Development and Application of a Method for Fiber-Fiber Bonded Area Measurement

PhD Thesis

Lisbeth Kappel

Institute for Paper, Pulp and Fiber Technology

Graz, February 2010

Statutory Declaration

I declare that I have authored this thesis independently, that I have not used other than the declared sources / resources, and that I have explicitly marked all material which has been quoted either literally or by content from the used sources.

Graz, 05.02.2010

Acknowledgment

Abstract

In this thesis a method for measuring the bonded area of individual fiber-fiber bonds is presented. It is based on microtome serial sectioning and image analysis. The size and the three-dimensional structure of the bonded area are assessed together with the cross sectional fiber morphology. Additionally holes and unbonded fiber regions can be measured. Individual fiber-fiber bonds are cut with the microtome and the cutting area is imaged after every cut with a light microscope, yielding cross sectional images at distinct positions through the bond. In these images the fibers are drawn by hand and the region where the fibers are optically bonded is determined using image analysis and bonded area is calculated. This method is applied to the determination of the development of the size of bonded area and of morphological parameters during refining.

The measurement also provides a basis for the evaluation of non-destructive reference methods. As far as needed the results obtained with these methods were calibrated with the microtome results. Polarized light microscopy was applied in combination with a physical model that simulates the path of light through the fibers and the microscope. This led to a comprehensive fundamental understanding of the theory of polarized light microscopy for fiber-fiber bonded area measurement. Comparison of bonded area measured with both methods showed that the bonded area is over- or underestimated with polarized light microscopy depending on the refining state of the pulp that is used. A factor for this over- and underestimation was determined for unrefined and refined pulp, respectively. Additionally the general applicability of confocal laser scanning microscopy for fiber-fiber bonded area measurement could be shown.

The methods presented in this thesis lead to a deeper understanding of fiber-fiber bonds and provide a basis for specific bonding strength measurements.

Keywords: fiber-fiber bond, bonded area, microtome serial sectioning, fiber morphology, polarized light microscopy

Kurzfassung

In dieser Arbeit wird eine Methode für die Bindeflächenmessung von einzelnen Faser-Faser Bindungen vorgestellt. Die Methode basiert auf Mikrotomserienschnitten und Bildanalyse und liefert die Größe und die dreidimensionale Struktur der Bindefläche zusammen mit Informationen über die Faserquerschnittsmorphologie. Zusätzlich werden Fehlstellen in der Bindung und ungebundene Faserränder gemessen. Einzelne Faser-Faser Bindungen werden mit dem Mikrotom geschnitten und die Schnittfläche wird nach jedem Schnitt mit einem Mikroskop aufgenommen. Dadurch erhält man Querschnittsbilder an bestimmten Positionen durch die gesamte Bindung. In diesen Bildern werden die Fasern händisch eingezeichnet, die Regionen wo die Fasern optisch gebunden sind werden bildanalytisch bestimmt und die Bindefläche wird berechnet. Mit dieser Methode wurde die Entwicklung der Bindefläche und der Fasermorphologie mit der Mahlung untersucht.

Die Mikrotomie diente als Basis für die Evaluierung zerstörungsfreier Referenzmethoden für die Faser-Faser Bindeflächenmessung. Wenn nötig wurden die Ergebnisse der zerstörungsfreien Methoden mit den Mikrotomergebnissen kalibriert. Polarisationsmikroskopie wurde in Kombination mit einem physikalischen Modell, das den Weg des Lichts durch Fasern und Mikroskop simuliert, angewandt. Das führte zu einem umfassenden Verständnis der theoretischen Grundlagen der Polarisationsmikrsokopie für die Faser-Faser Bindeflächenmessung. Die Bindefläche wurde mit beiden Methoden gemessen und ein Vergleich der Ergebnisse zeigte, dass die Polarisationsmikroskopie die Bindefläche über- bzw. unterschätzt, je nach Mahlungszustand des eingesetzten Zellstoffs. Ein Faktor für diese Über- bzw. Unterschätzung wurde für ungemahlenen und gemahlenen Zellstoff bestimmt. Zusätzlich wurde gezeigt, dass Konfokalmikroskpopie prinzipiell für die Faser-Faser Bindeflächenmessung anwendbar ist.

Die in dieser Arbeit vorgestellten Methoden führen zu einem besseren Verständnis von Faser-Faser Bindungen und dienen als Basis für spezifische Bindekraftmessungen.

Schlagwörter: Faser-Faser Bindung, Bindefläche, Mikrotom-Serienschnitte, Fasermorphologie, Polarisationsmokroskopie

List of publications

This thesis is based on the following papers:

1. L. Kappel, U. Hirn, W. Bauer and R. Schennach: A novel method for the determination of bonded area of individual fiber-fiber bonds. Nordic Pulp and Paper Research Journal, 24(2):199-205, 2009.

2. L. Kappel, U. Hirn, E. Gilli, W. Bauer and R. Schennach: Revisiting polarized light microscopy for fiber-fiber bond area measurement - Part I: Theoretical fundamentals, Accepted for publication in Nordic Pulp and Paper Research Journal, 2010.

3. L. Kappel, U. Hirn, E. Gilli, W. Bauer and R. Schennach: Revisiting polarized light microscopy for fiber-fiber bond area measurement - Part II: Proving its applicability, Accepted for publication in Nordic Pulp and Paper Research Journal, 2010.

4. E. Gilli, L. Kappel, U. Hirn and R. Schennach: An Optical Model for Polarization Microscopy Analysis of Pulp Fibre-to-Fibre Bonds. Composite Interfaces 16: 901–922, 2009.

Contributions of the author:
Paper 1, 2 and 3: Experiments, analysis, first version of the manuscript.
Paper 4: Experiments in part, manuscript in part.

Other publications and relevant conference presentations not included in this thesis:

Oral presentations

1. L. Kappel, U. Hirn, W. Bauer and R. Schennach: Measuring the bonded area of individual fiber-to-fiber bonds. In Workshop "Characterization of the fine structure and properties of paper making fibers using new technologies", COST Action E 54, Budapest, Hungary, 2008.

2. L. Kappel, U. Hirn and W. Bauer: A novel method for the analysis of fiber-to-fiber bonded area. In International Annual Symposium DITP, Bled, Slovenia, 35: 37, 2008.

3. L. Kappel, W. Bauer, U. Hirn, R. Schennach, E. Gilli, F. Schmied and C. Teichert: Untersuchung von Faser-Faser Bindungen im Micro- und Nanometerbereich. In Österreichische Papierfachtagung, Graz, Austria, 2008.

4. L. Kappel, U. Hirn and W. Bauer: A novel method for the analysis of fiber-to-fiber bonding area. In COST Action E 54 Fine Fibre, Graz, Austria, 2008.

5. E. Gilli, F. Schmied, C. Teichert, U. Hirn, L. Kappel, W. Bauer and R. Schennach: An interdisciplinary view on the strength of fiber-fiber bonds in paper. In Workshop "Single fiber testing and modeling", Stockholm, Sweden, 2009.

6. L. Kappel, U. Hirn, W. Bauer and R. Schennach: Revisiting polarized light microscopy for fiber-fiber bond area measurement. In Workshop "New methods for paper fibre characterization", COST Action E 54, 61-62, Tampere, Finland, 2009.

7. L. Kappel, U. Hirn, W. Bauer and R. Schennach: Anwendung der Polarisationsmikroskopie zur Bestimmung von Faser-Faser Bindeflächen. In Österreichische Papierfachtagung, Graz, Austria, 2009.

8. L. Kappel, U. Hirn, W. Bauer and R. Schennach: Grundlagenforschung zur Papierfestigkeit. In Minisymposium Verfahrenstechnik, 479-183, Wien, Austria, 2009.

Poster contributions

1. F. Schmied, C. Teichert, L. Kappel, U. Hirn and R. Schennach: Characterization of cellulose fiber surfaces. In 57. Jahrestagung der Österreichischen Physikalischen Gesellschaft, Leoben, Austria, 2007.

2. R. Schennach, L. Kappel, F. Schmied, E. Gilli, U. Hirn, W. Bauer and C. Teichert: Christian Doppler Labor für Papierfestigkeit. In Herbsttagung der Österreichischen Papierindustrie, Frantschach, Austria, 2007.

3. F. Schmied, C. Teichert, L. Kappel, U. Hirn and R. Schennach: Quantitative investigation of precipitated lignin on kraft pulp fibers with AFM. In AFM Forum and Workshop, Dublin, Ireland, 2008.

4. F. Schmied, C. Teichert, L. Kappel, U. Hirn, R. Schennach and H. Schröttner: Surface characterization of cellulose fibers. In Micro and Nano Scale Characterization of Fibres, Belfast, United Kingdom, 2008.

5. F. Schmied, C. Teichert, L. Kappel, U. Hirn and R. Schennach: Surface morphology of treated paper fibers. In 58. Jahrestagung der Österreichischen Physikalischen Gesellschaft, Leoben, Austria, 2008.

6. F. Schmied, C. Teichert, L. Kappel, U. Hirn, R. Schennach and H. Schröttner: Comparative AFM and SEM investigations on kraft pulp fiber surfaces. In Instrumentation and Methodology: Multinational Congress on Microcopy, 299-300, Graz, Austria, 2009.

7. L. Kappel, U. Hirn, W. Bauer and R. Schennach: Measuring the bonded area of individual fiber-fiber bonds. In Workshop "Single fiber testing and modeling", Stockholm, Sweden, 2009.

Printed papers

1. L. Kappel, U. Hirn, W. Bauer and R. Schennach: Measuring the bonded area of individual fiber-to-fiber bonds. Papiripar LII, 6: 246-250, 2008.

Contents

Chapter 1

Introduction

1.1 Background of the research project

This thesis was performed in the course of the CD-Laboratory for Surface Chemical and Physical Fundamentals of Paper Strength. The research group is formed by three university institutes (Institute of Solid State Physics, Institute of Paper, Pulp and Fiber Technology, Graz University of Technology and Institute of Physics, University of Leoben) and two industrial partners (Mondi and Lenzing), as depicted in figure 1.1.
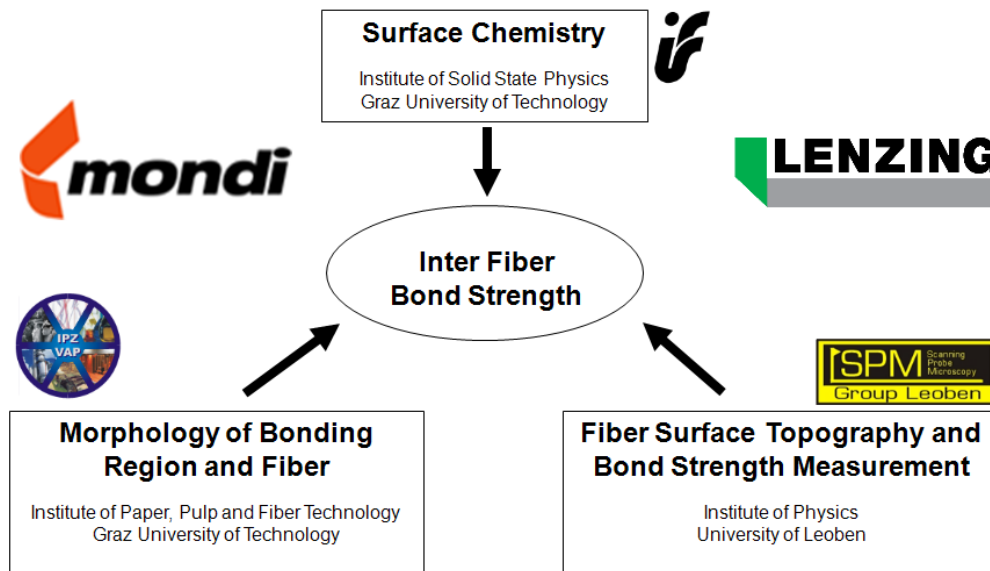
Fig. 1.1 Buildup of the CD-Laboratory for Surface Chemical and Physical Fundamentals of Paper Strength

The research in a CD-Laboratory consists of a fundamental and an applied part. The university institutes mainly focus on the fundamental research, while the major part of

the applied research is carried out directly at the industrial sites. Quarterly meetings and constant communications between the research groups ensure lively exchange of knowledge and achieving a common purpose.

The main aim of this CD-Laboratory is to gain insight into the bonding strength of fiber-fiber bonds and to quantify the contribution of the various chemical and physical forces that determine the fiber-fiber bonding strength, as suggested by Lindström et al. [1].

The fundamental research part focuses on three aspects of the fiber-fiber bonds:

- Surface chemistry of the fibers: At the Institute of Solid State Physics the surface chemistry of the fibers and of paper is analyzed using attenuated total reflection Fourier transform infra red spectroscopy (ATR-FTIR). Model systems of cellulose and hemicellulose films help to evaluate the respective influence on fiber-fiber bonding strength.

- Morphology of bonding region and fiber-fiber bonded area: The morphology of the bond and the bonded area are analyzed at the Institute of Paper, Pulp and Fiber Technology in a three dimensional representation of the fiber-fiber bonds obtained from a light microscopic imaging technique based on microtome serial sectioning and image analysis. Non-destructive methods for fiber-fiber bonded area measurement, like polarized light microscopy and confocal laser scanning microscopy are validated on the basis of the results obtained with the microtome.

- Fiber surface topography and bonding strength: The breaking load of the bond and the fiber surface topography prior to and after bond breakage are examined using atomic force microscopy (AFM) at the Institute of Physics. Additionally embedded fiber-fiber bond cross sections are analyzed to gain information on the fiber-fiber interface on the nanometer scale.

The applied research goes into two distinct directions. The industrial partner Mondi focuses on improving the dry strength of the paper by means of chemical additives or modified pulping and chemical post-pulping treatment of the fibers. The film formation of xylan on cellulose substrates is of major interest for the industrial partner Lenzing.

1.2   Scope of the thesis

Paper strength is mainly determined by the strength of individual fibers, the fiber-fiber bonds and the structure of the fiber network. In this thesis the focus is set on fiber-fiber bonds, because the research was carried out in cooperation with Mondi, a manufacturer of

kraft paper. Kraft paper mainly consists of unbleached, moderately beaten kraft softwood fibers. Therefore individual fiber strength is high, whereas sheet density (and thereby bonded area and cumulative bonding strength) is low. For that reason Mondi is more interested in improving the fiber-fiber bonding strength than in improving the single fiber strength. To understand the fundamental mechanisms of bonding strength, individual fiber-fiber bonds have to be analyzed in order to eliminate influences from the fiber network.

Apart from the surface chemical and the nano-topographical factors influencing the fiber-fiber bonding strength, morphological characteristics of the fibers and the bonding region also have a large impact. Thus measuring and understanding the fiber-fiber bonded area is the principal topic of the present thesis. In a first approach bonded area was measured based on microtome serial sectioning and image analysis. Investigations in this field can be divided into the following two subcategories:

- The morphology of the fiber-fiber bond, i.e. the three dimensional area and shape of the bonded area as well as the fiber wall deformation around the bonding zone.

- The cross sectional morphology of the fibers forming the bond, i.e. cell wall thickness, lumen collapse, fiber cross sectional dimensions and crossing angle.

Measuring the bonded area together with morphological parameters of fibers and bonding region allowed to build multiple linear regression models that explain the impact of fiber morphology on the size of bonded area. This comprehensive view of bonded area and morphology leads to a deeper understanding of fiber-fiber bonds. However, to measure the specific bonding strength the bonded area has to be measured non destructively. Therefore other non-destructive methods were evaluated and as far as needed calibrated on the basis of the microtome results.

1.3   Outline of this thesis

The PhD thesis is compiled in the form of a cumulative thesis. It is based on four papers that were published in the course of this work and that are listed above. The organization of the thesis is described in the following paragraphs.

In chapter 2 the relevant aspects of paper strength are discussed. A literature review of methods for fiber-fiber bond preparation and measurement of fiber-fiber bonded area is given in chapter 3 and chapter 4 respectively.

In Paper I a novel method for the measurement of fiber-fiber bonded area, which was developed in the course of this thesis, is described. The method is based on microtome serial sectioning and image analysis, bonded area is measured together with morphological parameters of fibers and bonding region. A detailed description of the image analysis routines and a discussion of the method can be found in chapter 5.

Measuring only the bonded area is not sufficient to get a comprehensive picture of fiber-fiber bonds. Therefore analyzing the specific bonding strength, being the bonding strength per bonded area, is the target. This is only possible if a non-destructive method for fiber-fiber bonded area measurement is used. On the basis of the fundamental understanding of fiber-fiber bonds that is gained with microtome serial sectioning other non-destructive methods for fiber-fiber bonded area measurement were evaluated and as far as needed calibrated using the microtome results. This allowed understanding the non-destructive methods and applying them correctly.

Polarized light microscopy was used as a non-destructive method for fiber-fiber bonded area measurement. The theoretical background of this method is discussed in Paper IV. The prove of its applicability and a comparison with the microtome method can be found in Paper II and Paper III. The description of sample preparation before analyzing fiber-fiber bonds under the polarized light microscope is given in chapter 6. Also the applicability of polarized light microscopy for refined pulp and for mechanical pulp is discussed.

The three-dimensional structure of a specimen can be analyzed non-destructively with confocal laser scanning microscopy (CLSM). This method has already been applied for fiber morphology analysis. In this work its applicability for fiber-fiber bonded area measurement was investigated. Sample preparation and experimental procedure are covered in chapter 7.

With microtome serial sectioning not only bonded area is measured, but also morphological parameters of fibers and bonding region. Based on these results the development of bonded area with refining is treated in chapter 8. Multiple linear regression modeling was performed to determine the influence of fiber morphology on the size of bonded area.

Finally the conclusions and an outlook are given in chapter 9.

Chapter 2

Background

Paper strength is mainly determined by the strength of single fibers and by the strength of fiber-fiber bonds. The influence of these parameters has already been discussed in the literature ([2], [3], [4], [5]). In this chapter the complex paper structure will be covered in consideration of individual fibers, fiber-fiber bonds and bonds in the fiber network. The influence of each of these factors together with characterization methods will be discussed.

2.1 Fiber strength

Fiber properties   The cellulosic fiber is the basic unit of paper, so attention will be drawn to its structure, components and properties in this section.

The most important component of a pulp fiber are the cellulose fibrils. Their hierarchical structure is depicted in figure 2.1[1]. The basic module are the cellulose molecules, that collocate to elementary cells. The elementary cells form elementary fibrils, which string together side by side and bundle to micro fibrils. Macro fibrils originate from bundled micro fibrils. They spiral around the fiber axis in differently oriented layers. The layered structure of a wood fiber results from these oriented macro fibrils.

Figure 2.2 shows that the cell wall of a wood fiber is built up in four layers (primary wall P, two secondary walls S1 and S2 and tertiary wall S3 or T). In the wood structure the middle lamella (ML) lies between the individual fibers, it is largely removed in the process of chemical pulping. The cell wall layers consist of cellulose fibrils embedded in an amorphous matrix of lignin and hemicelluloses. In the outer layer (primary wall P) the fibrils show the least ordered structure. The order increases in the secondary wall S1, here the fibril angle, being the angle between the fibrils and the fiber axis, is huge. The secondary wall S2 has the

---

[1]Available from lecture notes R. Eichinger: Faserphysik, 2009

5

Element	Cross section	Width	Depth	Length
Molecule		0.82	0.39	0.52
Elementary cell		0.82	0.78	1.03
Elementary fibril		6-10	3-5	15-20
Micro fibril		20-30	8-10	50-80
Macro fibril		-400	-100	-3000
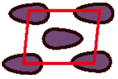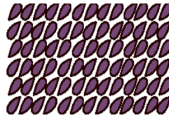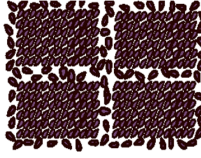
Fig. 2.1 Hierarchical structure of cellulose fibrils, length specifications in nm

highest thickness and is mostly responsible for the mechanical properties of the fiber. The fibrils show a highly ordered structure and the fibril angle is low. The tertiary wall T closes the cell wall towards the lumen. Here the fibril angle is higher again.

Apart from the fibrillar structure the cell wall layers also differ in thickness (see figure 2.2) as well as in chemical composition. The distribution of cellulose, hemicellulose and lignin changes through the individual cell wall layers, as it is depicted in figure 2.3. The lignin content decreases towards the lumen, while the cellulose content increases.
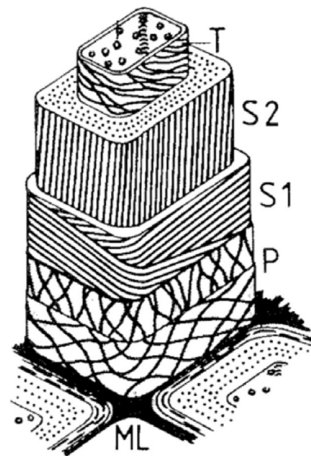
Fig. 2.2 Cell wall structure of a wood fiber

The fiber dimensions differ depending on type of wood, function in the wood (e.g. storage and transport of nutrients or strengthening) and time of growing (springwood or summerwood). For this thesis pulp from spruce and pine wood was used. Typical fiber properties of this
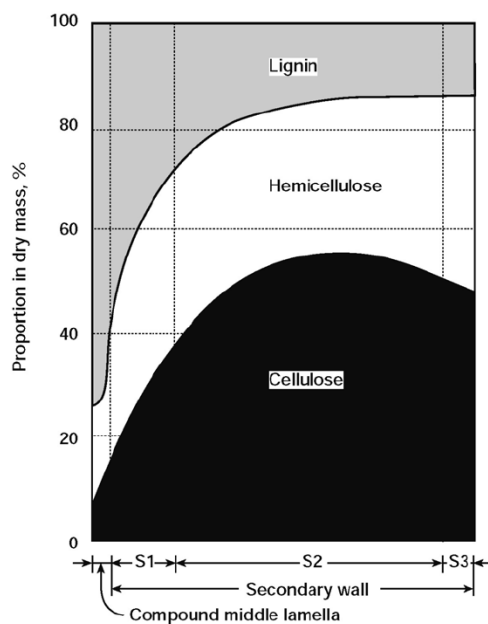
Fig. 2.3 Chemical composition of the fiber cell walls [5]

pulp are given in table 2.1 [5]. A more detailed characterization of the pulp used in this work is given in chapter 5.2.

	Mean fiber length [mm]	Mean fiber width [μm]
European spruce	3.5	27
Scots pine	3.6	39

Tab. 2.1 Fiber dimensions of spruce and pine wood [5]

Factors influencing fiber strength Pulp fibers are natural fibers, that are highly inhomogeneous. This leads to a wide distribution of the tensile strength of single fibers, as is shown in figure 2.4. In this graph the values for bleached sulphite spruce fibers are given, they range from 10 mN up to 350 mN. [5]

The fibril angle has a big influence on the load-elongation behavior of the fibers and varies considerably not only between different types of wood, but also between springwood and summerwood. A huger fibril angle leads to lower fiber strength. Pits in the fiber wall act as natural defects, just like micro-compressions or dislocations, that arise during the pulping process. Also the pulping process itself has a big impact on the fiber properties. Apart from the different processes (mechanical pulping, sulphite, sulphate), also the post-pulping processing like bleaching and refining has direct impact on the fiber strength. Removal of hemicelluloses impairs the fiber strength, while a high α-cellulose content increases fiber
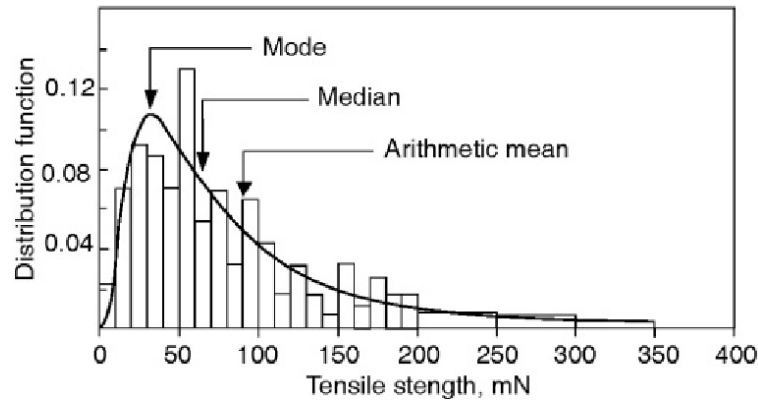
Fig. 2.4 Tensile strength distribution of bleached spruce pulp fibers [5]

strength. Another factor that has to be considered when fiber strength is measured is the tendency of fibers to curl and form kinks during drying, which may distort the measuring result. [5], [6]

Measuring the fiber strength Generally there are two different approaches to measure the strength of pulp fibers:

- Measuring the load elongation characteristic of <u>individual fibers</u>. The big advantage of this method is that there are no network effects and each fiber is loaded parallel to the fiber axis. After rupture the fiber cross sectional area can be measured and taken into account. However, the tests are time consuming and tedious. Because of the inhomogeneity of pulp fibers many tests are needed to get significant results. Clamping of the fibers often is a problem, as the weak and thin fibers tend to break or slip during clamping or loading. Gluing the fibers to the testing tabs is also challenging. Van den Akker et al. [2] tried several different glues and found that a hard-setting glue gives a good grip, but most of the fibers broke at one of the glue joints. They suggest that the hardened glue created a stress concentration in the fiber. When softer glues were used, the holding of the fibers often was insufficient. Finally they developed their own glue that showed satisfactory results. Another aspect that has to be considered is that the glue must not spread on the fiber. Leopold and McIntosh [7] used colored glue to show its distribution on the fiber.
  Hardacker [8] described an apparatus for single fiber testing and concentrated his attention to gripping and clamping the fibers. This is less problematic when regenerated cellulose fibers are used, as for example in [9], because the larger fiber length simplifies the handling of the fibers.

- In the zero-span tensile test a strip of paper is tested, the distance between the jaws of a tensile tester is set to zero and load is applied only to the fibers crossing the line between the jaws and not to the bonds. This comparatively fast and easy method was first introduced by Hoffmann Jacobsen [10] and is widely used for measuring fiber strength, e.g. [11] and [12]. However, it also has to be questioned critically, as there are many unknown issues. It is impossible to set the span between the jaws exactly to zero, this has been shown microscopically [11] and using an analytical model [13]. Boucai [11] found a typical span length between 0.15 mm and 0.4 mm. This means that it is almost impossible to measure only fiber strength without having any influence from the fiber network. A possibility to exclude the influence of the fiber network is to use wet sheets, as in this case the fiber-fiber bonds will be weakened enough to show insignificant influence on the results obtained for fiber strength. Still, fiber strength properties will also be influenced in the wet state. Further it has to be considered that the angle of the load applied to the fibers cannot be controlled, as at least part of the fibers are oriented randomly in a sheet. Seth et al. [14] showed that the zero-span test yields reliable results, as long as the fibers are straight. They came to the conclusion that if the precondition of straight fibers is fulfilled, bonding has little effect on the zero-span test and they do not follow the idea of measuring wet sheets in order to eliminate bonding.

Van den Akker et al. [2] analyzed the relationship between single fiber strength and zero-span tensile strength with comparative measurements. They came to the conclusion that the values show quite good agreement and found that the zero-span test is a meaningful measure of the fiber strength.

Influence of fiber strength on paper strength It is well known that pulp fibers have a very high breaking length in comparison to paper. Still, it has to be considered, that these high strength values are only obtained if the fiber is loaded parallel to its main axis. Usually the fibers are oriented rather randomly in a sheet of paper and they are loaded in any given direction, hence they show considerably lower strength. Another important point that has to be considered in this discussion is that due to drying tensions during bond formation the fiber is weakened because of so called micro-compressions. This is why an individual fiber shows higher strength and its mechanical properties cannot be related directly to the mechanical properties of a fiber in the paper network. [5]

In order to evaluate the role of fiber strength in a sheet of paper Van den Akker et al. [2] prepared laboratory sheets containing a small percentage of dyed fibers. These sheets were

tested in a "tensile-break inspection apparatus", where the rupture of the paper could be observed directly using a microscope. The dyed fibers were followed during breaking of the sheet. This showed that a substantial percentage of fibers (approximately 50%) was actually broken. In the case of beaten pulp this percentage increased to about 70%. This shows that fiber strength has considerable influence on sheet strength. Also Wathén [3] came to the conclusion that fiber strength has a significant influence on paper strength. Niskanen et al. [4] showed the importance of fiber strength to sheet strength using computer simulations. Page [15] investigated the importance of fiber strength and bond strength on the tensile strength of paper and came up with an explicit equation for the tensile strength (see equation 2.1).

$$\frac{1}{T} = \frac{9}{8 \cdot Z} + \frac{12 \cdot A \cdot \rho \cdot g}{b \cdot P \cdot L \cdot RBA} \tag{2.1}$$

with:

T = tensile strength of the paper sheet, expressed as breaking length $[cm]$
Z = zero-span tensile strength of the fiber, expressed as breaking length $[cm]$
A = average fiber cross section $[cm^2]$
ρ = fiber density $[g/cm^3]$
g = acceleration due to gravity $[cm/s^2]$
b = shear bond strength per unit bonded area $[dyn/cm^2]$
P = fiber perimeter $[cm]$
L = fiber length $[cm]$
RBA = relative bonded area [-]

In this equation the first term on the right side represents the contribution of fiber strength to the sheet strength. The second term on the right side displays the contribution of the bond strength to the sheet strength. According to this equation fiber strength gains importance with increasing paper strength. Experiments proved the validity of this mathematical relation.

2.2   Fiber-fiber bonds

Bond formation   When water is removed from the fiber suspension, surface tension forces pull the fibers closer together. This is known as the Campbell effect [16]. When the fiber surfaces are close enough, polymer chains that protrude from the fiber surfaces entangle and also contribute to the bonding. Hydrogen bonded chains are formed between the fibers and

as water removal progresses, hydroxylic groups on the fiber surfaces form direct hydrogen bonds. As a consequence of the swellability of fibers in water, the fibers shrink during drying, preferably in the lateral direction. This causes tensions in the bonding region and so called micro-compressions. [5]

Nanko and Ohsawa [17] identified four different structural features of the fiber-fiber bonds using electron microscopy (see figure 2.5):

- The bonding layer formed by external fibrils and polymer chains.

- The skirt formed at the edge of the bond due to out-drawn S1-layers. This deformation of the fiber wall enlarges the contact area between the fibers.

- The covering layer formed by external fibrils and fines and covers the edges of the bond.

- The wrinkles cannot always be observed.
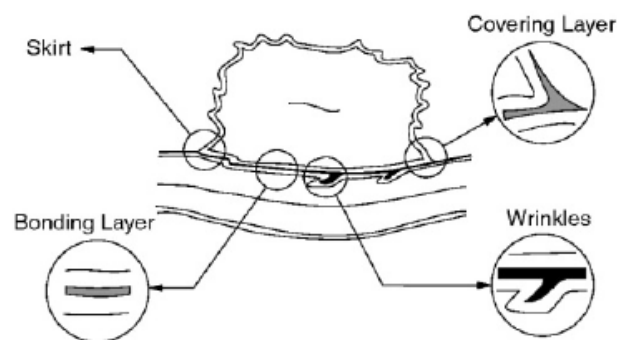
Fig. 2.5 Structural features of the fiber-fiber bonds [17]

Bonding mechanisms   Lindström et al. [1] defined five possible bonding mechanisms that may play a role in fiber-fiber bond strength: mechanical interlocking, inter-diffusion of cellulose molecules, hydrogen bonding, induced dipoles and electrostatic interactions (see figure 2.6).

- Mechanical interlocking: This mechanism is highly influenced by the roughness of the fiber surface and by the number of fibrils that protrude from the fiber surface and entangle during bond formation. It is mainly based on friction and does not necessarily require direct molecular contact of the entire fiber surfaces.
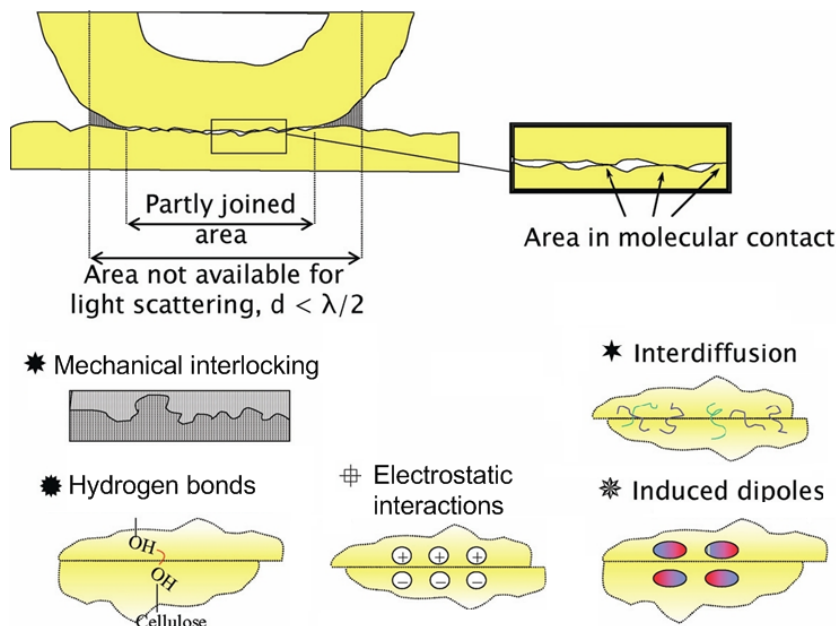
Fig. 2.6 Five possible bonding mechanisms [1]

- Inter-diffusion of cellulose molecules: Depending on the degree of swelling cellulose molecules can migrate from one fiber into the other. This effect can be enhanced by adding hydrophilic polymer molecules.

- Hydrogen bonds: Cellulose and hemicellulose are built up of glucose units that provide a large number of hydroxyl groups for hydrogen bond formation. During fiber-fiber bond formation the fibers are pulled towards each other due to capillary forces. As a result of the fibers conformability they will be in close enough contact so that hydrogen bonds can form.
  However, the impact of hydrogen bonds on bond strength is not totally clear. There is no quantitative statement on the contribution of hydrogen bonds to bond strength in the literature. Linhart [18] for example traced back the entire bond strength to mechanical interlocking and entangling of fibrils. He states that due to the relatively rough fiber surface the fibers cannot get into close enough contact to form a significant number of hydrogen bonds. Corte and Schaschek [19] on the other hand attributed the entire paper strength to the formation of hydrogen bonds.

- Induced dipoles: Contrary to hydrogen bonds the induced dipoles (Van der Waals interactions) are non-specific and long range [20]. The importance of these attractive forces between cellulosic fibers has recently been discussed by Notley et al. [21].

12

- Electrostatic interactions: Due to acid groups on the surface a pulp fiber is negatively charged. Positive counter ions of the acid groups can lead to electrostatic bonding. Stratton [22] investigated the strength of single fiber-fiber bonds treated with two different polymeric strength aid systems, one forming covalent as well as ionic bonds and one forming only ionic bonds. These results were compared with the results from untreated fibers to evaluate the influence of electrostatic interactions. He found that with both systems the same increase in fiber-fiber bonding strength can be observed and concluded that covalent bonds only play a minor role for bonding strength.

Until now it is only agreed that each of these mechanisms must play a role, but the respective impact has not been quantified. For each of the mechanisms the size of the bonded area is of major importance. Here it has to be distinguished between optically and chemically bonded fiber surfaces. Most of the methods used for fiber-fiber bonded area measurement are restricted to optical methods and cannot be used to make statements about the area in molecular contact. The methods for measuring fiber-fiber bonded area will be discussed in chapter 4.

Factors influencing fiber-fiber bonding strength   The chemical composition of the bonded fibers has an influence on the fiber-fiber bonding strength. Lignin reduces the strength, while hemicelluloses increase the strength. Fiber morphological parameters, like fibrillation, fiber wall thickness or fiber surface roughness also play a role. Fibrils protruding from the fiber surface promote mechanical interlocking. This can be facilitated by beating the fibers. Fibers with thin fiber wall show higher flexibility and can form stronger bonds. The surface roughness should preferably be low, as smooth surfaces allow higher bonded area and therefore higher bonding strength. [6]

Measuring the fiber-fiber bonding strength   Measuring the bonding strength of individual fiber-fiber bonds is challenging, especially because of the small sample size and the low bonding forces. Several researchers developed their own sample preparation techniques and testing devices.
Stratton [22] prepared the fiber-fiber bonds for strength measurement as it is shown in figure 2.7. He placed the fiber-fiber bond on a Mylar mount, only the ends of one of the bonded fibers were glued to the Mylar. The slot indicated in figure 2.7 was cut by a laser. This Mylar mount was then clamped in the tensile tester. This sample preparation technique was used by several others, sometimes in a slightly modified way, e.g. [2], [9].
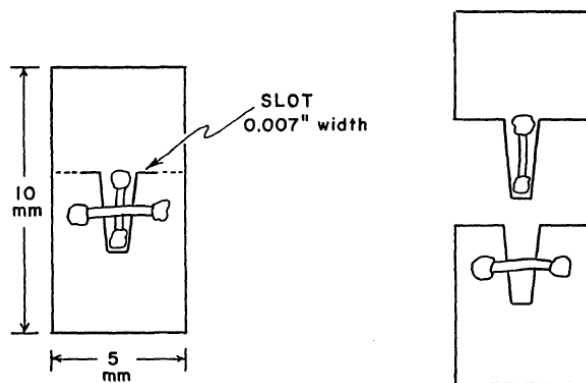
Fig. 2.7 Sample preparation for fiber-fiber bonding strength measurements [22]

Torgnysdotter and Wågberg [23] used a tensile testing stage that was designed at Mid Sweden University especially for this purpose. Also Thorpe et al. [24] as well as Stratton and Colson [25] designed their own load-elongation apparatus. Contrary to them Schniewind et al. [26] used a table model of the Instron tensile tester.

Despite the differences in the applied apparatus, the breaking loads given in the articles show quite good agreement. The average values range from 50 mN to 280 mN. There is a strong scatter in the values, but considering that the used pulps show wide differences these variations are not surprising.

Burgess [27] used a mathematical model to calculate fiber-fiber bonding strength. Experiments with hand sheets with varying basis weight yielded a linear relationship between $\frac{Basis\,weight}{Breaking\,length}$ and basis weight. An analytical model was built, which suggests that an extrapolation of this relationship to zero basis weight may be a reasonable estimate of fiber-fiber bonding strength.

2.3 Bonds in the fiber network

The bonds in the fiber network, will be discussed from the following two perspectives:

- Paper structure

  - Coverage

  - Corte Kallmes theory

- Relative bonded area (RBA)

Paper structure - Coverage   The coverage, c, is widely used to characterize random two-dimensional networks. It is defined as the average number of fibers at any point of the network and can be calculated with equation 2.2, where N is the number of fibers, l_f is the fiber length, w_f is the fiber width, A is the sheet area, b is the basis weight of the paper and β_f is the basis weight of the fibers. [5]

$$c = \frac{N \cdot l_f \cdot w_f}{A} = \frac{b}{\beta_f} \tag{2.2}$$

Figure 2.8 shows how the local coverage can be determined using a paper cross sectional image. A reference line is drawn through the cross section of a sheet of paper and then the fibers that intercept with this line are counted. The example here shows a kraft paper with a basis weight of 80 g/m^2, the coverage in this case is 15.

The coverage gives the effective number of fiber layers in a sheet. However, one has to keep in mind that actually there is no distinct number of fiber layers in a sheet of paper, as the structure is always random and partly felted. The local coverage values, c', are Poisson distributed.
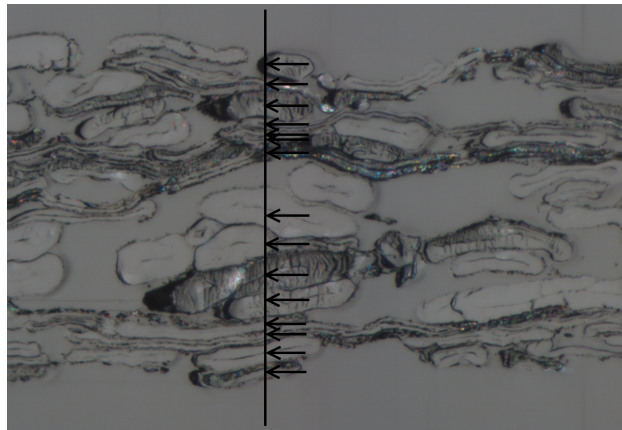
Fig. 2.8   Determination of the coverage

As the coverage is not easy to measure, mathematical models can be applied to get an estimate of this value. An approach to describe the paper structure mathematically is to assume that the paper consists of a pile of thin layers, i.e. two-dimensional sheets [28]. The advantage of the two-dimensional sheets is that all geometric elements are visible. Kallmes et al. [29] compared the results from the modeled multi-planar sheets that consist of several two-dimensional sheets with measurement results from standard hand sheets. They found good agreement and concluded that the pile of two-dimensional sheets is a suitable approximation for the paper structure. Sampson [30] also came to the conclusion that it is feasible to model

the paper network as a pile of two-dimensional thin sheets.

Paper structure - Corte Kallmes theory   The Corte Kallmes theory is a mathematical approach to describe the structure of a fiber network and the number of bonds in the paper. Corte and Kallmes studied the statistical geometry of two-dimensional random fiber networks [28]. They compared their mathematical model with microscopic measurements and found good agreement in the results.

A fiber is divided into square segments, as shown in figure 2.9 (left). The number of segments per fiber, K, is calculated with equation 2.3, where l_f is the average fiber length and w_f is the average fiber width.

$$K = \frac{l_f}{w_f} \tag{2.3}$$

Then the probability of having k neighboring fiber segments without bonding is calculated using equation 2.4. In the example in figure 2.9 (right) there are 5 neighboring fiber segments without bonding.

$$P(c = 0)^k = e^{-k \cdot c} \tag{2.4}$$
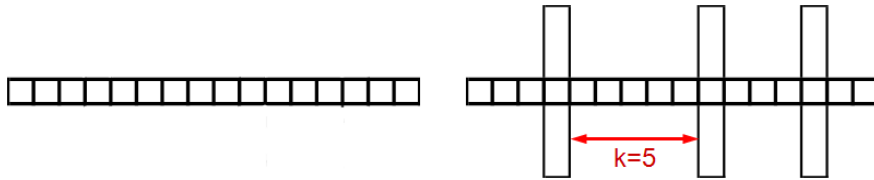
Fig. 2.9   Corte Kallmes theory - fragmentation of a fiber in square segments

This theory is only an approximation, as the model assumes that the fibers cross at right angles and at discrete locations.

To account for the random locations and orientations of the fibers a different approach has to be taken. Figure 2.10 shows an area A that is considered. The probability of two fibers crossing each other in this area is calculated using equation 2.5. Again l_f is the average fiber length and φ is the angle between the fibers. Based on this general equation the probability of two fibers crossing each other can be calculated.

$$P_c(\varphi) = \frac{l_f^2 \cdot sin\varphi}{A} \tag{2.5}$$

The average distance between two crossings, l_s, is calculated using equation 2.6, where w_f is the average fiber width and c is the average coverage.

$$l_s = \frac{\Pi \cdot w_f}{2 \cdot c} \qquad (2.6)$$
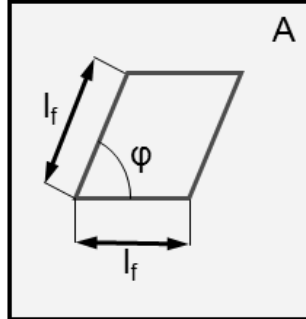
Fig. 2.10 Corte Kallmes theory - accounting for random locations and orientations of fibers

Relative bonded area The relative bonded area, RBA, is defined as the bonded fiber surface area, A_B, divided by the total fiber surface area, A_T, and characterizes the bonding degree of the paper (see equation 2.7).

$$RBA = \frac{A_B}{A_T} \qquad (2.7)$$

Calculation of RBA using the coverage, c, is only possible in the case of two-dimensional networks, for three-dimensional networks RBA has to be measured. Different approaches to measure RBA and a theoretical model for the fractional contact area (FCA) will be discussed in the following. For all measurement methods that are described below the total unbonded fiber surface area, A_T, has to be quantified. Rennel [31] compared three drying techniques for obtaining unbonded fibers: solvent-exchange drying, freeze drying and spray drying of an aqueous suspension with very low consistency (0.1 g/l). For all three cases the BET surface area and the light scattering coefficient were measured. The major difference between these methods was that in the case of solvent dried fibers hydrogen bonds could not form, so the fiber surface was more open, yielding a higher light scattering coefficient. During spray drying hydrogen bonding is possible, so the fiber surfaces should be comparable to those in a dry sheet of unbonded paper. Some inter-fiber bonding cannot be avoided in this case, but experiments showed that this effect is negligible. Also in the case of freeze drying some hydrogen and inter-fiber bonds can form, but in negligible magnitude. All results were compared to surface area values that were obtained by extrapolating the curve for the relationship between breaking length and unbonded area to zero breaking length. This turned out to be an unreliable method. In conclusion the author suggests that spray

drying of a suspension with low consistency is best suited to obtain unbonded fibers.

- Light scattering: Based on the assumption that all unbonded fiber surfaces are able to scatter light, Nordman and Gustaffson [32] used the light scattering coefficient, $s \ [m^2/g]$, to evaluate the increase in bonding with beating and higher wet pressing. They only aimed at investigating qualitative changes in degree of bonding, but not at actually measuring the relative bonded area. In order to calculate RBA also the total unbonded dry fiber surface area available for bonding has to be known. Ingmanson and Thode [33] used solvent dried paper sheets and state that RBA values based on these results are too high. They note that in the case of highly beaten pulp it is likely that a significant amount of fines is lost in the process of displacing water with acetone, which will have an impact on the light scattering coefficient. Therefore they determined the unbonded surface area by extrapolating the tensile strength as a function of s for different degrees of wet pressing. This curve turned out to be independent of the degree of beating. An explanation for this independency could be that the fibrils bond back to the fiber surface during sheet drying so that the total surface area of water dried fibers remains constant. This theory is not supported by Batchelor and He [34], who state that correlating s with sheet tensile strength and with sheet density is not useful, because changes in fiber cross sectional shape with wet pressing have to be considered. They gave a new formula for calculating RBA, where s is corrected for changes in fiber cross sectional shape.

- Gas adsorption: Instead of using the light scattering coefficient, gas adsorption can provide a measure of fiber surface area. Haselton [35] compared the adsorption of nitrogen, butane and carbon dioxide on pulp fibers. For computing the surface area from adsorption data the Brunauer, Emmett and Teller (BET), the Harkins-Jura and the Fu-Bartell methods were compared. He found that the combination of nitrogen adsorption with the BET method was best suited for measuring the RBA.

- Polarized light microscopy: Page et al. [36] used polarized light microscopy to investigate fiber-fiber bonds in a sheet of paper. With the information contained in the polarized light microscopy images they calculated the percentage of bonded fiber surface using equation 2.8.

$$Percentage\,bonded = \frac{Mean\,bonded\,area \cdot 100}{Mean\,fiber\,width \cdot Intercrossing\,distance} \tag{2.8}$$

With this method they got a fraction of bonded fiber surface of 16 % for unbeaten pulp

and 36 % for beaten pulp. These values are slightly lower than those given by Ingmanson and Thode [33], who give an RBA value of approximately 25% for unbeaten pulp. The results for beaten pulp cannot be compared, as too few specifications concerning intensity of beating are given.

- Theory of fractional contact area: This theory is based on the assumption that paper can be modeled as a pile of two-dimensional fiber networks [30]. The grammage of the two-dimensional networks is determined using the porosity. The interaction of fibers between the distinct layers is also considered in the model. Sampson [30] calculated the fractional contact area and the results showed very good agreement with data from the literature for thick sheets with known porosity. Kallmes and Bernier [37] also modeled RBA assuming that a sheet of paper can be approximated as a pile of two-dimensional sheets. They additionally measured RBA both with gas adsorption and using the specific light scattering coefficient and found good agreement between all results.

Although the RBA measurement methods using light scattering or gas adsorption differ significantly they seem to yield results with good agreement. Haselton [38] compared the BET surface area with the specific light scattering coefficient at various degrees of beating and wet pressing, he found a linear relationship. This was also shown by Swanson and Steber [39] and Kallmes and Bernier [37].

2.4 Conclusions

The relevant aspects of paper strength are discussed above: fiber strength, fiber-fiber bonds and bonds in the fiber network. However, the focus of this thesis will be only on fiber-fiber bonds. The industrial partner Mondi is a manufacturer of kraft paper that mainly consists of unbleached and moderately beaten kraft softwood fibers. The individual fiber strength is high, therefore Mondi is more interested in improving the fiber-fiber bonding strength. Methods for fiber-fiber bond preparation and fiber-fiber bonded area measurement are discussed in chapter 3 and chapter 4, respectively.

Chapter 3

A review of methods for fiber-fiber bond preparation

The methods for fiber-fiber bond preparation are either based on manipulation of individual fibers or on using a highly diluted fiber suspension. Both options will be discussed in the following. In the literature also preparation techniques for bonds between a fiber and a shive or between a fiber and a strip of cellophane can be found. These methods are also described here, as they can as well be applied for preparation of fiber-fiber bonds.

3.1 Fiber-fiber bonds prepared from individual fibers

McIntosh [40] placed a wet shive on a glass microscope slide and applied a drop of water to the shive. A single pulp fiber was placed across the shive at an angle of 90°. This was covered with another glass slide and dried over night at 90°C and under the weight of 300 g. The glass slides were both covered with a foil, in order to prevent the shive and the fiber from adhering.

Practically the same method was used by Mohlin [41] to prepare bonds between a pulp fiber and a strip of cellophane. The glass slides were covered with aluminium foils and the samples were dried over night at 95°C and under the weight of 120 g.

Thorpe et al. [24] sandwiched fiber-shive bonds between two surface treated glass slides and clamped them under a pressure of 1500 psi. This assembly was then heated for 60 minutes in a pressure cooker or for 15 minutes in an autoclave at 210°C. The samples were then put into an oven at 105°C for 30 minutes without pressure, after that they were allowed to rest at room temperature over night to complete the drying.

Stratton [22] positioned two fibers at right angles on a teflon-faced rubber disc under water.

The fibers were clamped under tabs that were cut in the teflon film (see schematic drawing in figure 3.1), to ensure a constant crossing angle. The clamped fibers were covered with a second teflon faced disc. This sandwich was then dried at 105°C under a nominal pressure of 0.12 MPa for one hour. After drying the fiber-fiber bond was glued to a Mylar film for further analysis.
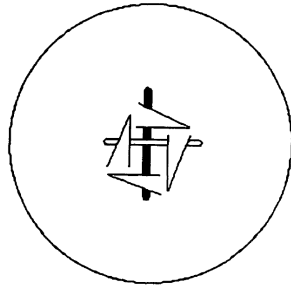
Fig. 3.1 Fiber-fiber bond preparation from individual fibers as described in [22]

A very similar approach was taken by Schniewind et al. [26], who also placed two wet fibers between two teflon plates. This assembly was pressed in a screw press with a pressure of 75 *psi* at a temperature of 23°C. The pressure was remained for three days, then the specimen were mounted on paper tabs for strength measurement.

Kang et al. [42] placed two fibers on a glass with a diameter of 9 mm under water, covered this with another piece of glass, pressed the sample for 2 minutes under 0.1 MPa and then dried it at 105°C for 5 minutes. Contrary to the citations given above, here no statements about problems with the fibers sticking to the glass are mentioned, they also do not make any indications on covering the glass with some anti-stick coating.

3.2   Fiber-fiber bonds prepared from suspension

Mayhood et al. [43] prepared fiber-fiber bonds by dewatering an extremely dilute suspension on a wire. The samples were dried under the same conditions as standard laboratory sheets. By that they obtained single fibers, fiber-fiber bonds and small fiber mats. Fibers that were bonded at right angle were chosen for further analysis. Twisted fiber ends or other involved fibers were trimmed and the fiber-fiber bond was fixed directly on the testing mount.

A small volume of a very dilute fiber suspension was dried between two teflon-faced silicon discs by Forsström et al. [44]. In this way thin fiber mats were formed that were allowed to dry for two hours at 105°C and under a nominal compressive load of 0.12 MPa. Then perpendicular fiber-fiber bonds were chosen for further testing.

A more complex setup was used by Lowe et al. [45]. A dilute suspension was drained onto a piece of filter paper and the fibers were wet pressed in a standard hand sheet mold onto glass slides. The samples were dried between two wet blotters for two minutes at 50 *psi*. An illustration of the wet pressing setup is shown in figure 3.2. The fiber-fiber bonds remained on the glass slides for microscopic analysis.
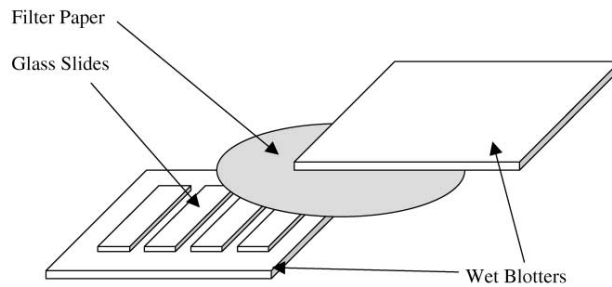
Fig. 3.2 Fiber-fiber bond preparation from suspension as described in [45]

Thomson et al. [46] filtered a suspension with a concentration of 50 *mg/l* onto filter paper. From this filter paper fiber-fiber bonds were transferred to glass slides with light pressing. The bonds were then air dried for at least six hours and remained on the glass slides for microscopic analysis.

3.3   Discussion of fiber-fiber bond preparation

When working with single fibers or individual fiber-fiber bonds, the pre-selection of only a certain kind of fibers can be problematic. This is especially true when single fibers are manipulated, as straight and long fibers are separated more easily from the pulp. This effect is strongly reduced when the bonds are made from suspension. In this case also the bond forming conditions are more related to bond formation in sheets, as fibers can settle freely on top of each other. An advantage of fiber-fiber bond preparation from individual fibers is that the angle of crossing can be chosen freely.

Chapter 4

A review of methods for fiber-fiber bonded area measurement

Several methods for fiber-fiber bonded area measurement are described in the literature. These methods can be grouped in the following way:

- Dyeing methods

- Microtome methods

- Optical sectioning methods

- Polarization microscopy methods

- Measuring the common area

4.1 Dyeing methods

Torgnysdotter et al. [47] used a light microscope, operating in the diffraction interference contrast mode to investigate the fiber-fiber contact zone. Fiber-fiber bonds were dyed with an acetone based dye (hexamethyl-P-rosaniline). The acetone does not disrupt the molecular contact between the fibers, so the dye can only reach fiber surfaces that are not in molecular contact. The excess acetone was evaporated and then the bonds were ruptured. After that the fibers were analyzed with a light microscope and the undyed fiber surfaces were considered as formerly bonded. A schematic representation of how the microscope images were interpreted is shown in figure 4.1. The undyed areas were analyzed manually and the area of contact, $A_{contact}$, was calculated from the summed-up areas. Additionally the total

fiber-fiber overlap area, A_{total}, was measured. From these values the degree of contact was calculated according to equation 4.1. So no actual value for size of bonded area is determined, rather a qualitative expression for the degree of bonding is given. The number of contact points and the homogeneity of the contact points were also evaluated.
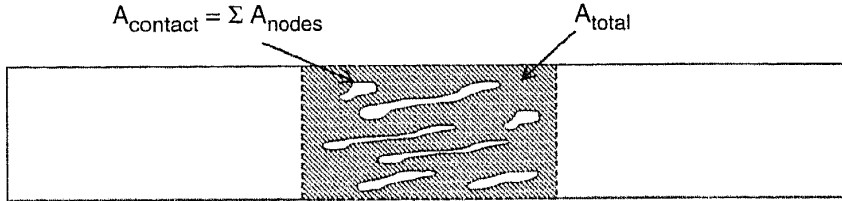
Fig. 4.1 Evaluation of fiber-fiber contact area as described in [47]

$$Degree\,of\,contact = \frac{A_{contact}}{A_{total}} \tag{4.1}$$

Another method based on dyed fibers was introduced by Thomson et al. [46]. They functionalized the bonded fibers with a pair of fluorescent dyes capable of fluorescence resonance energy transfer (FRET). Under the fluorescence microscope the relative energy transfer values were related to the distance between the bonded fibers. The results were corrected using the FRETN algorithm, where the measure of FRET is normalized for the concentrations of donor and acceptor [48]. An exemplary result is shown in figure 4.2. The color bar on the right indicates the distance between the fibers, the units of the legend are arbitrary units. Red, orange and yellow are areas with a higher FRETN value and hence a shorter distance between donor and acceptor fiber. For comparison of fiber-fiber bonds made from different fibers (viscose, various types of wood) only qualitative statements were made, the authors did not give any values for the size of bonded area.

4.2 Microtome methods

Transmission electron micrographs of ultra thin paper cross sections were analyzed by Asunmaa and Steenberg [49]. Fibers and structures in the bonding region were observed with a resolution of 20 Å. This high resolution allowed seeing ultra structural contacts like merging of the fibers. Even micro-fibrils could be seen in the images. Values for size of bonded area were not obtained as too many images would have had to be analyzed. The authors just evaluated whether the contact between fibers consisted of areas of many small scattered point contacts or there were fewer but considerably larger areas. Local interruptions due to fiber morphology could also be observed. Furthermore they investigated between
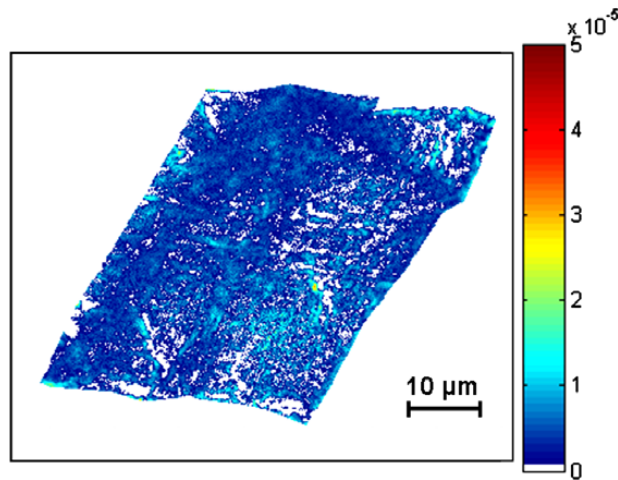
Fig. 4.2 FRETN surface plot of a fiber-fiber bond as shown in [46]

which fiber wall layers bonding had occurred: S1-S1, S1-S2, S2-S2 or contacts involving lumen.

A similar approach was taken by Yang et al. [50]. Slices with a thickness of 4 to 8 μm were cut off an embedded paper sample and each slice was examined in a microscope using phase contrast and transmitted polarized light. From these microscope images the fiber aspect ratio, the fiber moment of inertia and the degree of bonded surface area were determined. Figure 4.3 shows the method for determination of bonded surface area from the cross sectional images. The fiber perimeter was divided into equal sections and the number of sections that were in contact with another fiber was determined. With this information the ratio of bonded fiber surface could be calculated. Furthermore it was evaluated to how many other fibers one fiber was bonded, yielding a probability density of bonding state for each fiber. Again, only a degree of bonding is given and no value for size of bonded area.

4.3 Optical sectioning methods

Confocal laser scanning microscopy (CLSM) was used by Jang et al. [51] to investigate fibers and fiber-fiber bonds. Top and cross sectional view of fiber-fiber bonds as shown in figure 4.4 were analyzed. However, the authors did not really measure the bonded area quantitatively, they rather made qualitative statements on the extent of bonding.

Also Somwang et al. [52] used CLSM measurements to characterize the degree of bonding in hand sheets. Fiber-fiber bond cross sections were evaluated concerning conformability and quality of contact. But again, no measure for size of bonded area was given.
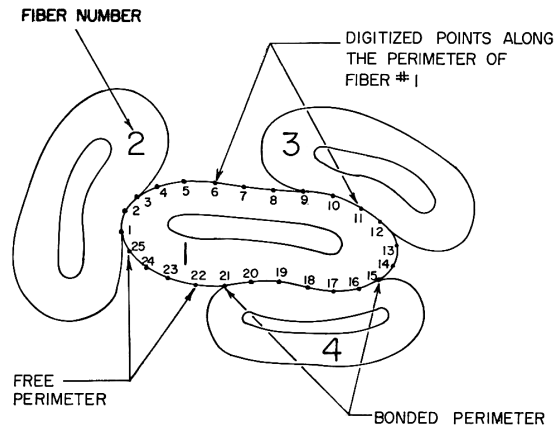
Fig. 4.3 Determination of bonded surface area after [50]
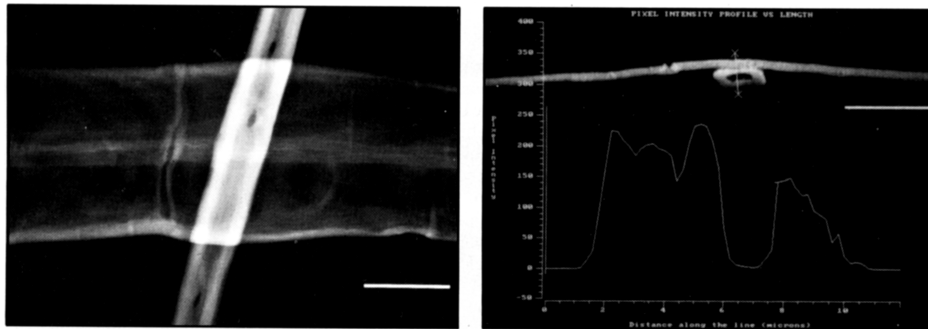
Fig. 4.4 Top and cross sectional view of a fiber-fiber bond under the CLSM [51]

4.4 Polarization microscopy methods

Page [53] introduced polarized light microscopy for fiber-fiber bonded area measurement. The method is based on polarized vertical illumination and the phenomenology can be explained with the drawing in figure 4.5. The light passes the first polarizing filter, the polarizer, and is linearly polarized, so that only waves with one plane of oscillation can pass. The light is directed through the objective and to the specimen, where it is reflected. The second polarizing filter, the analyzer is rotated 90° towards the polarizer, so that only optically modified waves can pass it. In the case of a single fiber, the light is able to pass the analyzer (see figure 4.5, left) and the fiber appears bright, in the case of fiber-fiber bonding the light cannot pass the analyzer (see figure 4.5, right) and bonded area appears dark. An example of a fiber-fiber bond under the polarized light microscope is shown in figure 4.6. Page [53] investigated bonds in thin sheets. To reduce unwanted reflected and scattered light from surrounding fibers 70 % of the fibers were dyed black. By that the remaining undyed fibers became clearly visible. Furthermore he found that the contrast was exceptionally high
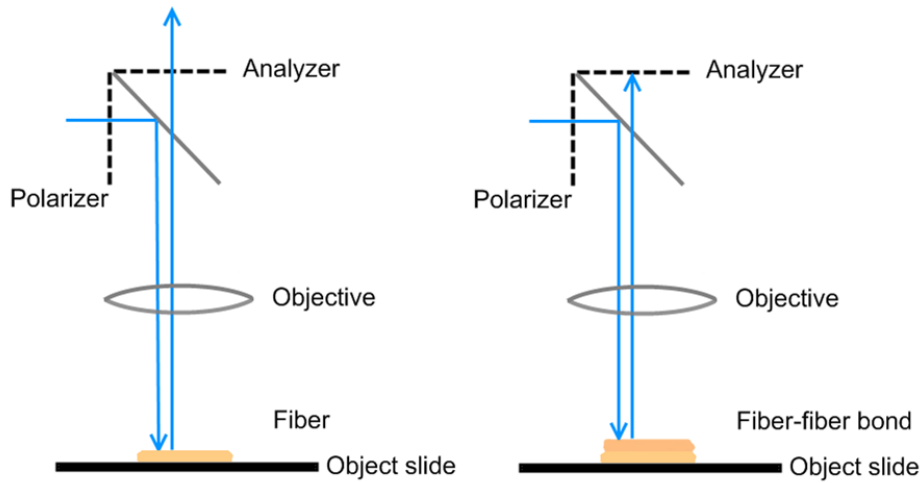
Fig. 4.5 Phenomenology of polarized light microscopy
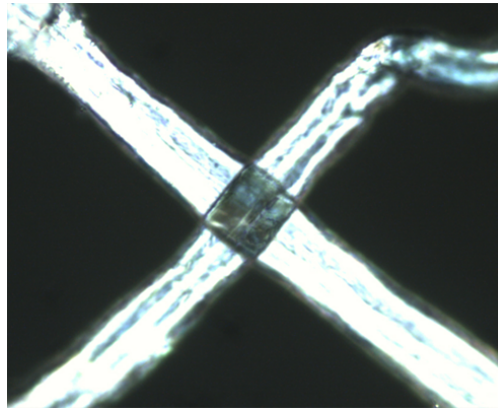
Fig. 4.6 Fiber-fiber bond under the polarized light microscope

when a dyed and an undyed fiber were bonded.

This work was continued in [36]. Again bonds in sheets were analyzed, but now the authors also gave values for the size of bonded area. Furthermore they divided the bonds into distinct forms of appearance: simple bonds (only two fibers are bonded) and obstructed bonds (a third fiber is involved). It was found that the effect of dark bonded area tends to be more clearly visible if the fibers are completely collapsed early wood fibers. This is why preferably bonds between such fibers were analyzed.

4.5 Measuring the common area

Mohlin [41] tried to measure the bonded area between a fiber and a strip of cellophane with polarized light microscopy, but the method turned out to be unsuitable for this purpose. The

author suggests that the low degree of crystallinity of the cellophane might be the reason for this. Scanning electron images of ruptured bonds showed a very good replica of the fiber in the cellophane. This is why it was assumed that the fiber was bonded to the cellophane over the entire crossing region. So bonded area was measured planimetrically from photo micrographs.

Also Schniewind et al. [26] found that polarized light microscopy was not generally applicable for their fiber-fiber bonds. Instead the gross overlap area was measured microscopically. This area was treated as a rectangle and the size of the bonded area was calculated by multiplying the two sides.

4.6   Discussion of fiber-fiber bonded area measurement

Most of the methods described above were applied to obtain qualitative statements on the degree of bonding between two fibers. Quantitative measurement of bonded area has only been performed applying polarized light microscopy [53]. One has to notice that almost all approaches described here are restricted to the resolution of light microscopy. Information on molecular contact is not provided, only optically bonded area is measured.

Holes in the bond cannot be identified with all methods. No information is available whether holes in the bond can be detected with dyeing methods, as for example used by Torgnysdotter et al. [47]. According to Mayhood et al. [43] it is also unclear whether holes in the bond can be determined with polarized light microscopy.

Another aspect that has to be considered is whether the method is destructive or non-destructive, as this is of relevance for e.g. specific bonding strength measurements. This is only possible with the methods described in [46], [51], [53], [41] and [26].

Finally the results may differ depending on whether individual fiber-fiber bonds or bonds in a sheet of paper are analyzed. The conditions during bond formation (temperature, pressure) may have a significant influence on bonding morphology and fiber conformability, thus influencing the fiber-fiber bonded area.

Chapter 5

A novel approach for fiber-fiber bonded area measurement

5.1   Introduction

In chapter 4 existing methods for fiber-fiber bonded area measurement were introduced. A novel method based on microtome serial sectioning and image analysis that has been developed in the course of this thesis is presented in Paper I. Individual fiber-fiber bonds are embedded in resin and serially sectioned in a microtome thus yielding cross sectional images of the bond that show where the fibers are optically bonded. From these images the bonded area is calculated using image analysis. This method allows a more comprehensive view of fiber-fiber bonding, because the bonded area is measured together with the morphological parameters of the fibers and the bonding region. Holes in the bond and overlapping but unbonded fiber edges can be identified correctly. The method is restricted to light microscopy, so optical bonded area is measured.

In this chapter additional information not given in Paper I regarding sample preparation and image analysis is provided.

5.2   Used pulp

All experiments were performed with an unbleached softwood kraft pulp that was a mixture from spruce and pine wood. It had a kappa number of 42 and was once-dried and unbeaten. Fiber analysis was performed with the Kajaani fiber lab, the results are summarized in table 5.1. The fiber length distribution is shown in figure 5.1.

Coarseness [mg/m]	0.2530
Fiber length (arithmetic average) [mm]	0.9025
Fiber length (length weighted average) [mm]	2.1300
Fiber length (width weighted average) [mm]	2.7850

Tab. 5.1 Characterization of the used pulp (Kajaani)
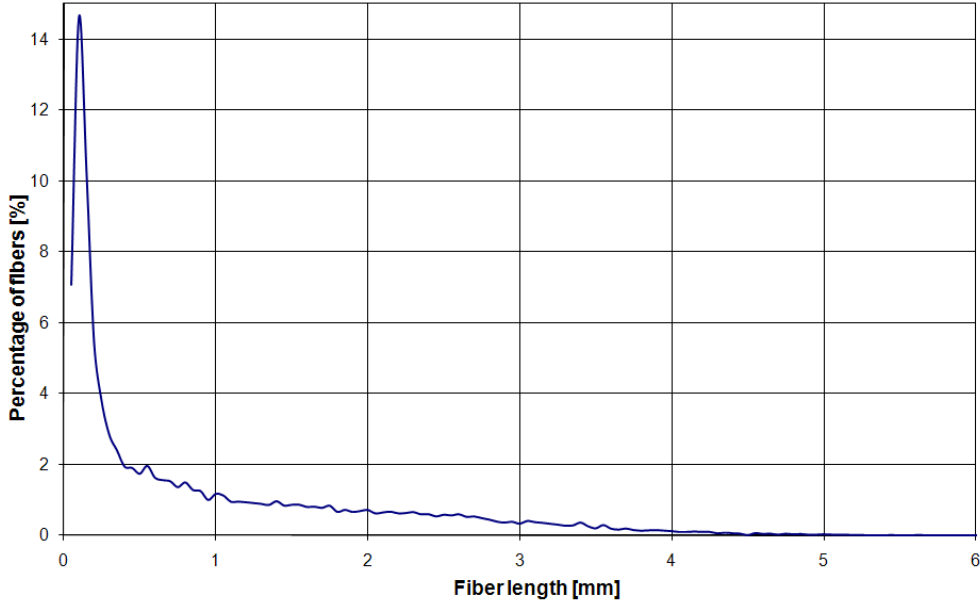
Fig. 5.1 Fiber length distribution of the used pulp

5.3   Sample preparation

Most of the methods for the preparation of fiber-fiber bonds described in chapter 3 have been tried in this work. These experiments showed that the manipulation of individual fibers is time consuming and that either bond formation was not possible, or that the bonds were very weak and most of them broke during handling. This is why we decided to make the fiber-fiber bonds from suspension, similar to the procedure described in [44]. Small drops of a suspension with a consistency of 0.01 % are dried between two teflon plates in a conventional laboratory sheet dryer. Small fiber mats are produced and from these fiber mats individual fiber-fiber bonds are chosen for further analysis. Only fiber-fiber bonds where no third fiber is involved are used for bonded area measurement. The fiber-fiber bonds are then fixed with glue[1] on a strip of paper across a hole and embedded in a cold polymerizing resin[2] using a gelatine capsule. A precise description of fiber-fiber bond preparation and embedding is

---

[1]Loctite Super glue Gel, 3g
[2]Technovit 7100

given in Paper I.

5.4 Imaging of the samples

The capsule is then clamped in a microtome and sections with a thickness of 3 μm are repeatedly cut off the sample. After every cut the cutting area is imaged. In order to have a large field of view with a high resolution several images are taken along the cutting area. The individual images are taken with an overlap of approximately 25 % and stitched into one composite image (see figure 5.2). This example shows the fiber cross sections before the fibers are bonded. In this case three images were taken after the microtome cut. The overlap is indicated by the red rectangle. After stitching one ends up with an image of the entire cutting area. The process of stitching is fully automatic. A description of the algorithm can be found in [54].
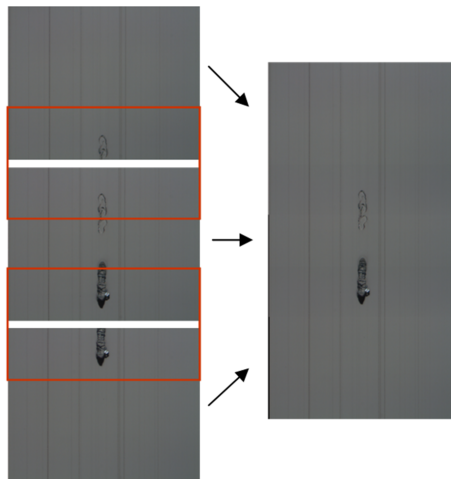
Fig. 5.2 Stitching of the images after microtome serial sectioning

The positioning accuracy of the microtome in the upper position after every cut is limited. This causes some vertical displacement in the order of a few micrometers between subsequent slice images. To obtain a correct picture of the fiber-fiber bond, these subsequent images have to be aligned in one image plane. Figure 5.3 shows the process of aligning. In the upper part of the image the fibers change their position in every picture randomly. In the lower part of the image the correct movement of the fibers is depicted. The black line indicates a reference line to show the effect of aligning. A description of this automatic process can also be found in [54].
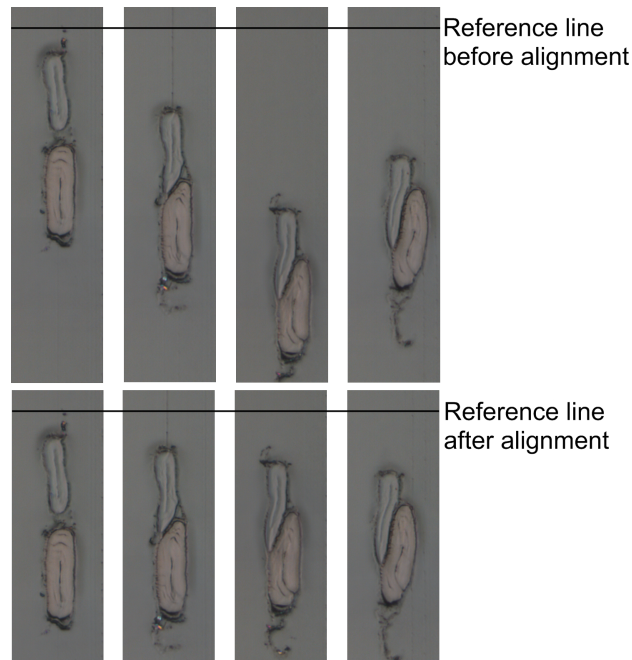
Fig. 5.3 Consecutive images of the fiber-fiber bond, before and after aligning

First trials showed that stitching and aligning is problematic if there are only two fibers in the images. If no fiber was caught in an image, the software did not have any information of how to position the image. This occurred at least once in every cut and even if stitching worked, the movement of the fibers in the cutting direction could not be reproduced correctly without having any fixed points. Therefore a material providing additional structural information in the images has to be embedded next to the bond. In a first approach small cellophane strips were glued sidewise of the hole where the bond is fixed, as shown in figure 5.4. This should function as a reference feature.
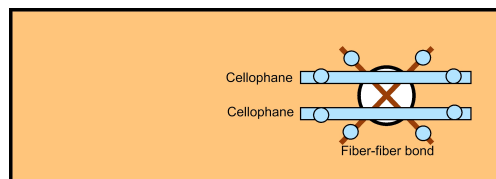
Fig. 5.4 Embedding the bond together with two strips of cellophane to gain structural image information

Stitching and aligning images of fiber-fiber bonds that had been embedded together with two strips of cellophane still was problematic, as the structural information provided by the cellophane was not sufficient. Between the cellophane and the fibers there were again regions without any elements in the image, so that stitching was not possible for lack of structural

information.

Some other material had to be chosen to be embedded next to the bond that ranges from the top to the bottom of the cutting area. As this material had to be embedded together with the bond, additionally the following criteria had to be met:

- The embedding resin must be able to penetrate the material.

- The structure has to be distinguishable from the fiber-fiber bond.

- The structure has to be small because of the small field of vision with the 50x objective.

- The structure has to be close to the bond, as the microtome images have a width of only 200 μm.

Experiments with the following materials embedded next to the fiber-fiber bond were performed:

Cellophane and a strip of paper: The fiber-fiber bond was fixed on the strip of paper, then a strip of cellophane was fixed on the paper strip and this was finally covered with another strip of paper. The cellophane should help to distinguish the fibers of the bond from the fibers in the paper and the second strip of paper should provide structural information. The scheme of sample preparation and the cross sectional view in a microtome image are shown in figure 5.5.

(a) Scheme of sample preparation

(b) Corresponding picture of the cutting area
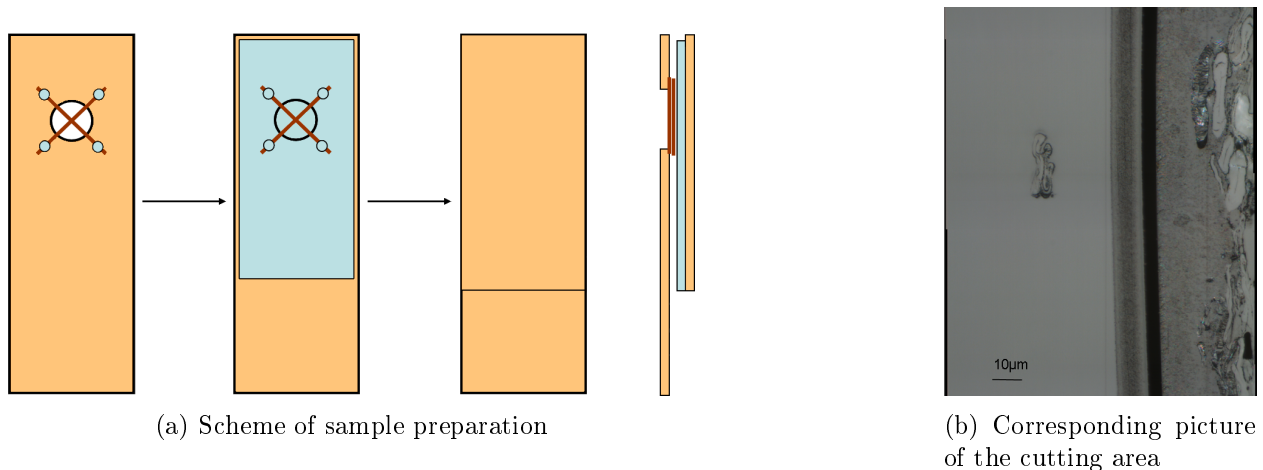
Fig. 5.5 Bond covered with cellophane and paper

The microtome image in figure 5.5(b) shows that the three layers (paper with the bond, cellophane, paper) were separated during embedding and so only a small part of the second paper strip can be seen in the picture of the cutting area. Because of the too big distance

between bond, cellophane and paper only a few fibers of the paper strip were caught in the image. They provided too few structural information to allow correct stitching and aligning.

Forming wire: Again the fiber-fiber bond was fixed on the strip of paper as usual. Then a small piece of a forming wire was glued to the paper strip. Since the forming wire is made of a synthetic material, the structure should be clearly distinguishable from the fibers. In figure 5.6 the set-up of the sample and the corresponding image of the cutting area are depicted.

(a) Scheme of sample preparation

(b) Corresponding picture of the cutting area
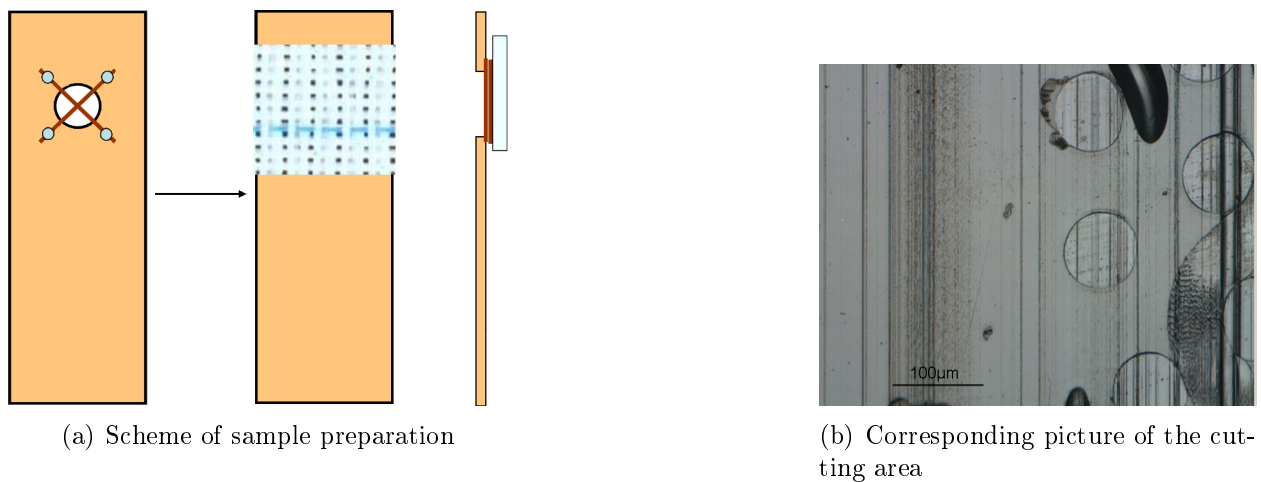
Fig. 5.6 Bond covered with forming wire

As figure 5.6(b) shows, the structure of the forming wire is much bigger than the fibers. This exemplary picture was made with a 10x objective. Nevertheless, hardly any structure of the wire is visible. Usually for all samples a 50x objective is used. This high magnification is needed for the measurement of the fiber-fiber bonded area to see the bonding structure as detailed as possible. For this sample the field of vision with the 50x objective is by far not sufficient, so embedding the forming wire together with the bond was not pursued further.

Woodfree coated paper: Also in this case there was no change in preparation of the bond. After the bond had been fixed on the strip of paper, it was covered with a piece of woodfree coated paper (see figure 5.7). The coating layer helps to distinguish between the fibers of the bond and the fibers of the paper strip without needing an additional layer in the sample (like in the case of cellophane above).

Figure 5.7(b) shows that the structure of the woodfree coated paper is in the range of the structure of the fibers. Furthermore the coating layer separates the two fibers of interest exactly from the fibers in the sheet of coated paper. Despite the high magnification enough structure is provided, so that stitching and aligning were possible without problems. The
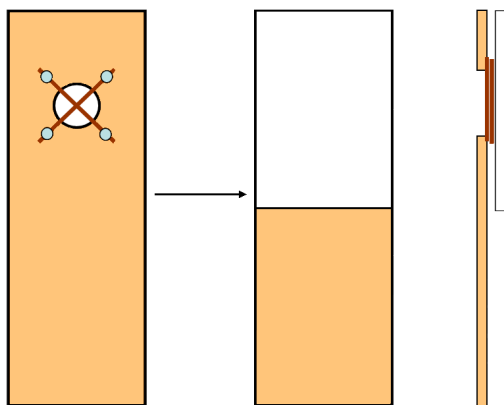
(a) Scheme of sample preparation
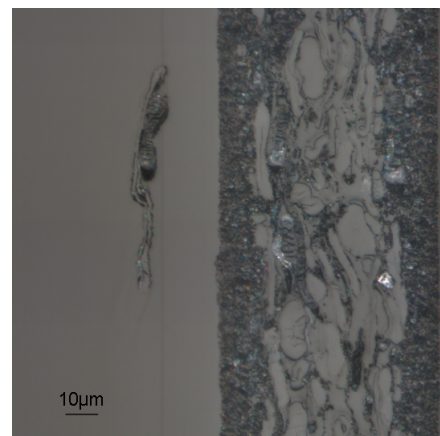
(b) Corresponding picture of the cutting area

Fig. 5.7 Bond covered with woodfree coated paper

sheet of coated paper hardly ever separated from the fiber-fiber bond during the embedding procedure, so that in most cases all criteria listed above were met.

Fiber-fiber bond fixed directly on woodfree coated paper: In order to minimize the distance between the bond and the coated paper, a bond was fixed directly on a strip of coated paper, as it is shown in figure 5.8. Two scratches were made in the coating layer sidewise of the bond (dashed line in figure 5.8(a)) to find the bond after embedding in the microtome images more easily. Additionally the paper strip was notched at the position of the bond.

The image of the cutting area in figure 5.8(b) shows that this does not give the desired results as the distance between the coated paper and the bond is even bigger than in the example in figure 5.7(b), as the fiber-fiber bond cannot be stretched during gluing. In addition sample preparation is much more tedious and more difficult in this case, so also this idea was not used.

The results of these four trials were compared and the third possibility (embedding the fiber-fiber bond together with woodfree coated paper) turned out to be the best solution. In pretests several samples were embedded like that and stitching and aligning worked stable in these trials. In less than 5% of all samples the bond was too far away from the coated paper, so that the microscope could not catch both, the bond and the coated paper. In all other cases half of the image was filled with the coated paper (see figure 5.7(b)), so that there was enough image structure to stitch and align the images. The movement of the bonded fibers through the images could be reproduced correctly.

(a) Scheme of sample preparation

(b) Corresponding picture of the cutting area
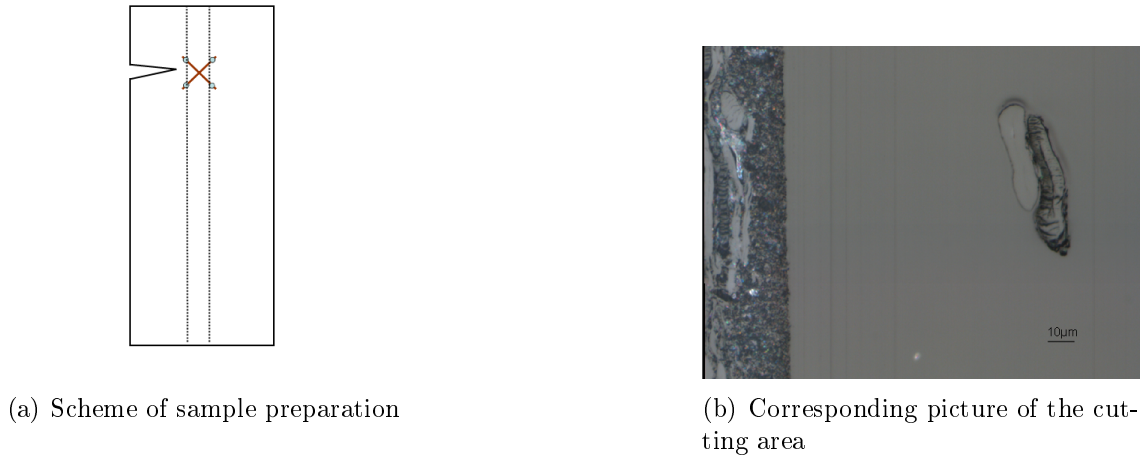
Fig. 5.8 Bond fixed directly on woodfree coated paper

5.5 Image analysis

For the measurement of bonded area the fibers in the microtome images are segmented by hand and a label image is created for every cut, as is also described in Paper I. In these label images, the region where there is no distance between the fibers is determined using image analysis. This yields a bonding line for every cut. The length of the line is measured and then multiplied with the cut thickness, yielding the bonded area. One has to notice that with this method only the optical bonded area is measured, as it is restricted to light microscopy with an optical resolution of $0.161 \mu m/Pixel$. Statements on actual chemical bonds cannot be made. The procedure of line length measurement is described in the following.

5.5.1 Line length measurement

The length of the bonding line is determined with an algorithm for line length measurement that considers the position of the pixels in the line towards each other. The possible arrangements of the pixels are demonstrated with two simple examples in figure 5.9. If the pixels are arranged in a straight line, the length can be calculated by simply multiplying the amount of pixels with the pixel size. In the case of shifted pixels, the amount of pixels has to be multiplied with the pixel size and with $\sqrt{2}$, so that the length of the diagonal is considered.

The algorithm for line length measurement that is used in this thesis will be described with the help of an exemplary part of a bonding line, as shown in figure 5.10. In this image the

(a) Straight pixels, scaled with 1   (b) Shifted pixels, scaled with $\sqrt{2}$
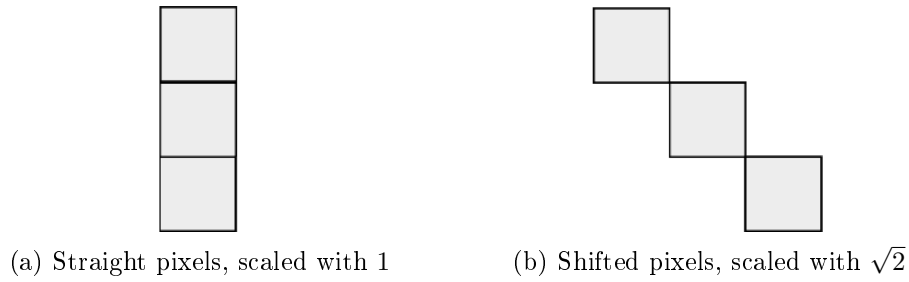
Fig. 5.9 Possible arrangements of pixels in the bonding line

focus is set on a 3x3 square, starting in the upper left corner of the image (marked light gray in figure 5.10).
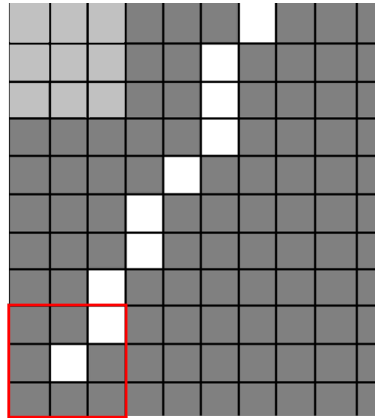
Fig. 5.10 Exemplary part of a bonding line

For the center of the focus the following three issues are examined:

1. Is the center part of the bonding line?

2. Does it have a neighbor that is part of the bonding line?

3. Where is that neighbor?

If the center is not part of the bonding line the position of the 3x3 square is moved one pixel, until the first question can be answered with "yes". In figure 5.10 the bonding line starts in the lower left corner of the image, this 3x3 square is framed red. The handling of the three questions listed above is demonstrated in figure 5.11 starting with this 3x3 square. In this example the first two questions are answered with "yes" (number 1. and 2. in figure 5.11). If the neighbor that is part of the bonding is located in one of the corners of the square, the length is scaled with $\sqrt{2}$, otherwise it is scaled with 1. If the center of the focus is part of

37

the bonding line, additionally the coordinates of the examined position are saved in a matrix (number 3. in figure 5.11). The neighbor of the examined pixel that is part of the bonding line is the new center of a 3x3 square (number 4. in figure 5.11). This is pursued for the entire bonding line. If the end of the line is reached, the rest of the image is searched for a new center of focus that is part of the bond. If there is a hole in the bond, the bonding line will be interrupted, so it has to be ensured, that no parts of the bonding line are left out. The procedure is continued for the entire picture, until the position of every pixel that is part of the bond is known and scaled either with 1 or with $\sqrt{2}$.
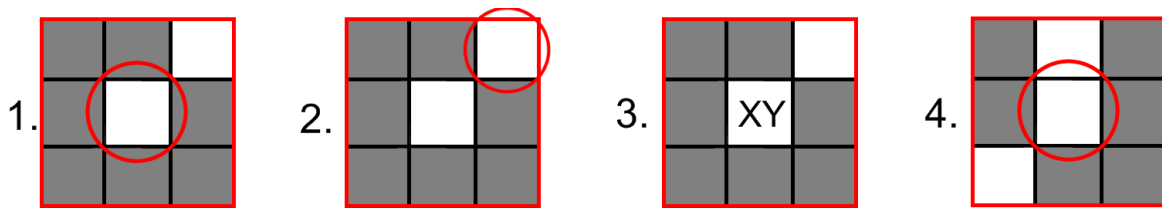
Fig. 5.11 Examining the focus of a $3x3$ square of the bonding line

5.5.2 Interpretation of image data

The bonded area is calculated by multiplying the length of all bonding lines with the cut thickness. A three-dimensional representation of the bonded area is obtained by plotting all bonding lines of one bond. Additionally several morphological parameters of the fibers and of the bond are measured image analytically from the cross sectional images. The fiber perimeter, fiber width, fiber cross sectional area, fiber collapse, fiber wall thickness, crossing angle and degree of bonding (holes in the bond and unbonded fiber edges) are measured using a method recently introduced by Kritzinger et al. [55].

With this data the influencing factors on the size of the bonded area are determined using multiple linear regression modeling. The model results can be found in Paper I.

5.6 Discussion of bonded area measurement with microtomy

5.6.1 Influence of the cut thickness on the accuracy of the method

The samples are cut with the microtome with a cut thickness of 3 μm. To find out how close the real shape of the bonded area could be measured and whether the accuracy of the microtome method could be enhanced, experiments with reduced cut thickness were

performed. Samples were cut with a cut thickness of 1 μm instead of 3 μm and bonded area was evaluated three times:

- With a cut thickness of 1 μm

- With a cut thickness of 2 μm

- With a cut thickness of 3 μm

A comparison of the results (size and shape of the bonded area) is shown in figure 5.12. There is only a difference of less than 0.5% in the results and the deviations with higher cut thickness go in both directions. So choosing a bigger cut thickness does not lead only to an over- or underestimation of the bonded area. This comparison showed that there is practically no gain in accuracy and that the higher evaluation time (threefold time for threefold number of images to be evaluated) does not pay off, so the cut thickness of 3 μm was kept for further experiments.

Cut thickness 1 µm
Bonded area: 2481 µm²

Cut thickness 2 µm
Bonded area: 2473 µm²

Cut thickness 3 µm
Bonded area: 2495 µm²
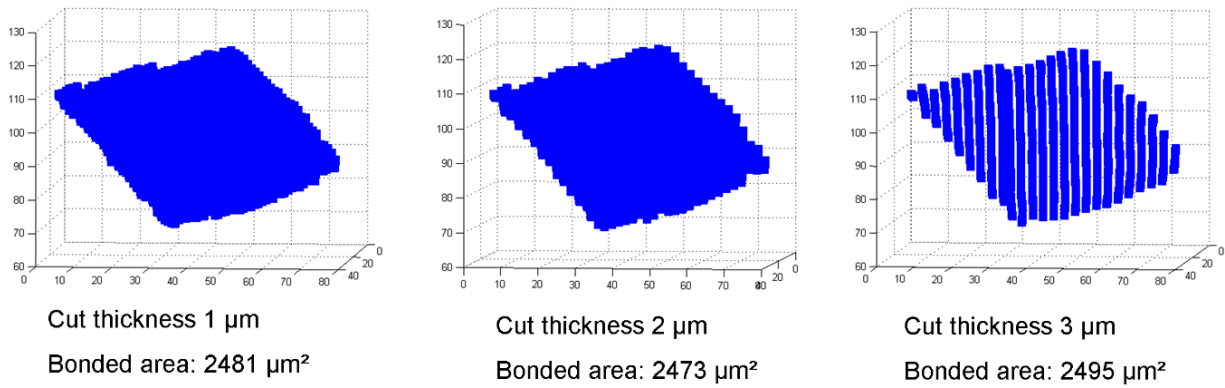
Fig. 5.12 Evaluating the influence of the cut thickness on the accuracy of the microtome method

5.6.2 Determination of the operator influence

Experiments were performed with the target to evaluate the operator influence on the result of bonded area measurement. Additionally the reproducibility of the segmentation of the fibers before bonded area measurement was to be tested when the operator stays the same. For three samples (sample 1, 2, 3) the fibers in the microtome images were segmented three times:

1. 2 x operator A (with more than one month time difference)

2. 1 x operator B

Figure 5.13 to figure 5.15 show the comparison of the three dimensional representation of the bonded area for all three determinations, the respective values for the bonded area are given in table 5.2.

Sample	Bonded area $[\mu m^2]$ Operator A (1)	Bonded area $[\mu m^2]$ Operator A (2)	Bonded area $[\mu m^2]$ Operator B
1	938	950	968
2	1186	1196	1236
3	1260	1273	1104

Tab. 5.2 Evaluation of the operator influence - comparison of the results for bonded area

For sample 1 and 2 the results are very similar in all three cases. Sample 3 showed a bit more complicated bonding morphology, because one of the bonded fibers was folded. Therefore it was sometimes difficult to distinguish between bonded and unbonded areas. This is the reason for the slight deviations in the shape of the bonded area in this case. But again generally the shapes show good agreement in all three cases.
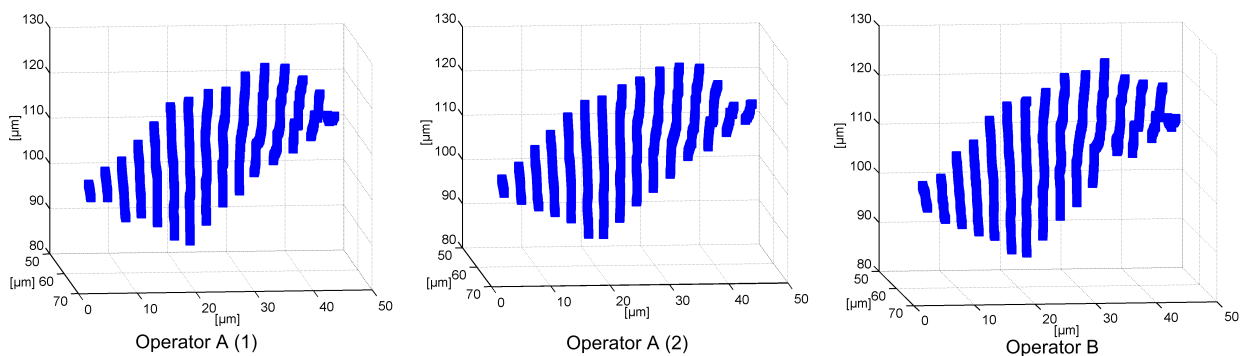
Fig. 5.13 Evaluation of the operator influence - sample 1
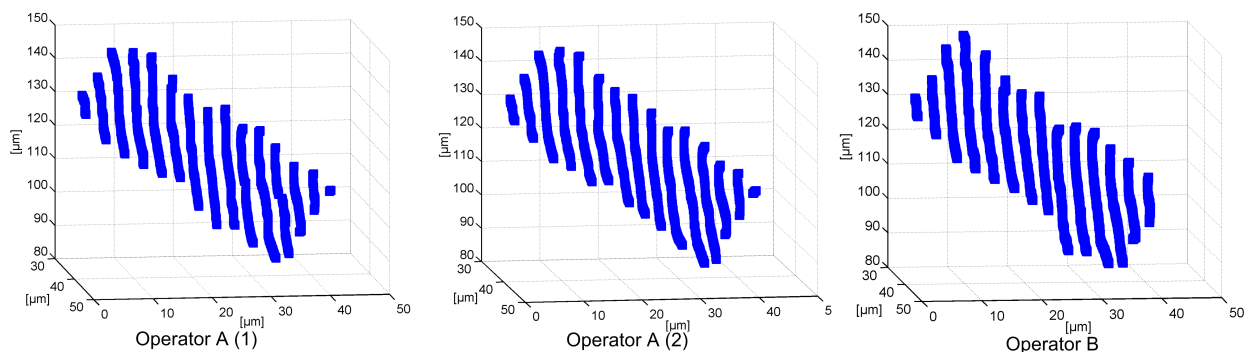
Fig. 5.14 Evaluation of the operator influence - sample 2
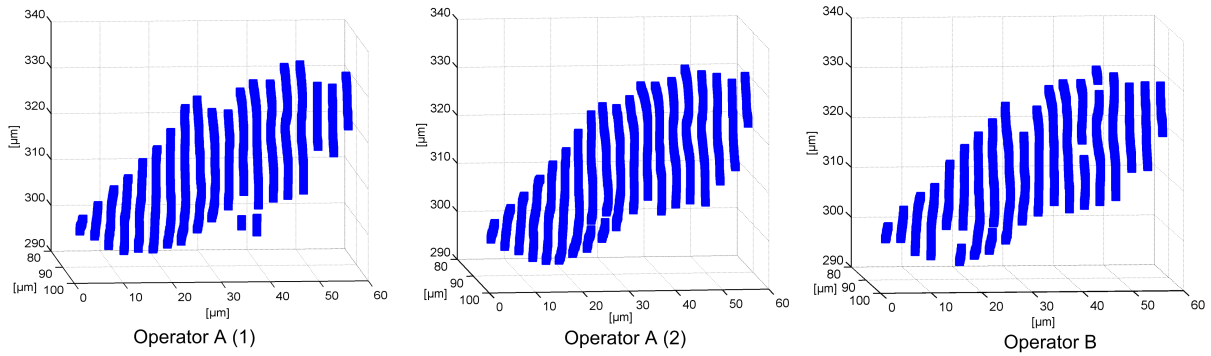
Fig. 5.15 Evaluation of the operator influence - sample 3

Comparing the results in figures 5.13, 5.14, 5.15 and table 5.2 and considering that there are several sources of errors in the method arising from the restriction to light microscopy and from the segmentation of the fibers by hand, it seems as if both accuracy and reproducibility of drawing the fibers by hand were sufficient. The values of bonded area in table 5.2 show that the variation is less than 5% in all cases for samples 1 and 2. For sample 3 the variations are approximately 10%.

The reproducibility of the overall method can only be tested with extreme high expenditure of time, as it is a destructive method and the microtome cutting cannot be repeated for one and the same sample. The only possibility would be to compare two large sets of identical samples, however this was not performed in the course of this thesis.

5.6.3 Discussion of the expenditure of time for bonded area measurement

The determination of one bonded area takes all in all about one day (including preparation of the fiber-fiber bond, embedding, cutting with the microtome, image analysis and evaluation of the images). Yet this does not mean that a person is occupied the entire time. It takes for instance one hour to dry the fiber-fiber bonds, where no presence is required. The same is true for the microtome cutting. As soon as the sample is clamped in the microtome and the required settings are made, the process of cutting is fully automatic. Also stitching and aligning only require some input parameters and work automatically after that. Solely the fiber segmentation in the microtome images is a time consuming process that is still done by hand. Depending on the number of cuts per bond the expenditure of time on average is two to three hours for each sample. An automated image analysis, where the fibers are tracked through the images is required to accelerate this procedure. Even though software for fiber tracking is available [56], it is not applicable at present. Investigating the influencing factors

on the size of the bonded area showed that unbonded areas (holes in the bond and unbonded fiber edges) have a big impact (see Paper I and chapter 8). This means that a high accuracy is required in fiber segmentation, especially in the border area of the bond, which is not achievable with automatic image analysis at the moment. However, for future application of the method some kind of automatic fiber segmentation will have to be developed to speed up the entire process.

5.7   Conclusions

Microtome serial sectioning seems to be a useful tool to investigate the bonded area as well as the morphology of the fiber cross sections and the bonding region. The method is able to measure the holes in the bond and overlapping but unbonded fiber regions. This combined measurement of fiber morphology and bonded area morphology thus contributes to a more comprehensive understanding of fiber-fiber bonding.

Adequate methods for sample preparation and measurement of the bonding line in the microtome images were developed and tested for reproducibility. A basis for the evaluation of other non-destructive reference methods is provided.

The major limitation of the method is the expenditure of time, as one fiber-fiber bonded area measurement takes approximately one day. Statements on how many bonds have to be analyzed to have a representative sample size are not possible at present. Kritzinger et al. [57] found that at least 250 individual fibers have to be analyzed with the serial sectioning method to obtain statistically meaningful results on fiber cross sectional properties. Measuring the bonded area of 250 fiber-fiber bonds is not possible within a reasonable time. Hence the method is not intended as a standard procedure for the investigation of a large number of samples. Rather it should help to evaluated faster and non-destructive reference methods.

Chapter 6

Polarized light microscopy for fiber-fiber bonded area measurement

6.1 Introduction

In the previous chapter a novel technique for fiber-fiber bonded area measurement based on microtome serial sectioning and image analysis was introduced. With this approach the optical bonded area can be measured with high accuracy and additional information on morphology of fibers and bonding region is obtained. However, it is a destructive method and therefore not applicable for specific bonding strength measurements. So a non-destructive reference method had to be found. Polarized light microscopy, as already introduced in chapter 4, was tried first, because it is easy to apply, no sample preparation is needed and all required laboratory equipment has already been available. The serial sectioning method was used to validate the results obtained with polarized light microscopy.

Polarized light microscopy was first introduced by Page [53]. He states that under polarized vertical illumination bonded areas are dark, while unbonded areas are bright. Fiber-fiber bonds in thin sheets were analyzed and to reduce unwanted reflected and scattered light 70 % of the fibers were dyed black using Chlorazol Black. Thus the bonds between the remaining undyed fibers became visible and bonds between one dyed and one undyed fiber showed exceptionally high contrast under the polarized light microscope. Page also found that the bonded area tends to be more clearly dark if two flat and ribbon shaped springwood fibers were analyzed [36].

A drawback of polarization microscopy seems to be that it works better for some types of bonds and less good for others. Mayhood et al. [43] investigated fiber-fiber bonds with polarized light microscopy. They found too, that the area in optical contact can be measured

more accurately if flat spring wood fibers are used. Schniewind et al. [26] state that polarized light microscopy was not generally applicable for their undyed bonds, but they do not discuss the problem or give any explanation. Bonds between a fiber and a shive were analyzed with polarized light microscopy by McIntosch [40]. An exemplary result given in this paper shows that bonded area is clearly brighter than the fiber or the shive, thus in the opposite way than suggested by Page [53]. However, the author does not discuss this further or give theoretical considerations about the applicability of this method for fiber-shive bonds. Mohlin [41] tried to measure the bonded area between a fiber and a strip of cellophane with polarized light microscopy, but the method turned out to be unsuitable for this purpose. The author suggests that the low degree of crystallinity of the cellophane might be the reason for this. Stratton [22] investigated fiber-fiber bonds between one dyed and one undyed fiber, which he found to be unproblematic.

The results given in the literature correspond with our first experimental observations. In some cases bonded area showed clearly dark, while in other cases no difference between bonded and unbonded areas could be seen. So fiber-fiber bonds were first analyzed with the polarized light microscope and then cut with the microtome to gain additional information on the fiber cross sectional morphology in the bonding region. Additionally a physical model was applied to understand the theoretical background of the method. This combination allowed better understanding and correct interpretation of the results obtained with polarized light microscopy.

6.2 Investigating the applicability of polarized light microscopy for fiber-fiber bonded area measurement

Measuring the bonded area of fiber-fiber bonds with polarized light microscopy turned out to be difficult in some cases, as bonded area did not always look dark. This is why we tried to clarify the physical mechanisms of bonded area measurement with polarized light microscopy. Although literature suggests that the method works better for bonds between one dyed and one undyed fiber, we first studied undyed bonds to investigate the fundamental theoretical background without any changes in reflection and transmission due to the dye. Fiber-fiber bonds were first analyzed with the polarized light microscope and then embedded and cut with the microtome. In this way the cross section of the fiber-fiber bond could be inspected and the result of polarized light microscopy could be related to the fibers' cross sectional morphology. This comparison explains why bonded area does not always show dark under polarized light.

The results of this investigation are discussed in Paper II. In order to understand the mechanism of polarized light microscopy we applied a physical model that simulates the path of light through the fibers and the microscope. This model is described in Paper IV. The experiments combined with the physical model provide a comprehensive interpretation of the polarized light microscopy results. The most important findings for undyed fiber-fiber bonds can be summarized as follows:

- If two completely collapsed springwood fibers, lying flat one upon the other are bonded, the bond resembles a system of plane parallel plates with equal thickness and polarized light microscopy yields correct results, bonded area appears dark.

- Model calculations showed that the fiber wall thickness of the bonded fibers has to be equal or at a certain ratio, as the intensity of returned reflection depends on the fiber wall thickness configuration. Experiments confirmed that the bonded area does not always look dark if fibers with unequal fiber wall thickness are bonded.

- Folds in the bonding region cause additional reflections and phase shifts of the light, the fibers no longer resemble a system of plane parallel plates. If one or both of the bonded fibers are folded, in most cases bonded area does not appear dark.

- Model calculations as well as experimental results showed that unbonded but parallel fibers show a dark crossing region under the polarized light microscope. This leads to incorrect interpretation of unbonded crossed fibers as bonded and to overestimation of bonded area if the fiber edges are not completely bonded.

The combination of Paper II and Paper IV offers a comprehensive interpretation of polarized light microscopy and explains its shortcomings for the analysis of undyed fiber-fiber bonds.

To analyze bonds between one dyed and one undyed fiber seems to be a more promising method. This has already been found experimentally by Page [53] and Stratton [22]. Still, they do not give any explanation for this improved mechanism. Based on these results we also investigated fiber-fiber bonds between one dyed and one undyed fiber with polarized light microscopy. Again the bonds were additionally cut with the microtome to get information on the fiber cross sectional morphology and some of the results were computed with the optical model. In Paper III an explanation is provided why polarized light microscopy works well with bonds between one dyed and one undyed fiber. Bonded area was measured with polarized light microscopy and with the microtome serial sectioning method. The results were compared and showed good agreement.

6.3 Dyeing of the fibers

Page [53] dyed the fibers with Chlorazol Black, the same dye was used in this study. Chlorazol Black is a dye powder that is dissolvable in water and in ethanol. Since Page does not specify which solvent was used for the dye, new experiments were performed to find out which was the most suitable solvent. For lack of further indications in the literature also an appropriate procedure for dyeing of the fibers had to be developed. To obtain fiber-fiber bonds between one dyed and one undyed fiber 50 % of the fibers were dyed and then the bonds were prepared as described in Paper I.

Characterization of the dye   Chlorazol Black is an acid dye and is also called direct black. Its chemical structure[1] is shown in figure 6.1. It is mainly applied as tissue stain and can be dissolved in de-ionized water and in ethanol.
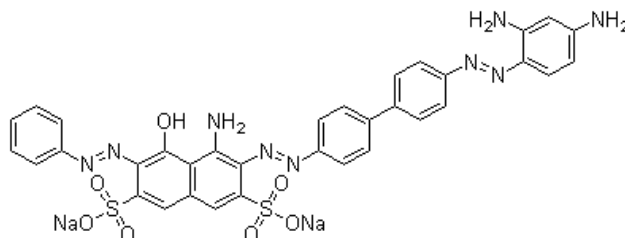
Fig. 6.1 Chemical structure of Chlorazol Black

Dyeing procedure   Independent of the solvent of the dye, the same dyeing procedure was kept for all experiments. 1 g of dye powder was dissolved in 100 ml solvent and stirred at room temperature with a magnetic stirrer for 30 minutes. In first experiments dry pulp was dyed and the dye did not reach fibers that were bundled, therefore dyeing was incomplete. To achieve sufficient dyeing the pulp was allowed to swell in water for at least four hours before dyeing. Then it was dewatered to a dry solids content of approximately 20 % and totally submersed in the dye. It was allowed to rest like this for one hour and stirred every now and then. After one hour the excessive dye was washed off the pulp over a vacuum filter. This procedure turned out to be highly time consuming because particularly in the beginning of the washing the filter was closed very quickly by undissolved dye particles. The washing was repeated until the the filtrate was absolutely clear.
This dyeing procedure showed satisfactory results and was kept for further experiments.

---

[1]Available from: `http://www.chemblink.com/products/1937-37-7.htm`, downloaded on December, 6th 2009

Solvent of the dye: de-ionized water In the first experiments de-ionized water was used as a solvent for the dye, because in this case the smallest influence on bonding strength properties was expected. The dye adsorbed well to the fibers, however, when the dyed fibers were suspended in water before bond formation the dye re-dissolved from the fibers and the suspension turned cloudy gray. Also sheets were formed from this pulp, they were only gray. The analysis of bonds between one dyed and one undyed fiber under the polarized light microscope showed that it was not always possible to distinguish the fibers. Figure 6.2 shows an exemplary result of polarized light microscopy. It is not possible to tell which fiber is dyed.
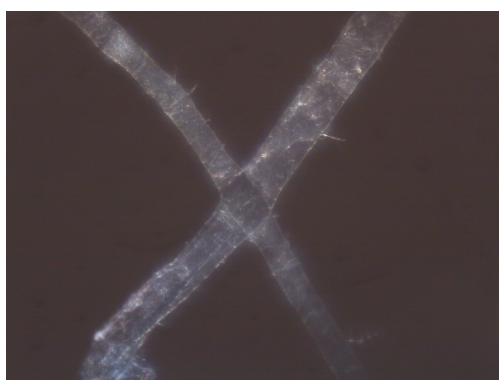
Fig. 6.2 Fiber-fiber bond under the polarized light microscope - one fiber dyed with Chlorazol Black dissolved in de-ionized water

A possible explanation for this behavior of the dyed fibers in suspension might be the poor solubility of Chlorazol Black in de-ionized water. Partly undissolved dye particles cannot adhere well to the fiber surface and redissolve when the pulp is suspended in water.

Solvent of the dye: ethanol The solubility of Chlorazol Black in ethanol (96 %) is higher than in de-ionized water, so dyeing of the fibers was more successful in this case. When the dyed pulp was suspended in water, the dye did not redissolve and the water remained clear. The sheets formed from this pulp were completely black. Figure 6.3 shows a comparison of the sheet color depending on the solvent of the dye. The sheet at the very bottom is undyed, the one in the middle was dyed with Chlorazol Black dissolved in de-ionized water, as mentioned above it is only gray. And the sheet on top was dyed with Chlorazol Black dissolved in ethanol, it is completely dark. The according brightness values for all three sheets are given in table 6.1.

As dyeing the fibers with Chlorazol Black that had been dissolved in ethanol yielded satisfactory results this procedure was kept for all further investigations.

Brightness undyed sheet	Brightness dyed sheet (solvent de-ionized water)	Brightness dyed sheet (solvent ethanol)
$28, 93$	$13, 5$	$4, 64$

Tab. 6.1 Comparison of sheet brightness before and after dyeing with Chlorazol Black

Fig. 6.3 Comparison of sheet color depending on the solvent of Chlorazol Black - undyed, solvent de-ionized water and solvent ethanol

6.3.1 Influence of dyeing on paper strength

Page has already investigated the influence of dyeing on paper strength and he states that dyeing of the fibers slightly changes paper strength, but he does not make any indications on the direction and the range of the change. It is also unknown which solvent was used for the Chlorazol Black by Page. This is why new experiments had to be performed to quantify the influence of dyeing on paper strength.

Several influencing factors may affect the strength properties of sheets prepared from dyed fibers:

- The surface chemistry of the fibers might be altered, which could have an influence on the bonding ability.

- After dyeing the pulp is washed several times, fines may be washed out.

- The swelling behavior of the fibers might be affected by the ethanol.

Predicting the respective influence is not possible, so hand sheets with basis weight between $20 \ g/m^2$ and $150 \ g/m^2$ were prepared from dyed and undyed unbeaten pulp. The tensile strength and the burst strength of the sheets were measured. Additionally the pH-value and the conductivity of the suspension were measured to evaluate changes in ion concentrations.

A possible loss of fines was controlled by characterizing the dewatering behavior with freeness measurements.

Suspension   A comparison of the suspension parameters of dyed and undyed unbeaten pulp is shown in table 6.2. The decrease in pH-value and the increase in conductivity after dyeing indicate that the dye might be cationic. Additional ions in the suspension would explain these changes of the suspension.

The comparison of freeness before and after dyeing shows that no fines are washed away when the pulp is washed after dyeing. If there is a difference in freeness value of less than $1°SR$ no statement about a significant change in dewatering ability can be made.

	Undyed pulp	Dyed pulp
pH	$8, 2$	$7, 3$
Conductivity [μS/cm]	432	482
Freeness [°SR]	$12, 1$	$12, 8$

Tab. 6.2   Comparison of the suspension parameters before and after dyeing

Hand sheets   Figure 6.4 shows a comparison of tensile index of dyed and undyed sheets. Tensile index after dyeing is slightly higher over the entire range of basis weight. Still, the overlapping confidence intervals indicate that the difference is statistically not significant on a 95% confidence level.
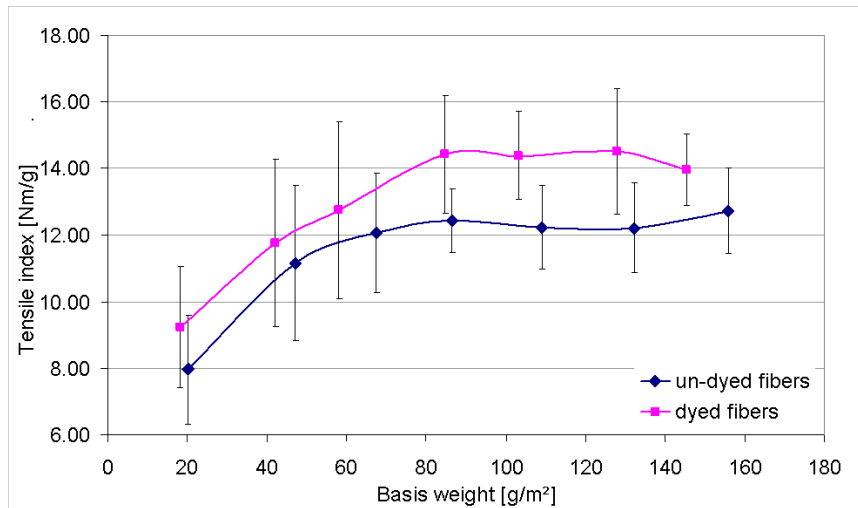
Fig. 6.4   Comparison of tensile index of dyed and undyed sheets

The results of burst strength measurements for the dyed and undyed sheets are shown in figure 6.5. Up to a basis weight of approximately 90 g/m^2 the influence of the testing mem-

brane is bigger than the influence of the sheet, so these measurements cannot be evaluated. At higher basis weight there is again a small difference between dyed and undyed pulp - dyed sheets show slightly higher strength - but this difference is again statistically not significant on a 95% confidence level, which shows by the overlapping confidence intervals.
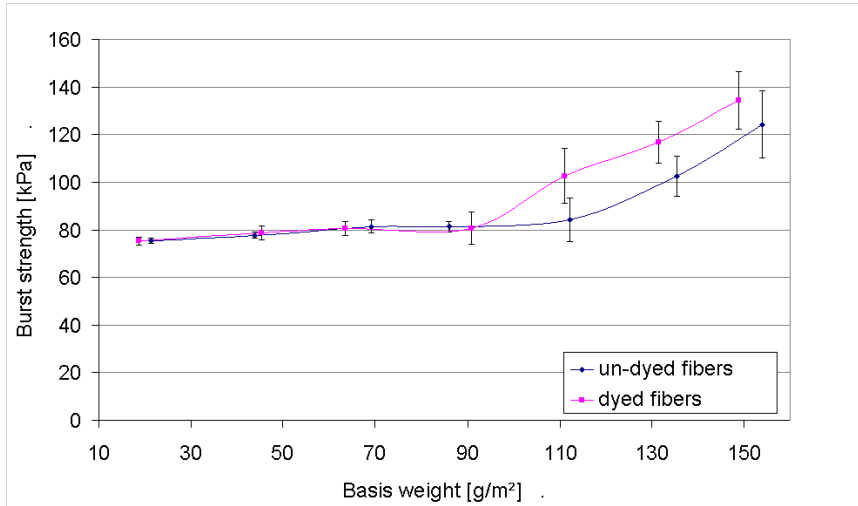
Fig. 6.5 Comparison of burst strength of dyed and undyed sheets

Summing up it can be said that dyeing the fibers with Chlorazol Black dissolved in ethanol works well for unbeaten pulp. No fines are lost during dyeing and washing the pulp. The paper strength was slightly higher after dyeing, however, the difference is statistically not significant on a 95 % confidence level.

The experiments described above were performed only with unrefined pulp and will have to be repeated with refined pulp. In this case the pulp contains more fines that might be lost during washing the pulp.

6.3.2 Proving the applicability of polarized light microscopy for bonds between a dyed and an undyed fiber

Fiber-fiber bonds between one dyed and one undyed fiber were prepared and analyzed with the polarized light microscope. These fiber-fiber bonds were also cut with the microtome to get additional information from cross sectional images. Some of the results were additionally computed with the mathematical model. Paper III explains why fiber-fiber bonded area measurement works better in the case of dyed fibers. In contrast to undyed fiber-fiber bonds now in most cases bonded area could be identified correctly. The improvements that can be achieved with dyeing one of the bonded fibers are:

- The fiber wall thickness does no longer have an influence on the visibility of dark bonded area. So bonds with all fiber wall thickness configurations can be analyzed with polarized light microscopy.

- The problems with folded fibers can be strongly reduced. If the dyed fiber is folded, bonded area still can be measured with polarized light microscopy, as the reflections at additional interfaces that are caused by the fold are almost completely absorbed by the dye. However, if the undyed fiber is folded, the dark bonded area is not always well defined.

- Unbonded fiber edges and holes in the bond are only in some cases problematic. The reason why parallel but unbonded fibers can only sometimes be identified is still under study and could not be completely clarified in this thesis.

6.4 Results

Bonded area of individual fiber-fiber bonds between one dyed and one undyed fiber was measured with polarized light microscopy and with the microtome method. The size and the shape of the bonded area were compared. This comparison was performed for the following pulps:

- Kraft pulp from spruce and pine wood, unbleached and unrefined

- Kraft pulp from spruce and pine wood, unbleached and beaten with 9000 revolutions in the PFI mill

- Mechanical pulp (type of wood unknown), unbleached and unrefined

6.4.1 Comparison of bonded area for unbleached and unbeaten kraft pulp

Bonded area of 73 fiber-fiber bonds was measured with polarized light microscopy and with the serial sectioning method, the results are compared in figure 6.6. The diagonal indicates equal values. In general the values show quite good agreement, although bonded area is overestimated more often by polarized light microscopy. On average the values measured with polarized light microscopy were 12.5 % higher.

Most of the deviations can be explained with the help of the microtome images. An exemplary comparison of polarized light microscopy and microtomy for overestimation and for
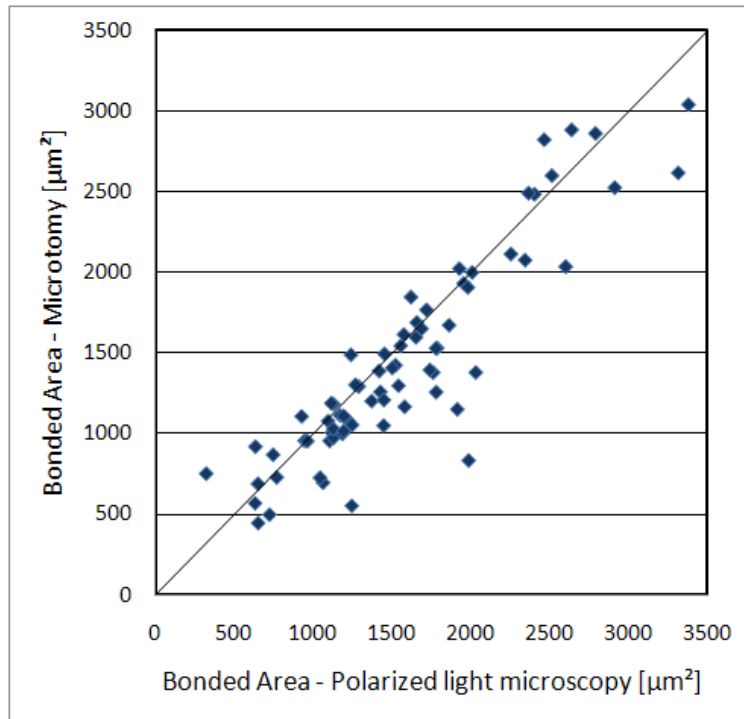
Fig. 6.6 Comparison of bonded area measured with polarized light microscopy and with microtomy - unbleached and unbeaten kraft pulp

underestimation of bonded area is given in Paper III. Also a multiple linear regression model is given, that shows that 60 % of the deviations can be explained with incomplete bonding, i.e. holes in the bond and unbonded fiber edges. This indicates that despite dyeing of one fiber, unbonded fibers cannot always be identified correctly with polarized light microscopy and lead to overestimation of bonded area.

6.4.2 Comparison of bonded area for unbleached kraft pulp - beaten with 9000 rev. PFI

After proving the applicability of polarized light microscopy for unbeaten pulp the method was also tested for beaten pulp. A highly laboratory beaten pulp was used, as in this case the biggest differences to unbeaten pulp were expected. Again bonds between one dyed and one undyed fiber were analyzed first with the polarized light microscope and then with the microtome. Size and shape of bonded area of 68 fiber-fiber bonds were compared. In figure 6.7 bonded area measured with polarized light microscopy is plotted plotted versus bonded area measured with the microtome. The diagonal indicates equal values. In contrast to the unbeaten case, now bonded area is underestimated by polarized light microscopy in

most cases (on average by 15.9 %). The respective mean values and standard deviations are given in table 6.3.
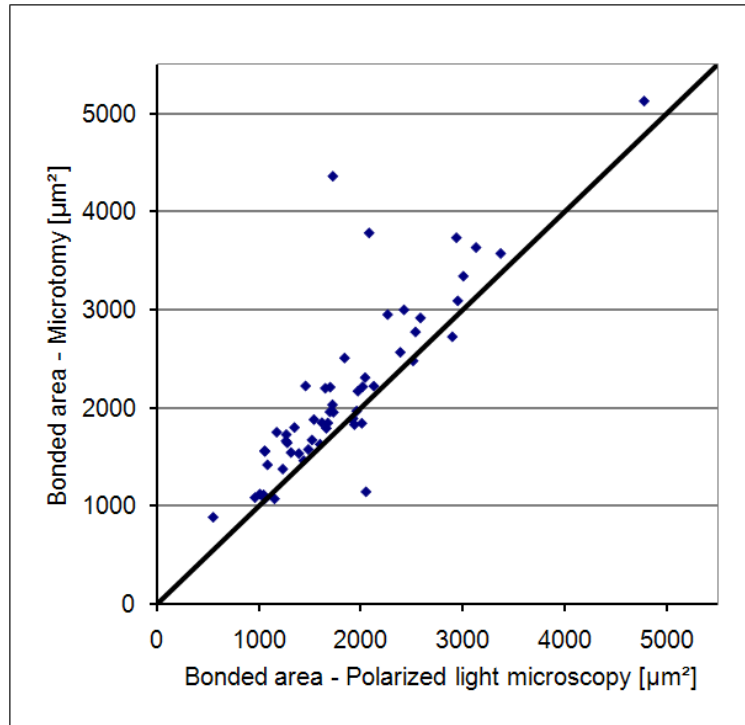
Fig. 6.7 Comparison of bonded area measured with polarized light microscopy and with microtomy - unbleached kraft pulp beaten with 9000 rev. PFI

	Mean bonded area $[\mu m^2]$	Standard deviation $[\mu m^2]$
Microtomy	2146	870
Polarized light microscopy	1847	734

Tab. 6.3 Comparison of bonded area measured with polarized light microscopy and with microtomy - unbleached kraft pulp beaten with 9000 rev. PFI

To explain the deviations between the measurement results again multiple linear regression modeling was performed. The morphological parameters that are measured in the microtome images were taken as explaining variables: fiber cross sectional area, fiber perimeter, fiber width, fiber wall thickness, fiber collapse, incomplete bonding (unbonded fiber edges and holes in the bond) and crossing angle. The deviation between the measurement results was the response variable. The mathematical model showed that not any of the morphological parameters has a statistically significant influence on the size of bonded area on a 95 % confidence level.

It seems as if most of the deviations between the measurement results can be explained only

with the fibrils on the beaten pulp fiber surfaces, which cannot be reproduced with any of the applied measurement methods. The fibrils cause additional reflections, so that the polarized light microscope images are brighter in total. In the crossing region these bright reflections are evaluated as unbonded fiber edges and holes in the bond. Two exemplary comparisons of a polarized light microscope image with the fiber-fiber bond cross section are given in figure 6.8 and figure 6.9. In the first example (figure 6.8) the center of the bond appears brighter under the polarized light microscope, suggesting that the fibers are unbonded in this area. But the microtome image on the right shows that the fibers are optically bonded over the entire length. This can as well be observed in figure 6.9. In this example also the fiber edges appear as unbonded, however, the microtome image on the right shows that the fibers are again optically bonded over the entire length. So these two examples seem to confirm the assumption that the additional reflections caused by the fibrils are the origin of the underestimation of bonded area in this case.
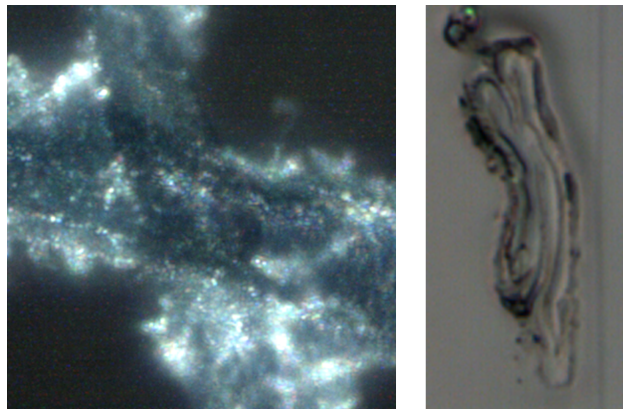
Fig. 6.8 Comparison of polarized light microscopy and microtomy image for beaten pulp (1)

The development of the bonded area and of some interesting morphological parameters with refining was investigated with the serial sectioning method, the results are given in chapter 8. The influence of dyeing on paper strength still has to be evaluated for this highly beaten pulp.

6.4.3 Investigating the applicability of polarized light microscopy for mechanical pulp

All experiments that have been described so far were performed with an unbleached kraft pulp that was a mixture of spruce and pine wood. The results of polarized light microscopy seem to depend a lot on the fiber morphology, so it was unclear whether this method can
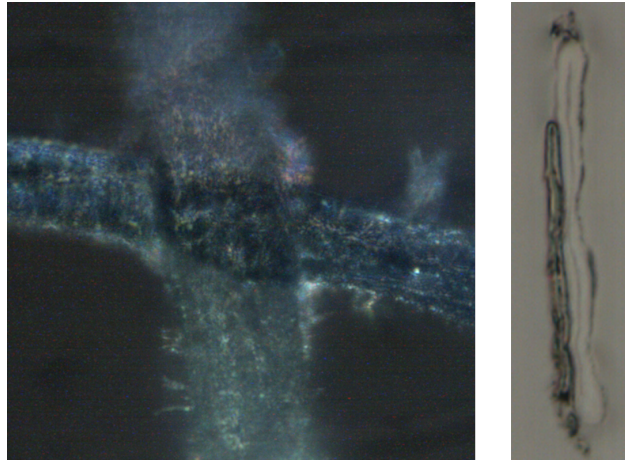
Fig. 6.9 Comparison of polarized light microscopy and microtomy image for beaten pulp (2)

also be applied for fiber-fiber bonds between two mechanical pulp fibers.

Fiber-fiber bonds were prepared from mechanical pulp and analyzed with the polarized light microscope. Some of the bonds were also cut with the microtome to gain additional information from the cross sectional images. In this case only a qualitative comparison of the methods was made, comparative bonded area measurements were not performed.

Preparation of fiber-fiber bonds Like in the case of kraft pulp 50 % of the fibers were dyed with Chlorazol Black. Then the fiber-fiber bonds between one dyed and one undyed fiber were prepared as it is described in Paper I. The handling of these bonds turned out to be more tedious and difficult than with kraft pulp, because the bonds were much weaker and broke easily during the preparation procedure. Fixing the fiber-fiber bonds on the strip of paper across the hole also was difficult in many cases, as the mechanical pulp fibers were much shorter than the kraft pulp fibers.

Polarized light microscopy Each bond was imaged in eight different rotary positions from both sides. Only in about one third of the samples the bonded area appeared dark. In all other cases no real difference between bonded and unbonded fibers was visible. To find an explanation why dark bonded area was observable only in a few cases, some bonds were cut with the microtome.

Microtomy of fiber-fiber bonds The microtome images provide additional information on fiber-fiber bond cross sections and explain why the effect of dark bonded area is not always visible with the polarized light microscope. This microtome analysis showed that as long as the fibers are undamaged and show regular cross sections, the bonded area looks

dark under the polarized light microscope. However, it seems as if a considerable number of fibers was damaged during mechanical pulping. These damaged fibers no longer show the typical cross sections that are well known, but they show various structures and shapes. It has already been demonstrated in Paper II that the bonded fibers have to resemble a system of plane parallel plates to show dark bonded area. This is definitely not the case if damaged mechanical pulp fibers are analyzed.

Measuring the bonded area of pulp that had been refined with 9000 revolutions in the PFI mill already showed that the fibrils protruding from the fiber surface cause additional reflections that are evaluated as unbonded fibers. This effect seems to be even intensified in the case of strongly damaged mechanical pulp fibers so that bonded area in many cases does not appear dark at all.

Conclusions   These experiments lead to the assumption that the applicability of polarized light microscopy for mechanical pulp fibers is only limited. The process of mechanical pulping seems to damage the fibers too much, so that most bonds no longer resemble a system of plane parallel plates, which is the main precondition for measuring the fiber-fiber bonded area with polarized light microscopy. Only approximately one third of the analyzed bonds showed dark bonded area.

6.5   Conclusions

The combination of polarized light microscopy with microtome serial sectioning and with an optical model that describes the behavior of fiber-fiber bonds under polarized vertical illumination led to a fundamental understanding of this non-destructive method for fiber-fiber bonded area measurement. Comparison of shape and size of bonded area measured with the respective methods showed that bonded area is overestimated with polarized light microscopy in the case of unrefined pulp, while it is underestimated if highly beaten pulp is used.

Provided that this over- and underestimation of bonded area is considered and that the number of analyzed fiber-fiber bonds is high enough, polarized light microscopy can be used as a basis for specific bonding strength measurement.

Chapter 7

Measuring the fiber-fiber bonded area with confocal laser scanning microscopy (CLSM)

7.1 Introduction

Confocal laser scanning microscopy (CLSM) is an optical sectioning method that provides information on the three-dimensional structure of a specimen. It is an easy and non-destructive analogue to the microtome serial sectioning method described in chapter 5. The applicability of the CLSM as a non-destructive measure of the fiber-fiber bonded area was evaluated.

The confocal laser scanning microscope combines the high resolution of light microscopy in the xy-plane with a comparable high resolution in the z-direction. Its principle is illustrated in figure 7.1. A high light intensity is required, so a laser beam is used as source of light. This beam is focused on a small circular aperture (A_1), reflected at a beam splitter (BS) and focused by the objective lens (L_2) on the plane $z = z_0$ in the specimen of interest. The light that is reflected at this plane is collected by the objective and imaged through the beam splitter on the aperture A_2. Behind the aperture A_2 there is a detector. Only light that is reflected from the plane $z = z_0$ is focused on the aperture A_2. Light reflected from other planes of the sample reaches the detector with almost zero intensity. If the z-position of the specimen (here marked as object) is altered, individual planes can be detected selectively one after the other. [58]

A special application of CLSM is fluorescence microscopy, where the laser excites fluorescent dyes and higher spatial resolution can be achieved. The acquired two-dimensional images

can be stacked to a three-dimensional reconstruction of the object.
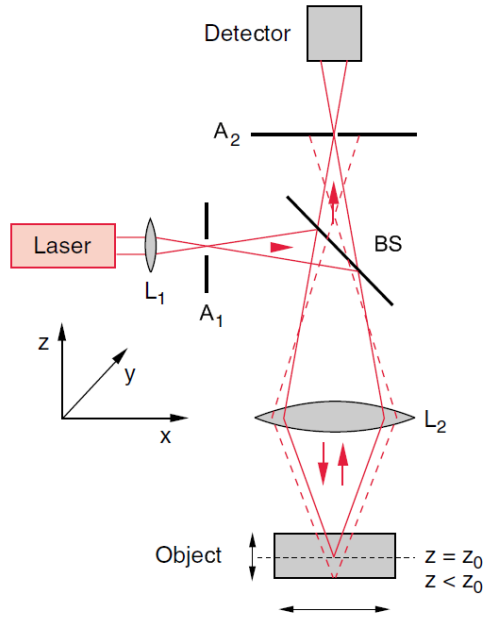
Fig. 7.1 Principle of confocal laser scanning microscopy [58]

The specimen can be scanned either in the xy-plane or in the xz-plane, as figure 7.2 shows. In the case of xy-scanning the microscope stage has to be moved vertically after every scan to obtain a series of images through the sample. Cross sectional views of the sample are obtained with xz-scans. [59]
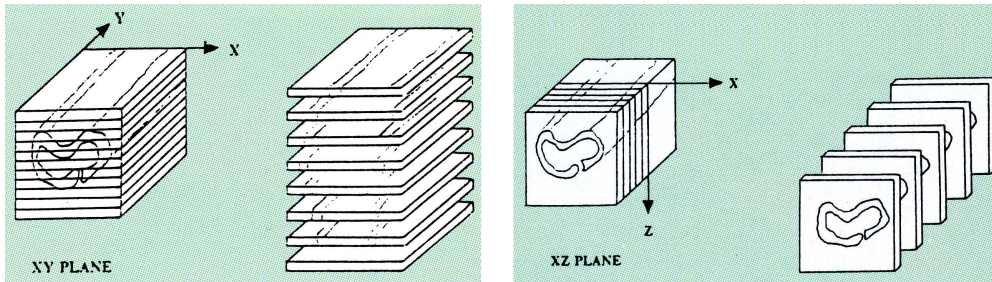
Fig. 7.2 Optical sectioning in the xy-plane or in the xz-plane [59]

For paper and fiber analysis both scanning methods have already been used. On the one hand the research focused on fiber characterization. Transverse fiber dimensions like fiber cross sectional area, fiber wall thickness, fiber collapse and lumen area were examined in [51], [60], [59], [61], [62], [63] and [64]. Jang et al. [63] simultaneously measured the fibril angle and related these results to the collapsibility of the fibers.

On the other hand the focus was set on fiber distribution in sheets, including fiber orientation, two-sidedness of a sheet, fines distribution, surface roughness, surface topography and porous sheet structure [59], [65], [66], [67] and [64].

Jang et al. [61] showed the validity of the CLSM results by comparing them with results obtained from conventional image analysis and surface profilometry. The same was demonstrated by He et al. [64], who compared the fiber dimensions measured in CLSM images with those measured on freely dried fibers on glass slides.

Horvath et al. [68] investigated the adsorption of polyelectrolytes to pulp fibers using confocal laser scanning microscopy. The polymer was labeled with a fluorescent dye (Sulforhodamine B), so the penetration into the fiber wall could be followed in the fiber cross sectional images.

This literature review shows that confocal laser scanning microscopy has already been successfully used for fiber characterization. In most cases the autofluorescence of the pulp fibers was enhanced by dyeing the fibers with fluorescent dyes, like for example Acridine Orange. However, no results have been found in the literature concerning the investigation of fiber-fiber interfaces with the CLSM.

7.2 Application of CLSM for fiber-fiber bonded area measurement

Fiber-fiber bonds were imaged with the Leica TCS 4d confocal microscope at the Institute of Molecular Biosciences (University of Graz). Figure 7.3 shows three exemplary fiber-fiber bond cross sections of unbleached and undyed kraft pulp fibers imaged with the CLSM. In the leftmost image the border of the bond can be seen, the fibers just start touching one another. The middle image shows that the fibers are in contact over about one third of their width, while they seem to be bonded over the entire width in the rightmost image. These bond cross sections show that the fibers cannot be distinguished, as both have the same autofluorescence. The interface between the fibers is not visible.
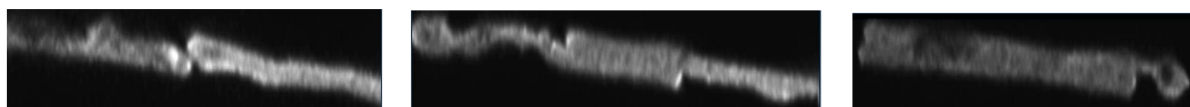
Fig. 7.3 Fiber-fiber bond cross sections imaged with the CLSM - undyed fibers

So this preliminary investigation demonstrated that in order to visualize the fiber-fiber interface the bonded fibers have to be dyed with two different fluorescent dyes. Finding suitable

dyes and development of a dyeing procedure will be covered in the following two sections. First measurement results will be shown in chapter 7.2.3.

7.2.1 Selection of fluorescent dyes

Before CLSM measurements can be performed each of the bonded fibers has to be dyed with another fluorescent dye, so that the fibers can be distinguished and the bonding line can be determined. For selection of suitable dyes the following requirements were considered:

- The dyeing of at least one of the bonded fibers should be visible with the naked eye, also at natural light.

- The dyed fibers have to be discriminable from each other, under natural light and under the CLSM.

- The dye has to be able to penetrate into the fiber wall, so that the entire cross section of the fiber is visible under the CLSM and not only the fiber surface.

According to the literature Acridine Orange and Rhodamine B have already been used for CLSM investigations of pulp fibers (see e.g. [68], [60]). So these two dyes were chosen for first experiments.

Acridine Orange   The orange dye is soluble in water and ethanol and shows green fluorescence. It is cell-permeable and is usually applied to distinguish between DNA and RNA, as it shows different emission maxima in the respective cases. Its chemical structure[1] and the fluorescence spectrum[2] are shown in figure 7.4 and figure 7.5, respectively. For this work the dye powder was dissolved in de-ionized water.
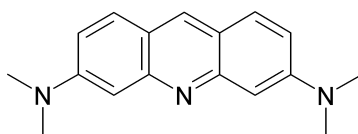
Fig. 7.4   Chemical structure of Acridine Orange

---

[1]Available from: `http://de.wikipedia.org/wiki/Datei:Acridine_Orange.png`, downloaded on December, 6th 2009

[2]Available from: `http://omlc.ogi.edu/spectra/PhotochemCAD/html/acridineorange.html`, downloaded on December, 6th 2009
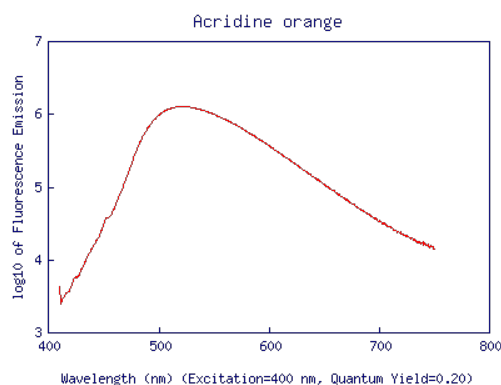
Fig. 7.5 Fluorescence spectrum of Acridine Orange

Rhodamine B The green dye powder turns pink when it is dissolved and shows red fluorescence. Figure 7.6 shows the chemical structure[3] of Rhodamine B, figure 7.7 shows the according fluorescence spectrum[4]. Amongst others it is applied in the paper and textile industry as colorant, but also in cell biology as a molecular marker. It is dissolvable in de-ionized water and in ethanol, both possibilities were applied in this work.
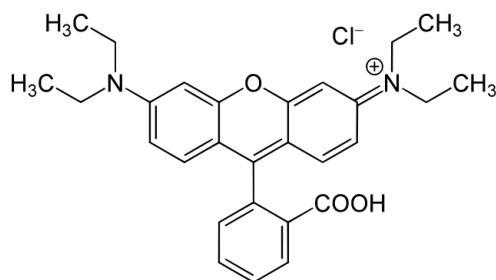
Fig. 7.6 Chemical structure of Rhodamine B

Optical brightening agents Another approach was to treat fibers that had been dyed with Chlorazol Black, as needed for polarized light microscopy (see chapter 6), with optical brightening agents. Chlorazol Black is not fluorescent, but all other requirements listed above are met. So fluorescence was added with two different optical brightening agents (Leukophor[5] and Tinopal[6]). This combination would allow measuring the bonded area with polarized light microscopy, CLSM and with the microtome, giving a comprehensive comparison of the methods.

---

[3] Available from: `http://de.wikipedia.org/wiki/Rhodamine`, downloaded on December, 6th 2009

[4] Available from: `http://omlc.ogi.edu/spectra/PhotochemCAD/html/rhodamineB.html`, downloaded on December, 6th 2009

[5] `http://www.clariant.com`

[6] `http://cibasc.com`
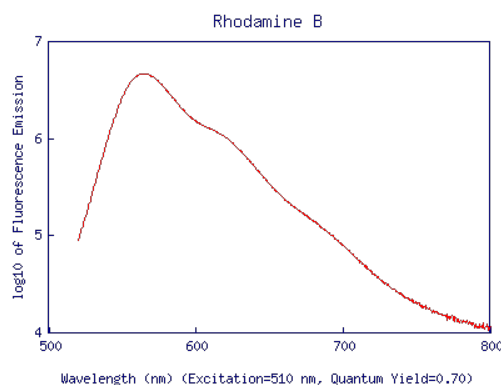
Fig. 7.7 Fluorescence spectrum of Rhodamine B

Optical brightening agents are fluorescent substances that are applied in the paper industry to enhance the brightness of the paper. They absorb light in the invisible ultraviolet spectrum (290 nm to 400 nm) and emit most of the absorbed energy in the visible range (between 400 nm and 480 nm). By that the emission can be raised above 100% and the paper appears brighter under UV-containing light.

7.2.2   Development of a dyeing procedure

Several different fluorescent dyes and optical brightening agents were used in the course of this work, independent of the dye or the optical brightening agent the same dyeing procedure was kept for all experiments.

If necessary the dye powder was dissolved in a suitable solvent (de-ionized water or ethanol) using a concentration as recommended by the manufacturer. The solution was stirred under ambient conditions with a magnetic stirrer for 15 minutes until the dye powder was completely dissolved. Before dyeing the pulp was allowed to swell in water for 4 hours. Then it was dewatered to a dry solid content of approximately 20 % and completely submersed in the dye or the optical brightening agent. The pulp remained like that for at least 30 minutes and was stirred several times until no undyed fiber bundles were visible. After that the pulp was washed several times using a vacuum filter until the filtrate was absolutely clear. In the case of the colorless optical brightening agents the filtrate is clear right from the beginning, so the pulp was washed in approximately 30 cycles.

For applying optical brightening agents on dyed fibers, the fibers were first dyed with Chlorazol Black, as described in chapter 6.3. Then the wet fibers were covered with the two optical brightening agents respectively and allowed to rest for 30 seconds, 10 minutes or 30 minutes. Ater 30 seconds, 10 minutes or 30 minutes the pulp was washed as described above.

Tinopal redissolved the Chlorazol Black from the fiber surface, so that after 30 minutes the pulp was only gray. This was also partly observable with Leukophor, but with far less intensity. So for further trials only Leukophor was used. The pulp that was treated with optical brightening agents for 30 minutes showed the highest fluorescence under the ultraviolet lamp, so this exposure time was kept.

7.2.3   Evaluation of the dyes

In chapter 7.2.1 the dyes that were applied in this work are described briefly. Here the experimental results obtained with various combinations are discussed. Also the experiments that were not successful will be described, in order to prevent others from trying the same things again. All of the measurements that are discussed in the following part were performed by Dr. Massimiliano Cardinale at the Institute for Environmental Biotechnology (Graz University of Technology).

Acridine Orange and Rhodamine B   Fiber-fiber bonds between one fiber dyed with Acridine Orange and one fiber dyed with Rhodamine B were analyzed with the CLSM. The volume and the surface of the fibers were recorded. Exemplary pictures of the three-dimensional surface reconstruction and of the volume of a fiber-fiber bond are shown in figure 7.8 and figure 7.9 respectively.
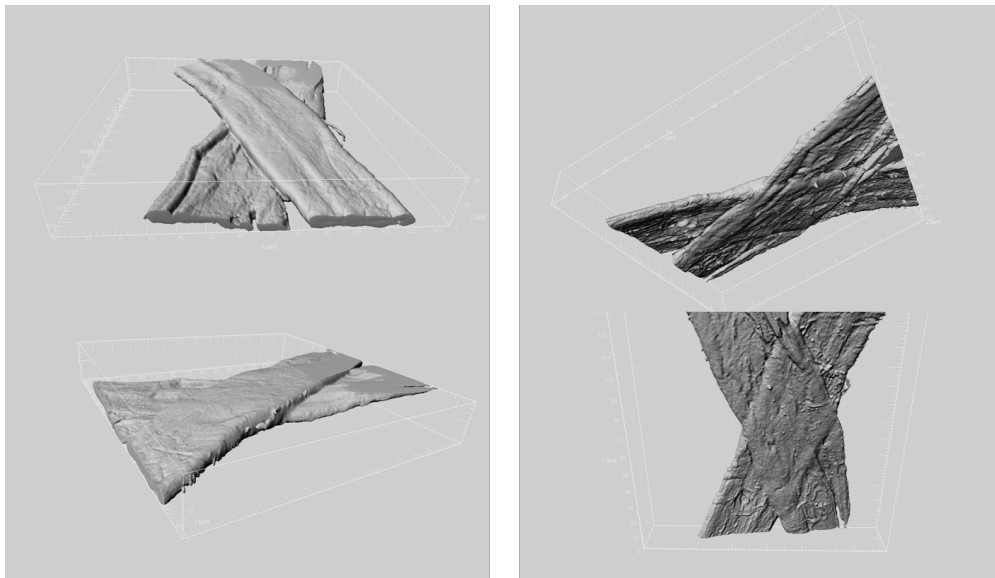
Fig. 7.8   Surface reconstruction of a fiber-fiber bond imaged with the CLSM
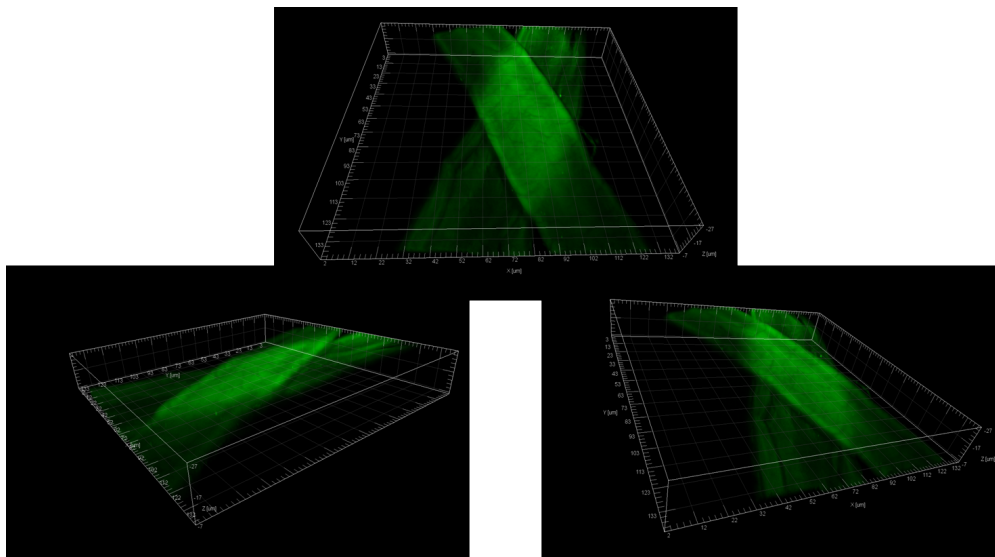
Fig. 7.9 Volume of a fiber-fiber bond imaged with the CLSM

The fluorescence of the fibers in the volume image is very similar, as the fluorescence spectra of Acridine Orange and Rhodamine B overlap over a too big range (see figure 7.5 and figure 7.7). Although there is a small difference in intensity between the bonded fibers this difference is too small to determine the bonding line and the size of bonded area. So the combination of Acridine Orange and Rhodamine B is not suited for fiber-fiber bonded area measurement with CLSM.

Chlorazol Black and Leukophor Only fibers that were treated with Leukophor were imaged with the CLSM, as Tinopal redissolved the Chlorazol Black from the fiber surfaces. In the CLSM images only the fiber surface was visible, imaging the volume was not possible. It seems as if the Chlorazol Black prevented the Leukophor from penetrating into the fiber wall, so that only the fiber surface fluoresced. Additionally the black dye absorbed most of the laser, which also reduced the signal from the fiber volume significantly.

In conclusion it can be said that also this dyeing is not suitable for fiber-fiber bonded area measurement with CLSM.

Rhodamine B (dissolved in water) and Leukophor In these experiments 50 % of the fibers were dyed with Rhodamine B that was dissolved in water and 50 % of the fibers were treated with Leukophor. Rhodamine B fluoresces red, while Leukophor fluoresces blue, so the spectra should be clearly discriminable in this case. Again bonds between differently dyed fibers were prepared and imaged with the CLSM. Both fibers showed in different colors. However, in the cross sectional images it seemed as if the Rhodamine B partly bled into the

second fiber. As the dye was based on water it may be assumed that part of the Rhodamine B redissolved from the fiber surface in the aqueous suspension during bond formation and penetrated into the second fiber. So again, determination of the correct fiber-fiber interface was not possible.

Rhodamine B (dissolved in ethanol) and Leukophor   In order to prevent the Rhodamine B from bleeding into the second fiber, ethanol was used as a solvent and again a Rhodamine B dyed and a Leukophor treated fiber were bonded. This time the dye did not redissolve from the fiber surface and imaging of the fiber-fiber bond with the CLSM was possible. A reconstruction of the surface as well as of the volume record of a fiber-fiber bond is shown in figure 7.10. These images were acquired with an xy-scan. The red knob on the blue fiber is an artefact from the measurement, as well as the elevated contour of the red fiber next to the bond. Neither of these structures was visible in the xz-scan images. Figure 7.11 shows exemplary fiber-fiber bond cross sections at various positions through the bond, scanned in the xz-plane. The contour of both fibers is well defined and the structure of the fiber-fiber bond and of the fibers is visible. The lower fiber seems to be folded, which causes a hole in the bond that is clearly observable in these images.
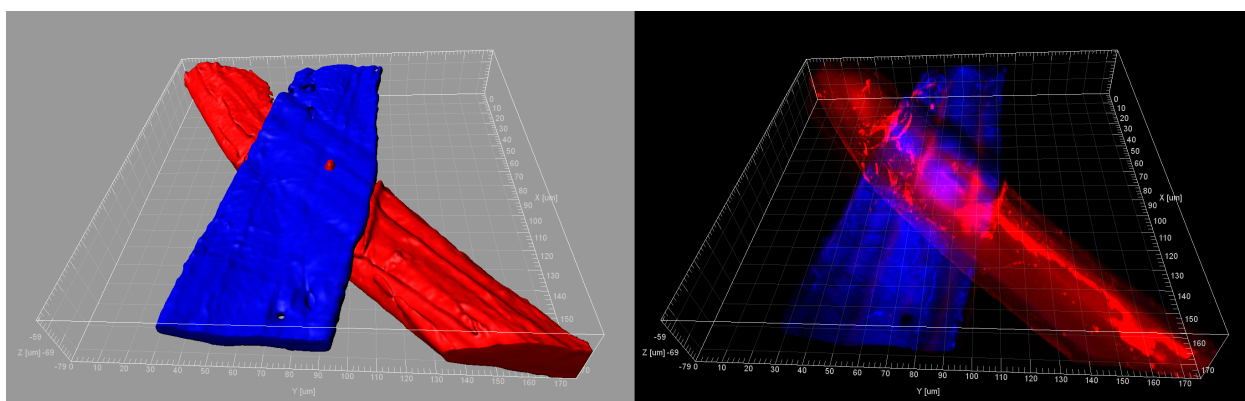
Fig. 7.10 Surface reconstruction and volume of a fiber-fiber bond imaged with the CLSM

Conclusions - evaluation of the dyes

Analyzing fiber-fiber bonds where one fiber was dyed with Rhodamine B dissolved in ethanol and the second fiber was treated with Leukophor turned out to be most promising. The fluorescence spectra of the fibers did not overlap and a clear fiber-fiber interface was visible (see figure 7.11). Hence this procedure was kept for all further experiments.
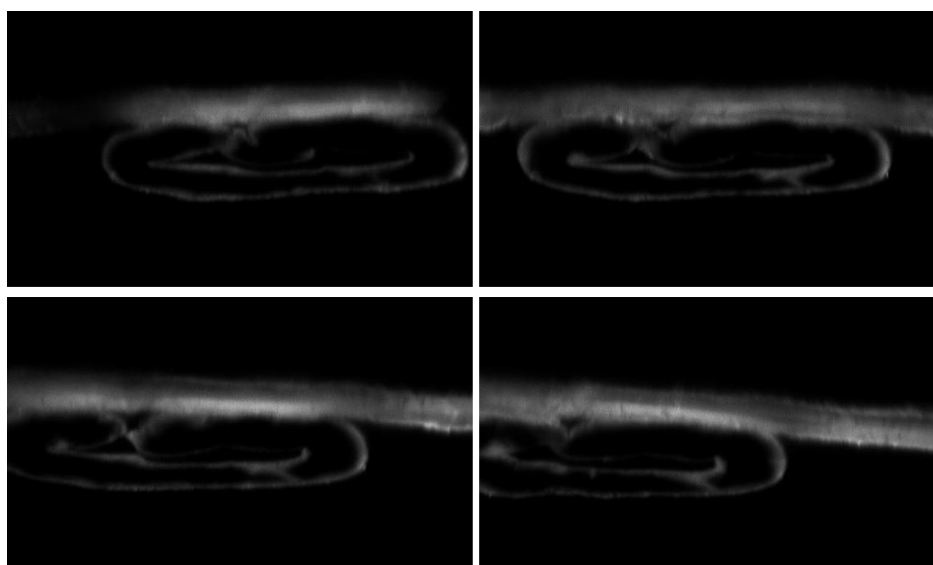
Fig. 7.11 Fiber-fiber bond cross sections at various positions through the bond imaged with the CLSM

7.2.4 Comparative bonded area measurements

After the fiber-fiber bond had been imaged with the confocal laser scanning microscope, the sample should be embedded and cut with the microtome to compare the size of bonded area and the fiber cross sectional dimensions. However, in first experiments there were some problems with the sample preparation that had to be solved first. Figure 7.12 (left) depicts how the fiber-fiber bond is prepared for CLSM measurements. The bond is fixed on a strip of paper, as described in Paper I, this strip of paper is fixed on a microscope slide and covered with a cover slip. In between antifadent is put, which has the same index of refraction as the cover slip. When the cover slip was removed again after the CLSM measurement, the bond stuck to it so that it could no longer be used for microtome analysis (see figure 7.12, right).
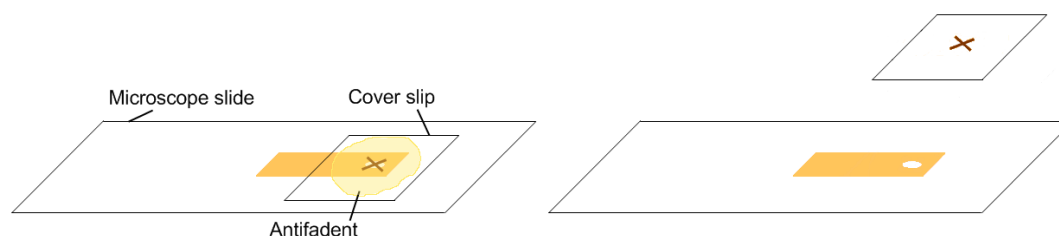
Fig. 7.12 Preparation of fiber-fiber bonds for CLSM measurement and problems with taking off the cover slip

The sample preparation before microtome serial sectioning is described in chapter 5.4. It is

shown that some material has to be embedded next to the bond to provide structural image information so that stitching and aligning of the microtome images is possible. Experiments led to the conclusion that the best solution is to embed a strip of woodfree coated paper next to the bond. The coating layer separates the fiber-fiber bond from the fibers in the paper and the paper itself provides structural image information.

An approach to solve the problem with detaching of the fiber-fiber bond after CLSM measurement was to glue this strip of coated paper to the sample before the CLSM analysis. By that the bond was fixed safely between the two papers. The problem here was that the coated paper contains optical brightening agents, so that its fluorescence was much stronger than the fibers' and CLSM measurements were not possible. Since most commercial available coated papers contain optical brightening agents something else will have to be used to protect the fiber-fiber bond.

New experiments will have to be performed, for example with a calendered packaging paper instead of the woodfree coated paper. The packaging paper consists of unbleached kraft fibers. The autofluorescence of these fibers is low, so that the fluorescence of the dyed fiber-fiber bond dominates. The calendering is necessary in order to prevent fibers from protruding from the paper surface. These fibers are unwanted as they may be mistaken for the fibers of the fiber-fiber bond in the microtome images.

7.3   Conclusions

To visualize the fiber-fiber interface with the confocal laser scanning microscope the bonded fibers have to be dyed with two different fluorescent dyes. The combination of Rhodamine B dissolved in ethanol and an optical brightening agent (Leukophor) turned out to be most suitable. Fiber-fiber bond cross sectional images obtained with the CLSM showed that the fibers can be distinguished in this case. The only drawback of this dye combination is that a three-fold measurement of the bonded area is not possible, as one of the bonded fibers has to be dyed black for polarized light microscopy.

Chapter 8

Development of fiber-fiber bonded area with beating

8.1 Introduction

Using microtome serial sectioning and image analysis not only the size of the bonded area is measured, but also several morphological parameters of the fibers and of the bond. The respective influence of these parameters on the size of the bonded area is determined with multiple linear regression modeling. Paper I contains a discussion of the modeling results for unbeaten pulp. In this case morphology had surprisingly little influence on the size of bonded area. To evaluate the influence of beating on the size of bonded area and on morphological parameters of fibers and bonding region, the experiments were repeated with pulp that was beaten with 9000 revolutions in the PFI mill. Again bonded area was measured together with morphological parameters. Multiple linear regression modeling was performed and the results were compared with those from the unbeaten pulp.

8.2 Comparison of bonded area - unbeaten and beaten pulp

All experiments were performed with an unbleached kraft pulp that was a mixture from spruce and pine wood. Fiber-fiber bonds were prepared from unbeaten as well as from beaten pulp. The beating was performed in the laboratory with the PFI mill (9000 revolutions). 73 fiber-fiber bonds from unbeaten pulp were analyzed and 68 fiber-fiber bonds from beaten pulp.

A comparison of bonded area from unbeaten and beaten pulp is given in table 8.1. The beating increased the bonded area by 45 %. The statistical significance of this increase is demonstrated with the box plots in figure 8.1. The notches in the boxes do not overlap, indicating that the difference between the results is significant on a 95 % confidence level. In both cases the values scatter strongly. Results that lie outside 1.5 IQR (interquartile range) of the lower or upper quartile are marked, these observations are considered outliers.

	0 rev. PFI	9000 rev. PFI
Mean bonded area	1433 μm^2	2082 μm^2
Standard deviation	622 μm^2	878 μm^2

Tab. 8.1 Comparison of bonded area - unbeaten and beaten pulp
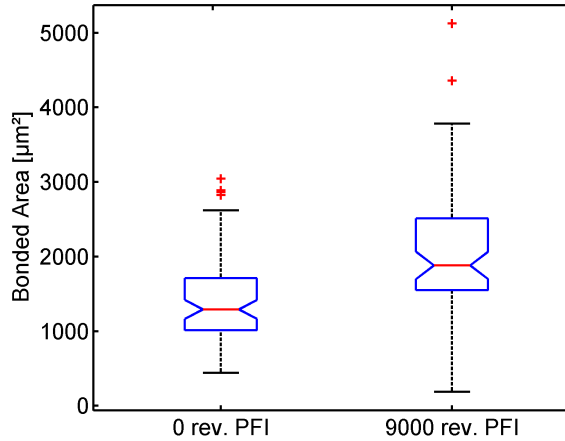
Fig. 8.1 Box plot: Bonded area of unbeaten and beaten pulp

The distributions of the results for unbeaten and beaten pulp are shown in figure 8.2. The peak is shifted from approximately 1000 μm^2 to 2000 μm^2, while the shape of the distribution does not change a lot.

8.2.1 Explaining the increase in bonded area with morphological parameters

The microtome images do not only provide information on bonded area, the following morphological parameters are additionally measured in the bonding region:

- Fiber cross sectional area

- Fiber perimeter
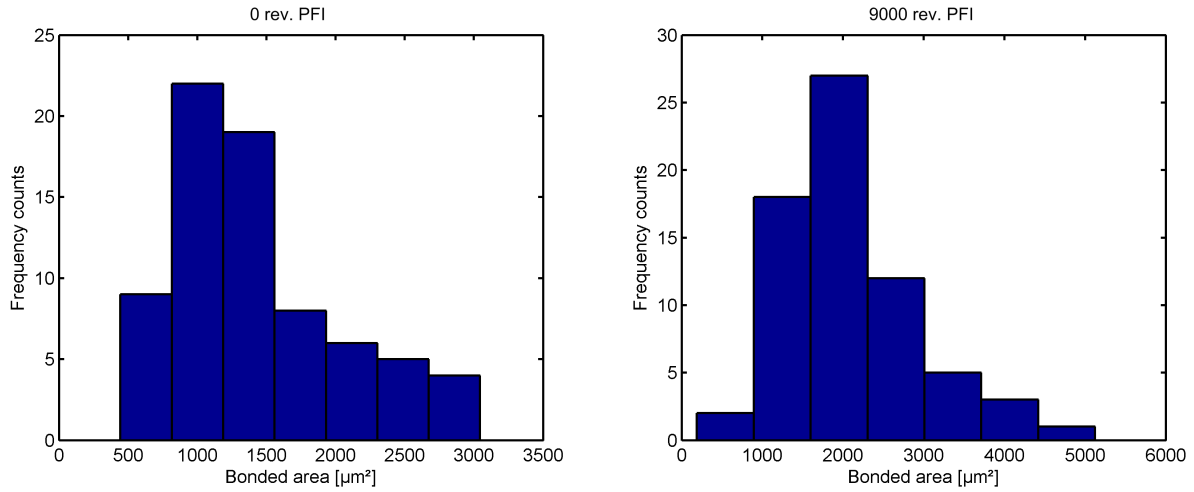
Fig. 8.2 Histograms: Distribution of bonded area of unbeaten and beaten pulp

- Fiber width

- Fiber wall thickness

- Fiber collapse

- Degree of bonding (i.e. a measure of holes in the bond and unbonded fiber edges)

- Crossing angle

The exact definition of these parameters and a description of how they are measured can be found in Paper I and in [55].

Figure 8.3 shows that the bonded area depends to a large extent on the basic geometry, being the fiber width and the crossing angle. According to figure 8.3 the calculated bonded area, A_{calc}, is given by equation 8.1, where w_1 and w_2 are the widths of the fibers and α is the crossing angle. This calculation was performed for all bonds.

$$A_{calc} = w_1 \cdot w_2 \cdot \frac{1}{sin\alpha} \tag{8.1}$$

The set of morphological data together with calculated and measured values for the size of bonded area for unbeaten and for beaten pulp were basis for further investigations of the development of fiber morphology with refining. In table 8.2 some interesting changes in fiber morphology and in degree of bonding with refining are summarized. The biggest difference can be found in the degree of bonding. Fiber-fiber bonds prepared from unbeaten pulp showed a degree of bonding of only 86 %, 14 % of the crossed fiber surfaces were unbonded. With refining the proportion of bonded fiber surface is raised to 98 %. However,
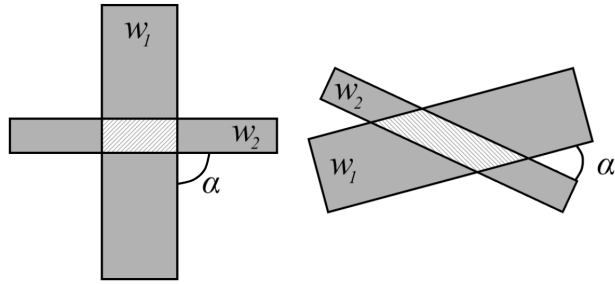
Fig. 8.3 Basic geometric parameters crossing angle and fiber width yielding calculated bonded area

this explains only part of the increase in size of bonded area. The residual increase is partly reflected in the increase of fiber width. At the same time the fiber wall thickness decreases, which may promote fiber conformability. The product of fiber width and fiber wall thickness stays almost constant, indicating that hardly any fiber material is lost during refining.

	0 rev. PFI	9000 rev. PFI
Degree of bonding	86 %	98 %
Fiber width	38 μm	42 μm
Fiber wall thickness	2.6 μm	2.3 μm
Fiber collapse	99.7 %	99.9 %

Tab. 8.2 Development of the degree of bonding and some morphological parameters with beating

In figure 8.4, 8.5 and 8.6 the box plots of degree of bonding, fiber width and fiber wall thickness are compared for unbeaten and beaten pulp. The increase in degree of bonding and in fiber width is statistically significant on a 95 % confidence level. This is indicated by the notches in the boxes that do not overlap. Only in the case of fiber wall thickness the notches slightly overlap.

All other morphological parameters did not show any differences worth mentioning. Unbeaten as well as beaten fibers showed a fiber collapse close to 100 % (see table 8.2). Also in size of cross sectional area no significant change could be found. The fiber perimeter is mainly influenced by the fiber width, so it overall shows the same behavior.

As the fiber-fiber bonds are made from suspension, the crossing angle cannot be influenced actively. On average the crossing angle was very close to right angle, however, the values scattered to some extent. This spread is reflected in the box plots of the crossing angle in figure 8.7. The overlapping notches indicate that the crossing angle did not differ in the unbeaten and the beaten case on a 95 % confidence level. So the crossing angle cannot be
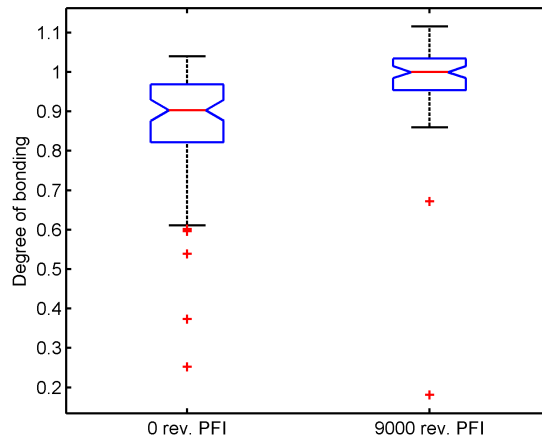
Fig. 8.4 Box plot: Degree of bonding of unbeaten and beaten pulp
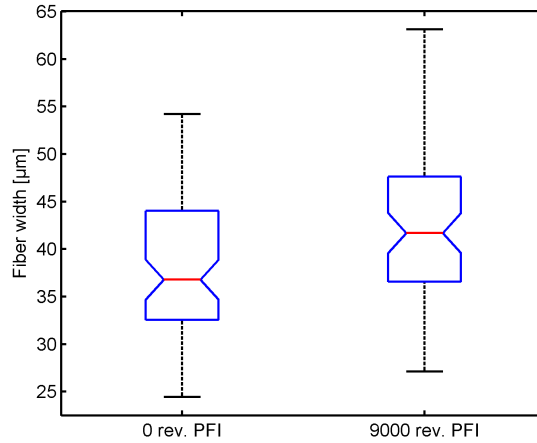
Fig. 8.5 Box plot: Fiber width of unbeaten and beaten pulp

related to the increase in bonded area with refining.

From the comparison of the morphological parameters it can be concluded, that the increase in fiber width and in degree of bonding mainly accounts for the increase in size of bonded area. However, fiber width is increased 10 % and degree of bonding is increased 12 %, while bonded area is 45 % larger. A possible approach for an explanation of this discrepancy is that the crossing angle has to be taken into account, even though there are no significant differences between unbeaten and beaten samples.

Figure 8.3 and equation 8.1 show how the bonded area can be calculated from the basic geometric parameters, fiber width and crossing angle. Especially in the case of beaten pulp the calculated bonded area is a very good approach for the measured bonded area. This is
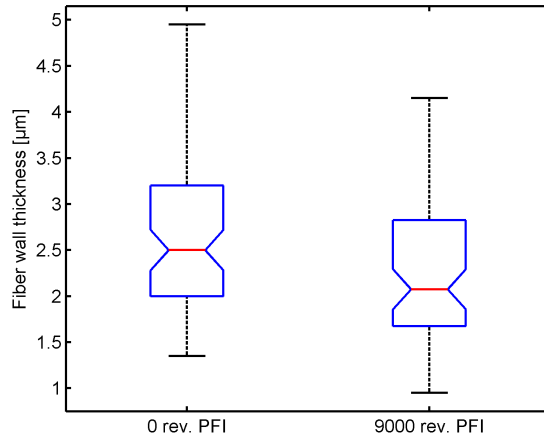
Fig. 8.6 Box plot: Fiber wall thickness of unbeaten and beaten pulp
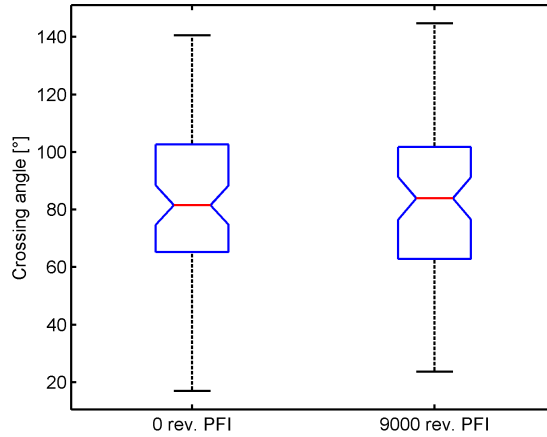
Fig. 8.7 Box plot: Crossing angle of unbeaten and beaten fiber-fiber bonds

also demonstrated in figure 8.8, where measured bonded area is plotted versus calculated bonded area. The mean calculated bonded area was very similar to the mean measured bonded area:

$\bar{A}_{calc} = 2068 \ \mu m^2$

$\bar{A}_{measured} = 2136 \ \mu m^2$

Still, if, according to equation 8.1, the mean fiber widths ($\bar{w}_1 = 42.4 \ \mu m$ and $\bar{w}_2 = 41.2 \ \mu m$) are multiplied with each other and then divided by the sine of the mean crossing angle ($\bar{\alpha} = 84.8°$) this does not result in the mean calculated bonded area, but in a value that is approximately 15 % lower (see equation 8.2). This indicates that weighting the fiber widths with the crossing angle for each bond separately is required to represent the mean bonded

area correctly.

$$\bar{w}_1 \cdot \bar{w}_2 \cdot \frac{1}{sin\bar{\alpha}} = 42.4 \cdot 41.2 \cdot \frac{1}{sin84.8°} = 1754 \ \mu m^2 \tag{8.2}$$

This might be an explanation, why the increase in bonded area also cannot be represented solely with the increase in degree of bonding and fiber width, as the weighting with the crossing angle has to be considered. Multiplying the average size of bonded area from unbeaten pulp (1433 μm^2) with 1.1 (accounting for the 10 % increase in fiber width), with 1.12 (accounting for the 12 % increase in degree of bonding) and with 1.15 (weighting with the crossing angle) yields approximately the average size of bonded area from beaten pulp (see equation 8.3).

$$1433 \ \mu m^2 \cdot 1.1 \cdot 1.12 \cdot 1.15 = 2030 \ \mu m^2 \tag{8.3}$$

8.2.2 Relating the increase in bonded area with the increase in tensile index

The tensile index, z-strength and freeness of unbeaten and beaten pulp were measured, the results are given in table 8.3. The increase in tensile index with beating is over 500 %, z-strength is enhanced 480% while bonded area is only increased 45 %. This indicates that the specific bonding strength also increases significantly with refining. Fibrils that originate from refining entangle and promote mechanical interlocking. Additionally hemicelluloses are exposed that are more capable of forming hydrogen bonds than cellulose. This emphasizes that the increase in bonded area is not solely responsible for the increase in bonding strength.

	0 rev. PFI	9000 rev. PFI
Tensile index [Nm/m]	15.12	82.04
Z-strength [N/cm^2]	14.7	71.4
Freeness [$°SR$]	13.65	29.55

Tab. 8.3 Tensile index, z-strength and freeness of unbeaten and beaten pulp

8.3 Explaining the bonded area with morphological parameters

8.3.1 Multiple linear regression modeling

Based on the measured bonded areas and morphological parameters, several factors that may affect the bonded area were investigated. Multiple linear regression was performed to quantify the significance (F^*-statistics) and the impact (ANOVA) of the explanatory variables [69]. For this statistical analysis the mean value of the morphological parameters of the two bonded fibers was taken.

Apart from fundamental geometry, the parameters that govern the bonded area were determined by multiple linear regression. A_{calc} and all of the morphological parameters were taken as predictor variables. The detailed results for the unbeaten pulp are discussed in Paper I, here only a summary of the explaining variables for bonded area is given in table 8.4. Fundamental bonding geometry (i.e. fiber width and crossing angle reflected in calculated bonded area) and incomplete bonding accounted for 87 % of the bonded area, while other morphological parameters had almost no influence.

Variable	R^2 stepwise	R^2 alone	p-Value	Sign of Coeff.
A_{calc}	0.547	0.547	$< 10^{-5}$	+
Edge fraction	0.853	0.280	$< 10^{-5}$	−
Hole fraction	0.873	0.017	$< 10^{-5}$	−
Fiber perimeter	0.879	0.219	0.027	−
Crossing angle	0.886	0.02	0.017	−

Tab. 8.4 Explaining variables for bonded area - unbeaten pulp

The same multiple linear regression model was built for the beaten pulp. Measured bonded area was the response variable, calculated bonded area and all morphological parameters were taken as predictor variables. The results of this model are summarized in table 8.5. Now the calculated bonded area explains almost 82 % of the bonded area (the R^2 is 0.817). An additional 10 % of variance is explained by the unbonded fiber edges, which is indicated by an increase from 0.817 to 0.914 of the R^2 stepwise. Finally the fiber perimeter explains another 1 % of the variance. Other morphological parameters that should be related to conformability (fiber wall thickness, fiber collapse and fiber cross sectional area) are not significant on a 95 % confidence level.

Figure 8.8 illustrates the fact that calculated and measured bonded area correlate very well. The diagonal indicates equal values and most results are located close-by. There are just

Variable	R^2 stepwise	R^2 alone	p-Value	Sign of Coeff.
A_{calc}	0.817	0.817	$< 10^{-5}$	$+$
Edge fraction	0.914	0.144	0.0005	$-$
Fiber perimeter	0.921	0.360	0.0078	$-$

Tab. 8.5 Explaining variables for bonded area - beaten pulp

three exceptions (marked with the numbers $1, 2, 3$), that can be explained with the microtome images.
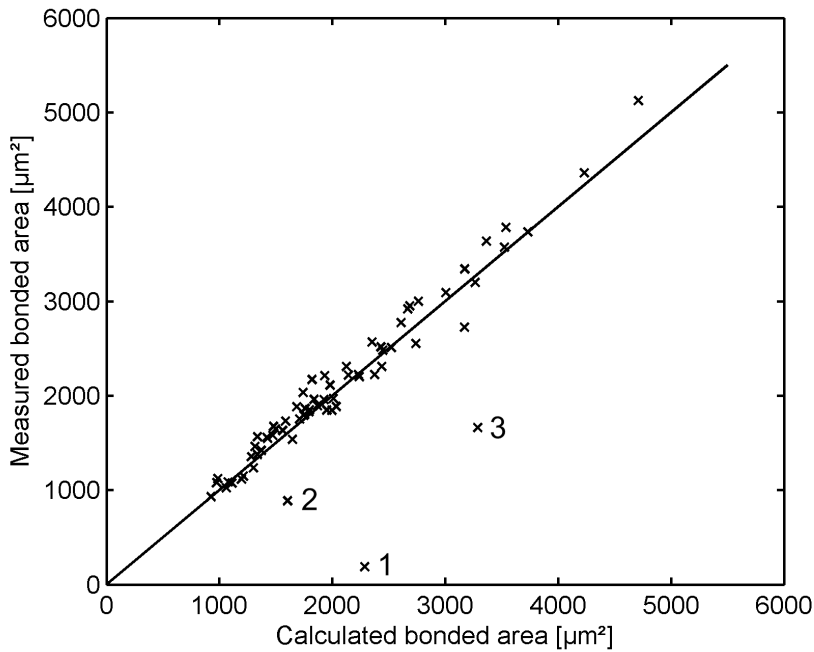
Fig. 8.8 Comparison of calculated and measured bonded area for beaten pulp

Explaining the deviations The microtome images provide additional information on fiber and bonding morphology. The cases where calculated bonded area deviates from the measurement will be discussed below using the respective microtome images.

1. In the first example measured bonded area was 188 μm^2, while calculated bonded area was 2286 μm^2. Figure 8.9 shows a series of microtome images through this bond. The fibers are only fractionally bonded, which is only reflected in the measurement, but not in the calculation.

2. Figure 8.10 explains the deviation between a measured bonded area of 887 μm^2 and a calculated bonded area of 1604 μm^2. The right fiber is shaped like an inverted U and

Fig. 8.9 Microtome images explaining the deviation between measured and calculated bonded area (1)

bonding is rather poor. So again the fiber width that is considered in the calculation of bonded area is not entirely used for bonding.

Fig. 8.10 Microtome images explaining the deviation between measured and calculated bonded area (2)

3. In the third example the attention has to be drawn to the right fiber in figure 8.11. The fiber width increases through the cuts, which may affect the calculation. So a measured bonded area of 1663 μm^2 is opposed a calculated bonded area of 3287 μm^2.

If these three exceptions are left out, the R^2 of the correlation between calculated and measured bonded area is 0.9713, compared to an R^2 of 0.817 under consideration of the exceptions (see table 8.5).
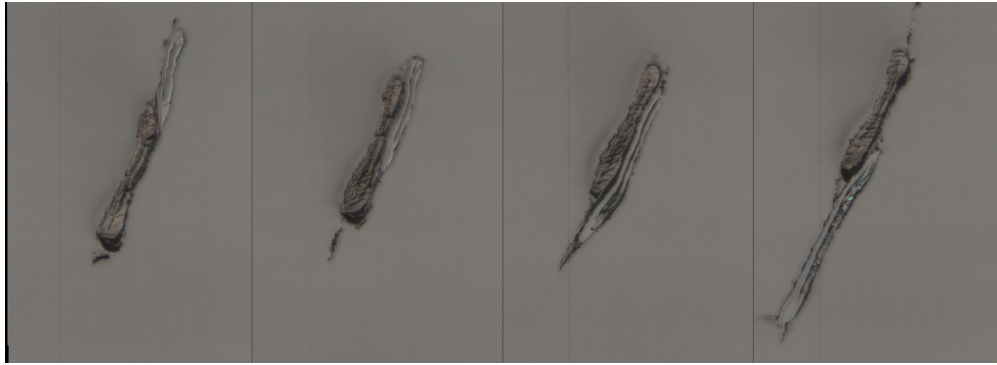
Fig. 8.11 Microtome images explaining the deviation between measured and calculated bonded area (3)

8.4 Conclusions

Bonded area is increased significantly with beating. Also some of the measured morphological parameters are changed. Fiber width and bonding degree increase significantly, while the fiber wall thickness slightly decreases.

Multiple linear regression modeling of results for unbeaten and beaten pulp showed that bonded area is dominated by the fundamental bonding geometry, being fiber width and crossing angle. Other morphological parameters that may be related to fiber conformability do not really play a role. Especially in the case of unbeaten pulp the degree of bonding (i.e. holes in the bond and unbonded fiber edges) also plays an important role, which is strongly reduced with beating.

Chapter 9

Conclusions and Outlook

In this thesis a novel method for fiber-fiber bonded area measurement based on microtome serial sectioning and image analysis is introduced. The bonded area is measured together with morphological parameters of the fibers and the bond, which leads to a deeper understanding of fiber-fiber bonds and its influencing factors. However, for measuring the specific bonding strength a non-destructive measure for fiber-fiber bonded area is required. Based on the microtome results non-destructive reference methods were evaluated and as far as needed calibrated.

In a first approach polarized light microscopy was applied. The comparison of polarized light microscopy images with microtome results indicated that polarized light microscopy is an appropriate method for fiber-fiber bonded area measurement as long as one of the bonded fibers is dyed black. An optical model which describes the behavior of fibers and fiber-fiber bonds under the polarized light microscope confirmed and explained these experimental results. It could be shown that bonded area is overestimated if fiber-fiber bonds between unrefined kraft pulp fibers are analyzed while it is underestimated in the case of refined kraft pulp. A factor for the over- and underestimation respectively was determined. Confocal laser scanning microscopy (CLSM) was also applied for fiber-fiber bonded area measurement. Provided that the bonded fibers are dyed with appropriate fluorescent dyes, this optical sectioning technique yields cross sectional images of the fiber-fiber bond similar to the microtome images that can be used to measure the bonded area.

Future applications

Microtome serial sectioning was successfully used for fiber-fiber bonded area measurement. The bonded area was evaluated together with morphological parameters for beaten and unbeaten pulp. The same experiments should be performed with chemically modified pulp.

One drawback of the microtome method for fiber-fiber bonded area measurement is the expenditure of time for the image analysis, as the fibers in the microtome images have to be drawn by hand. An automated fiber tracking algorithm would accelerate this process. The accuracy of this algorithm has to be high enough to identify unbonded fiber edges and holes in the bond correctly, as this will have a big influence on the results of fiber-fiber bonded area, especially if unbeaten pulp is used.

The applicability of polarized light microscopy and confocal laser scanning microscopy for fiber-fiber bonded area measurement has already been shown. Further non-destructive methods like for example nano-CT still have to be evaluated. Until now nano-CT has only been available with too low resolution for the required sample size, but today new devices can achieve the same resolution as CLSM or light microscopy. So this would be another approach to measure fiber-fiber bonded area non-destructively.

Comparison of bonded area measured with microtome serial sectioning and with polarized light microscopy showed that the bonded area is overestimated with polarized light microscopy if unbeaten kraft pulp is used, while it is underestimated if beaten kraft pulp is used (9000 rev. PFI). The same experiments should be performed with a pulp that was moderately beaten (e.g. 2000 rev. PFI), as this has more relevance in practice.

Understanding the polarized light microscopy and knowing the preconditions for the application of CLSM for fiber-fiber bonded area measurement is the basis for specific bonding strength measurements. A method for handling and testing individual fiber-fiber bonds will have to be developed.

In all experiments the focus was set on fiber-fiber bonds. In the future the work could be extended to the fiber network to analyze the following issues:

- Morphological factors influencing the size of bonded area: In the case of individual fiber-fiber bonds morphology had surprisingly little influence on the size of bonded area (see Paper I), maybe this is different in the fiber network.

- Investigation of the number of bonds per mm^2 depending on the basis weight.

- The bond/crossing ratio depending on the basis weight: Cross sectional images of ultra light weight sheets ($\sim 5\ g/m^2$) showed that a relatively large proportion of crossed fibers were not bonded. Here experiments on drying and pressing conditions for various basis weights should be performed.

- Applicability of polarized light microscopy for fiber networks: The fiber-fiber bonds have to fulfill certain geometrical preconditions to be analyzable with the polarized light microscope (see Paper II and Paper III). In a fiber network the geometry is not at all controllable and surrounding fibers will cause additional reflections and light scattering, which disturbs the effect of dark bonded area.

- Applicability of CLSM for fiber networks: The number of bonds per mm^2 should be analyzable with the CLSM without any difficulty. In the case of fiber-fiber bonded area measurement the precondition of having two bonded fibers dyed with different fluorescent dyes will be hard to fulfill for all bonds.

List of Figures

List of Tables

Bibliography

[1] T. Lindström, L. Wågberg, and T. Larsson. On the nature of joint strength in paper–A review of dry and wet strength resins used in paper manufacturing. *Advances in Paper Science and Technology*, 1:457–562, 2005.

[2] J.A. Van den Akker, A.L. Lathrop, M.H. Voelker, and L.R. Dearth. Importance of fiber strength to sheet strength. *Tappi Journal*, 41(8):416–25, 1958.

[3] R. Wathén. Studies on fiber strength and its effect on paper properties, 2006.

[4] K.J. Niskanen, M.J. Alava, E.T. Seppälä, and J. Aström. Fracture energy in fibre and bond failure. *Journal of pulp and paper science*, 25(5):167–169, 1999.

[5] K. Niskanen. *Paper physics*. Fapet Oy Helsinki, 2008.

[6] E. Duker and T. Lindstrom. On the mechanisms behind the ability of CMC to enhance paper strength. *Nordic Pulp and Paper Research Journal*, 23(1):57, 2008.

[7] B. Leopold. Chemical composition and physical properties of wood fibers. *Tappi Journal*, 44(3):230, 1961.

[8] K.W. Hardacker. The Automatic Recording of the Load-Elongation Characteristic of Single Papermaking Fibers; IPC Fiber Load-Elongation Recorder. *Tappi Journal*, 45(3):237–246, 1962.

[9] R.B. Adusumali, M. Reifferscheid, H. Weber, T. Roeder, H. Sixta, W. Gindl, RD Lenzing, and A. Lenzing. Mechanical Properties of Regenerated Cellulose Fibres for Composites. In *Macromolecular Symposia*, volume 244, pages 119–125. Basel; Oxford, CT: Huthig & Wepf, 1994-, 2006.

[10] P.M. Hoffmann Jacobsen. New method of determining the strength of chemical pulp. *Paper Trade Journal*, 53(22):216–217, 1925.

[11] E. Boucai. Zero-span tensile test and fibre strength. *Pulp Paper Magazine Canada*, 72(10):73–80, 1971.

[12] R.S. Seth and B.K. Chan. Measuring fiber strength of papermaking pulps. *Tappi Journal*, 82(11):115–120, 1999.

[13] R. Hägglund, P.A. Gradin, and D. Tarakameh. Some aspects on the zero-span tensile test. *Experimental Mechanics*, 44(4):365–374, 2004.

[14] R.S. Seth. Zero-span tensile strength of papermaking fibres. *Paperi ja puu - Paper and Timber*, 83(8):597–604, 2001.

[15] D.H. Page. A theory for the tensile strength of paper. *Tappi Journal*, 52(4):674–681, 1969.

[16] W.B. Campbell. The mechanism of bonding. *Tappi Journal*, 42(12):999–1001, 1959.

[17] H. Nanko and J. Ohsawa. Mechanisms of fiber bond formation. *Fundamentals of Papermaking*, 2:783–830, 1989.

[18] F. Linhart. Überlegungen zum Wirkungsmechanismus der Papierverfestigung. *Wochenblatt für Papierfabrikation*, 133(11-12):662–672, 2005.

[19] V.H. Corte and H. Schaschek. Physikalische Natur der Papierfestigkeit. *Das Papier*, 9(21/22):519–530, 1955.

[20] A.T. Horvath. *Chemical Methods for Improving the Fracture Toughness of Paper*. PhD thesis, KTH, Fibre and Polymer Technology, 2008.

[21] S.M. Notley, B. Pettersson, and L. Wågberg. Direct measurement of attractive van der Waals' forces between regenerated cellulose surfaces in an aqueous environment. *Journal of the American Chemical Society*, 126(43):13930, 2004.

[22] R.A. Stratton. Fundamentals of internal strength enhancement. Part two, Studies on the bonding of single fibers. Project 3526, Report three: A progress report to members of the Institute of Paper Science and Technology. 1992.

[23] A. Torgnysdotter and L. Wågberg. Tailoring of fibre/fibre joints in order to avoid the negative impacts of drying on paper properties. *Nordic Pulp and Paper Research Journal*, 21(3):411, 2006.

[24] J.L. Thorpe, R.E. Mark, A.R.K. Eusufzai, and R.W. Perkins. Mechanical properties of fiber bonds. *Tappi Journal*, 59(5):96–100, 1976.

[25] R.A. Stratton and N.L. Colson. Dependence of fiber/fiber bonding on some papermaking variables. 1990.

[26] A.P. Schniewind, L.J. Nemeth, and D.L. Brink. Fibre and Pulp Properties. I. Shear Strength of Single Fiber Crossings. *Tappi Journal*, 47(4):244–248, 1964.

[27] W.H. Burgess. Effect of basis weight on tensile strength. *Tappi Journal*, 53(9):1680–1682, 1970.

[28] O. Kallmes and H. Corte. The structure of paper, I. The statistical geometry of an ideal two dimensional fiber network. *Tappi Journal*, 43(9):737–752, 1960.

[29] O. Kallmes, H. Corte, and G. Bernier. The Structure of Paper, Part II. The Statistical Geometry of an Multiplanar Fiber Network. *Tappi Journal*, 44(7):519–528, 1961.

[30] W.W. Sampson. The statistical geometry of fractional contact area in random fibre networks. *Journal of pulp and paper science*, 29(12):412–416, 2003.

[31] J. Rennel, N. Hartler, and S.T. Stockholm. Opacity in relation to strength properties of pulps. Part 1. Method for producing unbonded fibers and determining their light scattering coefficient and surface area. *Svensk Papperstidning*, 1, 1969.

[32] L. Nordman and C. Gustaffson. On the relationship between tensile strength and bonded fibre area of paper. *Paperi ja puu*, (2):36–41, 1951.

[33] W.L. Ingmanson and E.F. Thode. Factors contributing to the strength of a sheet of paper. II. Relative bonded area. *Tappi Journal*, 42(1):83–93, 1959.

[34] W. Batchelor and J. He. A new method for determining the relative bonded area. *Tappi Journal*, 4(6):23, 2005.

[35] W.R. Haselton. Gas adsorption by wood, pulp, and paper. I. The low-temperature adsorption of nitrogen, butane, and carbon dioxide by sprucewood and its components. *Tappi Journal*, 37(9):404–412, 1954.

[36] D.H. Page, P.A. Tydeman, and M. Hunt. A study of fibre-to-fibre bonding by direct observation. *The formation and structure of paper*, 1:171–94, 1962.

[37] O. Kallmes and G. Bernier. The Structure of Paper, III: The Absolute, Relative, and Maximum Bonded Areas of Random Fiber Networks. *Tappi Journal*, 45(11):867–872, 1962.

[38] W.R. Haselton. Gas adsorption by wood, pulp, and paper. II. The application of gas adsorption techniques to the study of the area and structure of pulps and the unbonded and bonded area of paper. *Tappi Journal*, 38(12):716–723, 1955.

[39] J.W. Swanson and A.J. Steber. Fiber surface area and bonded area. *Tappi Journal*, 42(12):986–994, 1959.

[40] D.C. Mclntosh. Tensile and bonding strengths of Loblolly Pine kraft fibers cooked to different yields. *Tappi Journal*, 46(5):273–277, 1963.

[41] U.B. Mohlin. Cellulose fiber bonding. Determination of interfiber bond strength. *Svensk Papperstidning*, 77(4):131–137, 1974.

[42] T. Kang, H. Paulapuro, and E. Hiltunen. Fracture mechanism in interfibre bond failure: microscopic observations. *Appita Journal*, 57(3):199–203, 2004.

[43] C.H. Mayhood Jr, O.J. Kallmes, and M.M. Cauley. The mechanical properties of paper. Part II: Measured shear strength of individual fiber to fiber contacts. *Tappi Journal*, 45(1):69–73, 1962.

[44] J. Forsström, A. Torgnysdotter, and L. Wagberg. Influence of fibre/fibre joint strength and fibre flexibility on the strength of papers from unbleached kraft fibres. *Nordic Pulp and Paper Research Journal*, 20(2), 2005.

[45] R. Lowe, A. Ragauskas, and D.H. Page. Imaging fibre deformations. In *Advances in Paper Science and Technology: Transactions of the 13th Fundamental Research Symposium. SJ I'Anson. Cambridge, FRC*, pages 921–941, 2005.

[46] C.I. Thomson, R.M. Lowe, and A.J. Ragauskas. Imaging cellulose fibre interfaces with fluorescence microscopy and resonance energy transfer. *Carbohydrate Polymers*, 69(4):799–804, 2007.

[47] A. Torgnysdotter, A. Kulachenko, P. Gradin, and L. Wågberg. The Link Between the Fiber Contact Zone and the Physical Properties of Paper: A Way to Control Paper Properties. *Journal of Composite Materials*, 41(13):1619, 2007.

[48] G.W. Gordon, G. Berry, X.H. Liang, B. Levine, and B. Herman. Quantitative fluorescence resonance energy transfer measurements using fluorescence microscopy. *Biophysical Journal*, 74(5):2702–2713, 1998.

[49] S. Asunmaa and B. Steenberg. Beaten pulps and fiber-tofiber bond in paper. *Svensk Papperstidn*, 61(186):686–695, 1958.

[50] C.F. Yang, A.R.K. Eusufzai, R. Sankar, R.E. Mark, and R.W. Perkins Jr. Measurements of geometrical parameters of fiber networks. *Svensk Papperstidning,(13)*, pages 426–433, 1978.

[51] H.F. Jang, A.G. Robertson, and R.S. Seth. Optical sectioning of pulp fibers using confocal scanning laser microscopy. *Tappi Journal*, 74(10):217–219, 1991.

[52] K. Somwang, T. Enomae, and F. Onabe. Effect of Fiber Hornification in Recycling on Bonding Potential at Interfiber Crossings-Confocal Laser-scanning Microscopy. *Japan Tappi Journal*, 56(2):79–85, 2002.

[53] D.H. Page. Fibre-to-fibre bonds: Part 1 - A method for their direct observation. *Paper Technology*, 1(4):407–411, 1960.

[54] M. Wiltsche, M. Donoser, W. Bauer, and H. Bischof. A new slice-based concept for 3D paper structure analysis applied to spatial coating layer formation. *Proc. of the 13th Fundamental Paper Research Symposium*, pages 853–899, 2005.

[55] J. Kritzinger, M. Donoser, M. Wiltsche, and W. Bauer. Examination of Fiber Transverse Properties Based on a Serial Sectioning Technique. In *Progress in Paper Physics Seminar Proceedings, Helsinki*, page 152, 2008.

[56] M. Donoser and H. Bischof. Efficient maximally stable extremal region (MSER) tracking. In *Proceedings of the Conference on Computer Vision and Pattern Recognition*, pages 553–560. Citeseer, 2006.

[57] J. Kritzinger, M. Donoser, and W. Bauer. Representative analysis of fibre cross section properties using automated microtomy. In *Fundamental Research Communications, St. Annes's College, Oxford*, pages 28–31, 2009.

[58] W. Demtröder. *Experimentalphysik: Elektrizitat und Optik*. Springer Verlag, 2006.

[59] P.A. Moss, E. Retulainen, H. Paulapuro, and P. Aaltonen. Taking a new look at pulp and paper: applications of confocal laser scanning microscopy(CLSM) to pulp and paper research. *Paperi ja puu*, 75(1-2):74–79, 1993.

[60] H.F. Jang, A.G. Robertson, and R.S. Seth. Transverse dimensions of wood pulp fibres by confocal laser scanning microscopy and image analysis. *Journal of materials science*, 27(23):6391–6400, 1992.

[61] H.F. Jang, R. Amiri, R.S. Seth, and A. Karnis. Fiber characterization using confocal microscopy-collapsze behavior of mechanical pulp fibers. *Tappi Journal*, 79(4):203–210, 1996.

[62] H.F. Jang and R.S. Seth. Using confocal microscopy to characterize the collapse behavior of fibers. *Tappi Journal*, 81(5):167–174, 1998.

[63] H.F. Jang, G. Weigel, R.S. Seth, and C.B. Wu. The effect of fibril angle on the transverse collapse of papermaking fibres. *Paperi ja puu*, 84(2):112–115, 2002.

[64] J. He, W.J. Batchelor, R. Markowski, and R.E. Johnston. A new approach for quantitative analysis of paper structure at the fibre level. *Appita Journal*, 56(5):366–370, 2003.

[65] L. Xu, I. Parker, and C. Osborne. Technique for determining the fibre distribution in the z-direction using confocal microscopy and image analysis. *Appita journal*, 50(4):325–328, 1997.

[66] P.G. Auran. Surface structure analysis of paper based on confocal laser scanning microscopy (CLSM) imaging: aiming at the prediction of printability for wood-containing paper. In *Proceedings - SPIE The international society for optical engineering*, pages 161–169, 1998.

[67] L. Xu, I. Parker, and Y. Filonenko. A new technique for determining fibre orientation distribution through paper. In *TAPPI international Paper Physics Conference, San Diego, USA, Technical association of the pulp and paper industry*, 1999.

[68] A.T. Horvath, A.E. Horvath, T. Lindström, and L. Wågberg. Adsorption of Highly Charged Polyelectrolytes onto an Oppositely Charged Porous Substrate. *Langmuir*, 24(15):7857–7866, 2008.

[69] J. Neter, M.H. Kutner, C.J. Nachtsheim, and W. Wasserman. Applied linear statistical models . Illinois, IL: Richard D. Irwin, 1996.

Paper I

A novel method for the determination of bonded area of individual fiber-fiber bonds

Lisbeth Kappel, Ulrich Hirn, Wolfgang Bauer and Robert Schennach, Graz University of Technology, Austria

KEYWORDS: Fiber-fiber bond, Bonded area, Paper strength

SUMMARY: A method is presented for determining the bonded area of single fiber-fiber bonds, the method is based on microtome serial sectioning and image analysis. The size and three-dimensional structure of the bonded area are assessed together with cross sectional fiber morphology. Additionally, holes and overlapping but unbonded fiber regions can be measured.

87 fiber-fiber bonds from an unbleached and unbeaten softwood kraft pulp were analyzed. The statistical evaluation of the results showed that basic geometry (fiber width and crossing angle) explain only 55% of bonded area. Incomplete bonding (holes and overlapping but unbonded edges) additionally account for 27% of the bonded area, while fiber morphology only plays a minor role. This is a contradiction to the conventional theory that fiber conformability controls the bonded area in paper. An explanation for this might be that one cannot rationalize the three-dimensional network of paper directly from two-dimensional fiber-fiber bonds.

ADDRESSES OF THE AUTHORS:
Lisbeth Kappel (lisbeth.kappel@tugraz.at), **Ulrich Hirn** (ulrich.hirn@tugraz.at) and **Wolfgang Bauer** (wolfgang.bauer@tugraz.at): Graz University of Technology, Institute for Paper, Pulp and Fiber Technology, CD-Laboratory for surface chemical and physical fundamentals of paper strength, Kopernikusgasse 24, 8010 Graz, Austria.
Robert Schennach (robert.schennach@tugraz.at): Graz University of Technology, Institute for Solid State Physics, CD-Laboratory for surface chemical and physical fundamentals of paper strength, Petersgasse 16, 8010 Graz, Austria.
Corresponding author: Lisbeth Kappel

Paper strength is developed from the strength of single fibers and the strength of the fiber-fiber bonds. Furthermore, the strength of the fiber-fiber bonds depends on the size of the bonded area as well as on the specific bonding strength. Measuring the actual size of the bonded area helps to understand the governing factors for fiber-fiber bond strength. In this study the bonded area of individual fiber-fiber bonds and its distribution are investigated. We propose a novel method for determining the bonded area based on microtome serial sectioning of fiber-fiber bonds. Geometrical and morphological parameters of 87 single fiber-fiber bonds have been analyzed with statistical models in order to explain the factors that govern the size of bonded area.

Related research – preparation of fiber-fiber bonds
Various descriptions of how individual fiber-fiber bonds can be prepared are given in the literature. They are either based on manipulation of individual fibers or using a highly diluted fiber suspension.

McIntosh (1963), Thorpe at al. (1976) and Kang et al. (2004), prepared fiber-fiber bonds by placing two fibers (or one fiber and one shive) orthogonally on a glass slide in water and covering it with another glass slide. This sandwich was pressed and dried. Stratton (1992) placed two fibers at a right angle between two Teflon-coated discs under water. The fibers were clamped with tabs that were cut into the Teflon. The bonds were then dried under heat and pressure.

Mayhood et al. (1962) prepared fiber-fiber bonds by dewatering a very dilute suspension on a wire. After drying, single fiber-fiber bonds could be taken off the wire. Forsström, Torgnysdotter (2005) dried small drops of a very dilute fiber suspension between two Teflon-coated silicon discs under heat and pressure. Orthogonally crossed fibers were then selected from the small fiber mats.

Related research – determination of bonded area of fiber-fiber bonds
Several methods to analyze the bonded area of fiber-fiber bonds have been described in the literature. These methods can be grouped in *dyeing methods, microtome methods and polarization microscopy methods.* Torgnysdotter et al. (2007) dyed fiber-fiber bonds and then ruptured them. The un-dyed fiber surfaces were evaluated under the light microscope and considered as formerly bonded. Fluorescence microscopy was used by Thomson (2007). One fiber was dyed with a donor-fluorescence dye and one with an acceptor-fluorescence dye, so that under a fluorescence microscope bonded area becomes visible. Asunmaa, Steenberg (1958) and Yang et al. (1978) both used microtome cuts to determine the bonded fraction of the fiber surface by analyzing images of paper cross sections.

The most commonly used method was developed by Page (1960), who applied polarized light microscopy to determine the optically bonded area. He stated that bonded areas appear dark under vertical polarized illumination, while unbonded areas are bright. This method was also used by Jayme, Hunger (1961), who additionally analyzed broken bonds with electron microscopy and evaluated the roughness of the fiber surface.

Quantitative measurement of the bonded area has only been performed applying the method of Page (1960). These results will be addressed below in more detail. All other references did not give quantitative results for the bonded area, rather they provided qualitative information about the bond.

The method introduced in this paper provides additional information to the measurement of bonded area. It gives a more comprehensive view of fiber-fiber bonding,

because the bonded area is measured together with the morphological parameters of the fibers and the bonding region. Holes in the bond and overlapping but unbonded fiber edges can be identified correctly.

Materials and Methods

An unbleached softwood kraft pulp was used in all experiments. The pulp was a mixture from spruce and pine wood, it had a κ number of 42. The pulp was once-dried and unbeaten.

Preparation of fiber-fiber bonds

Fiber-fiber bonds were prepared from a dilute suspension, similar to the method described by Forsström, Torgnysdotter (2005).

Dry pulp was dispersed and allowed to swell in water for at least 12 hours. The fibers were disintegrated according to DIN EN ISO 5263-1.

A highly dilute suspension with a consistency of 0.01% was prepared. Small drops of the suspension were put on a piece of Teflon foil (4 cm x 4 cm), which was subsequently covered with another piece of Teflon foil. This sandwich was dried in a conventional sheet dryer for 45 minutes.

After drying, the thin fiber mats could be taken off the Teflon foil. From such fiber mats, seen in *Fig 1*, individual crossings were selected for further preparation (black circle mark).

Specimens were prepared as depicted in *Fig 2* (top). A single fiber-fiber bond was fixed with glue on a strip of paper across a hole. *Fig 2* (bottom left) shows a microscope image of such a fiber-fiber bond that is glued to a strip of paper. A magnification of this bond is shown in *Fig 2* (bottom right), with the crossing angle, α, and the vertical angle, β, shown.

Measurement of the bonded area

The method for the determination of the bonded area is based on microtome serial sectioning and image analysis. The size of the bonded area together with the three-dimensional structure of the bonded area and morphological fiber parameters can be obtained from this measurement.

The samples were embedded in a gelatin capsule using a cold-polymerizing resin based on hydroxyl-methyl-methacrylate (Technovit 7100[1]). After curing, the three-dimensional structure of the bonded region was analyzed using an automated microtomy system (Wiltsche et al. 2005). Slices having a thickness of 3 μm were sequentially cut off the embedded sample with the microtome. The cutting area was imaged automatically after every cut, pixel size was 0.161 μm. This process yields a stack of images of the fiber cross section, representing the three-dimensional shape of the fiber-fiber bond. In the images presented in following figures, the x- and y-coordinates correspond to the image plane, while the third coordinate is the slicing direction.
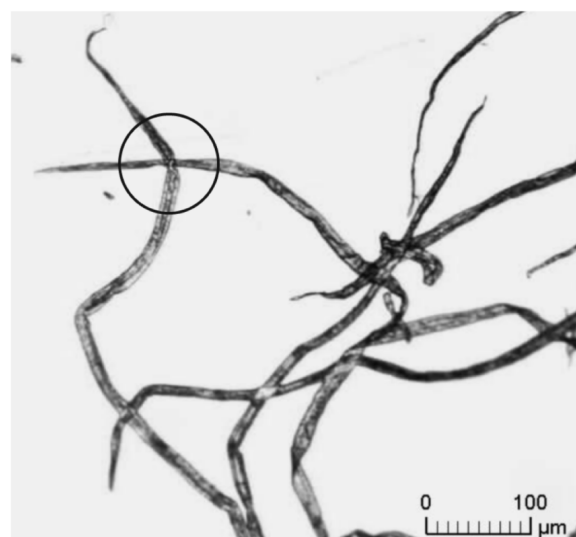
Fig 1. Thin fiber mat with orthogonally bonded fibers, which was used for measurement of the bonded area.
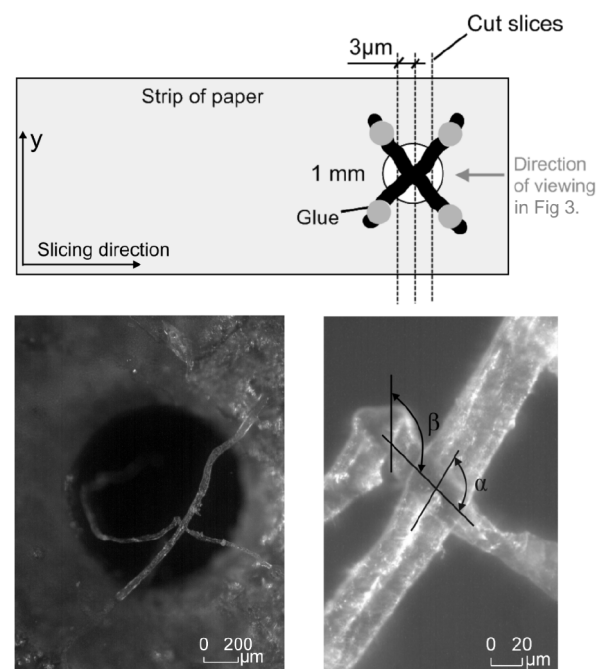
Fig 2. Top: A single fiber-fiber-bond fixed with glue on a strip of paper across a hole. Bottom left: Microscope image of a fiber-fiber bond glued across a hole. Bottom right: Image of the same bond as bottom left at higher magnification. The crossing angle, α, and the vertical angle, β, are drawn in.

Three light microscope images of the bond shown in *Fig 2* (bottom left) are presented in *Fig 3* at different cutting positions. The first image (*a.*) shows the edge of the bond, where the fiber contact region is small. The left fiber is fully collapsed and folded, whereas the right fiber is fully collapsed and unfolded. The following two images (*b.* and *c.*) proceed deeper into the bond. Because of the irregularity of the fold, the contact between the fibers is interrupted. *Fig 3* (*b.*) shows, that the fibers are separated in the upper part of the bond. In the next image (*c.*), the fibers are in contact over a greater length, although the contact is interrupted. Cut slices and the viewing direction of these images are also indicated in *Fig 2* (top).

Segmentation of the fiber regions was performed by
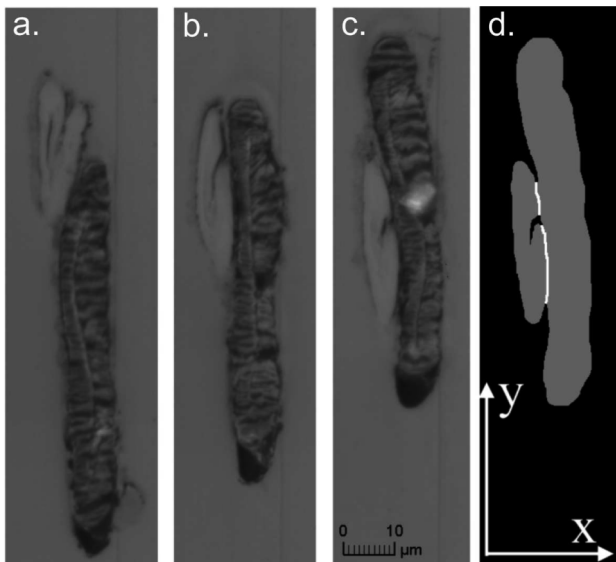
Fig 3. a., b., c.: Microscope images of fiber-fiber bond cross sections at different positions of the bond in *Fig 2* after microtome serial sectioning. d.: Manually segmented fibers from image c., the bonding line (white) was determined image analytically.

Fig 4. Three-dimensional representation of the bonded area. The bonding line for each cut is plotted, the distance between the lines equals the cut thickness (3 μm). The gray highlighted line corresponds to the bonding line in *Fig 3 (d.)*.

Fig 5. The run of the fiber cross section's center of mass through the cut slices defines the fiber main axis. This yields the crossing angle, α, and the vertical angle, β. The plot that is presented corresponds to the bond in *Fig 2* (bottom).

Fig 6. The angular face of a fiber cross section as it is seen in the images. The cutting area does not show the real fiber dimensions if the main fiber axis is not perpendicular to the x, y image plane, i.e. the vertical angle β does not equal π/2.

the operator, and the fiber outline was drawn into the microscope image by hand (*Fig 3d*).

The morphology of the bonded region and the fibers is determined from the fiber outline images using image analysis (*Fig 3d*).

For bonded area measurement, the fiber regions are considered to be bonded where the fibers in the microscope images are in direct contact. This region is determined using image analysis, resulting in a bonding line for every cut, as indicated by the white line in *Fig 3 (d)*. We are aware that the resolution of the optical microscope is too low to quantify whether the fibers are really in contact on a nanometer scale, we measure optically bonded area.

The bonded area is calculated from bond line length multiplied with the cut thickness (3 μm). It is inherently assumed that there is no change in bonding state in the cut slice, where no information is available.

A three-dimensional representation of the bonding region is obtained by plotting the bonding lines from each image taken within a bond (*Fig 4*). The rightmost line corresponds to the length where the fibers were in contact in the first cut (*Fig 3a*). The line which is marked gray belongs to the image in *Fig 3 (d)*. The interruption caused by the fold of the left fiber can be seen as break in the bonding line. The distance between the lines is equivalent to the cut thickness (3 μm).

Measurement of morphological parameters

In addition to bonded area, several morphological parameters of fibers and bonding region are measured from the images. Fiber cross sectional area, fiber perimeter, fiber wall thickness, fiber collapse, fiber width and incomplete bonding (holes and overlapping but unbonded edges) give comprehensive information regarding the fiber-fiber bond.

The position of the fiber cross section's center of mass through all cuts can be plotted for both fibers, which is shown in *Fig 5*. The main fiber axis is computed from

linear regression of the center of mass points. This yields the vertical angle, β, of each fiber, being the angle between the fiber axis and the image plane. Also, the crossing angle, α, between the fibers can be determined. *Fig 5* corresponds to the bond shown in *Fig 2* (bottom).

When the image plane is not perpendicular to the main fiber axis, the apparent fiber cross sectional area in the images is larger than the real area. The angular face that is seen in the image of the cutting area would therefore overestimate the real fiber dimension, as depicted in *Fig 6*.

The vertical angle, β, gives a reasonable approximation of the angle between image plane and main fiber axis. The real shape of the fiber cross section was computed from the apparent shape using a procedure similar to the

one described by Kritzinger et al. (2008). The apparent y-coordinate is transformed to the corrected y-coordinate, while the x-coordinate remains unchanged.

All morphological parameters were measured from this corrected fiber cross section.

Fiber width is measured directly as marked in *Fig 6*. For determining fiber wall thickness fiber collapse has to be considered. If the fiber is completely collapsed, the fiber wall thickness can be determined by dividing the fiber thickness by 2. Otherwise the uncollapsed lumen has to first be subtracted. Also, the fiber perimeter and cross sectional area are measured from the corrected fiber cross section. For quantification of the fiber collapse the fill factor was used (Kritzinger et al. 2008). The fiber cross sectional area is first determined with consideration of the lumen (A_L), as it is shown in *Fig 7* (left). Then the lumen area is filled, and the filled fiber cross sectional area (A_F) is determined (*Fig 7*, right). The fill factor is calculated using *Eq 1*.

$$Fill\ factor = \frac{A_L}{A_F} \qquad [1]$$

A fill factor of unity occurs if the fiber is completely collapsed. The fill factor becomes smaller with less fiber collapse.
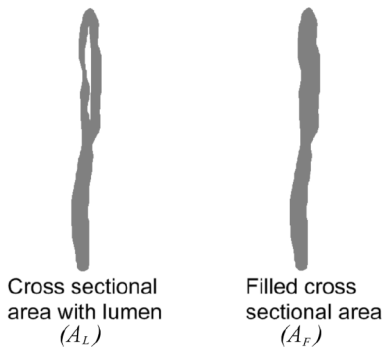
Fig 7. For the determination of fiber collapse, the fiber cross sectional area is first measured (A_L, left). Then the filled fiber cross sectional area is measured (A_F, right). Fiber collapse is the ratio of these two values (see *Eq 1*).

Cross sectional area with lumen (A_L)

Filled cross sectional area (A_F)

Three specific aspects of incomplete bonding have been evaluated: *holes, unbonded edge regions* of the bond and *fiber overlap area*. *Fig 8* shows the segmented fibers that are presented in *Fig 3*. In *Fig 8*, the bonded length (L_B) and unbonded edge length (L_{UE}) occur at both sides of the hole. *The total overlap length (L_O) is the maximum possible length that is available for bonding.* The hole fraction (F_H) and edge fraction (F_E) can be calculated to express incomplete bonding using *Eqs 2 and 3*.

$$F_H = \frac{L_H}{L_O} \qquad [2]$$

$$F_E = \frac{L_{UE}}{L_O} \qquad [3]$$

The corresponding areas (e.g. hole area) can be calculated by multiplying the various length scales with the cut thickness. For example, the bond in *Fig 4* contains one hole and unbonded parts at the edges of the bond (also see *Fig 3*). For this example, the hole fraction is 4.1% and edge fraction is 20.1%.
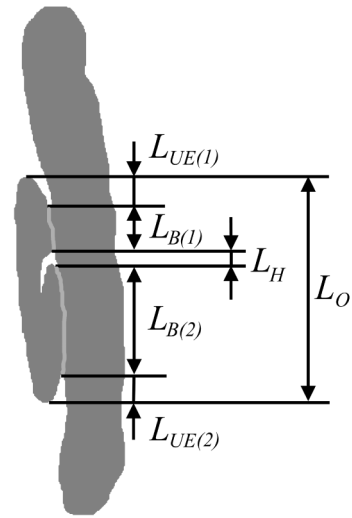
Fig 8. Diagram denoting the bonded length (L_B), hole length (L_H), unbonded edge length (L_{UE}) and the overlap length (L_O) that is available for bonding. The incomplete bonding can be calculated from these terms with *Eqs 2, 3 and 4*.

The hole fraction (F_H) and edge fraction (F_E) can further be combined to calculate the incomplete bonding ($B_{incomplete}$), as seen in *Eq 4*.

$$B_{incomplete} = F_H + F_E \qquad [4]$$

Results

The bonded area and morphological parameters of 87 fiber-fiber bonds of unbleached and unbeaten softwood kraft pulp were analyzed. Multiple linear regression modeling was performed to find factors influencing the size of bonded area.

The mean value for the bonded area was 1130 μm^2 and the standard deviation was 602 μm^2. *Fig 9* shows a histogram of all measured values of the bonded area. The distribution is positively skewed.

The origin of the strong variation and influencing factors on the size of bonded area are now discussed in greater detail.

Factors influencing the bonded area

Based on the measured bonded areas and morphological parameters, several factors that may affect the bonded area were investigated. Multiple linear regression was
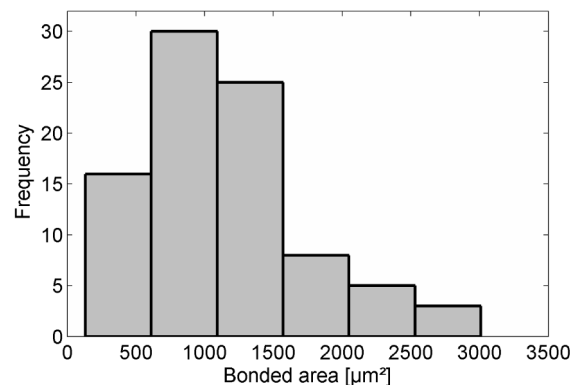
Fig 9. Histogram of values of the bonded area.
mean = 1130 μm^2, variance = 602 μm^2, skewness = 0.9495.

performed to quantify the significance (F*-statistics) and impact (ANOVA) of the explanatory variables (Neter et al. 1996). For this statistical analysis, the mean value of the morphological parameters of the two bonded fibers was taken.

Fig 10 shows that the bonded area depends to a large extent on the basic geometry, being the fiber width and the crossing angle.
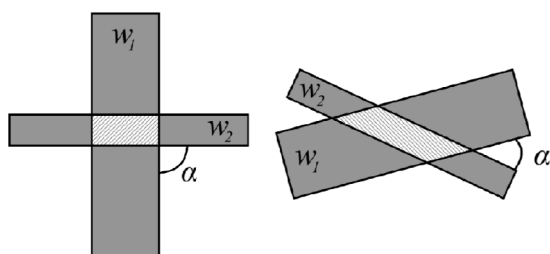
Fig 10. The basic geometric parameters crossing angle (α) and fiber width (w_1 and w_2) yield calculated bonded area, A_{calc}.

According to *Fig 10* the calculated bonded area, A_{calc}, is given by:

$$A_{calc} = w_1 \cdot w_2 \cdot \frac{1}{\sin \alpha} \qquad [5]$$

where w_1 and w_2 are the widths of the fibers and α is the crossing angle.

Apart from fundamental geometry, the parameters that govern the bonded area were found by multiple linear regression. A_{calc} and all of the measured morphological parameters were taken as predictor variables. The results of this model are listed in *Table 1*. The R^2 value is given for all parameters. Because of interactions and redundancies between the variables, interpreting this value is not straightforward. A parameter might have a significant R^2 value but still be redundant, because its information is also contained in other variables. In order to eliminate these redundancies a multiple variable linear regression model was built (Neter et al. 1996). The R^2 values are only given for the sake of completeness. Interpretations have been made on basis of the stepwise R^2 values, i.e. the ANOVA, of the linear multiple regression model. The p-Value shows the significance of the parameters on a 95% confidence level.

The significant parameters in *Table 1* have a white background, while some non-significant parameters that might be of interest are shaded gray.

Table 1. Results of multiple linear regression and ANOVA with the measured bonded area as the response variable and the calculated bonded area and morphological parameters as the predictor variables. Significant parameters have a white background, while non-significant parameters are shaded gray.

Variable	R^2 stepwise	R^2 alone	p-Value	Sign of Coeff.
A_{calc}	0.547	0.547	$<10^{-5}$	+
Edge fraction	0.853	0.280	$<10^{-5}$	-
Hole fraction	0.873	0.017	$<10^{-5}$	-
Fiber perimeter	0.879	0.219	0.027	-
Crossing angle	0.886	0.020	0.017	-
Fiber wall thickness	0.073	0.905		
Fiber collapse	0.018	0.149		
Fiber cross sectional area	0.017	0.934		

The R^2 value of the stepwise regression states that 54.7% of the size of bonded area can be explained in terms of the basic geometry of the bond, as the fiber width and crossing angle are accounted for in A_{calc}. An additional 30.6% of variance is explained by the unbonded edge regions, which is indicated by an increase from 0.547 to 0.853 of R^2 stepwise. Finally, the hole fraction explains another 2% of the variance. The signs of the model coefficients confirm the expected relationship: a high calculated bonded area (A_{calc}) corresponds to a larger bond area. A high edge fraction (F_E) and a high hole fraction (F_H) respectively correspond to smaller bond area.

The fiber perimeter and crossing angle together only explain 1.3% of variance. Although they are statistically significant, they only have a marginal impact. Other morphological parameters that should be related to conformability (fiber wall thickness, fiber collapse and fiber cross sectional area) are not significant on a 95% confidence level ($p > 0.05$), suggesting they did not significantly influence the bonded area.

In the linear model for the single fiber-fiber bonds, 87.3% of the variance in the bonded area is explained by basic geometry (A_{calc} accounts for 54.7% of the variance) and incomplete bonding (F_E and F_H, together account for 32.6% of the variance). It should be noted that the unbonded regions represented by F_H and F_E are not *causing* a reduction in the bonded area, rather they are the *result* of incomplete bonding in the overlapping regions of the fiber-fiber bond. The dominating effect was the unbonded regions at the edge of the bond, as their impact on the actual bond size is fifteen times larger than the effect of holes in the bond.

Fig 11 illustrates the fact that the potential bonded area was not fully exploited in the bonds that were examined. The plot compares the calculated bonded area (A_{calc}) with the measured bonded area. The diagonal indicates equal values. In most cases the bonded area was overestimated by the geometric calculations. The main reason for the deviations is incomplete bonding ($B_{incomplete}$), as previously discussed above and also seen in *Table 1*.
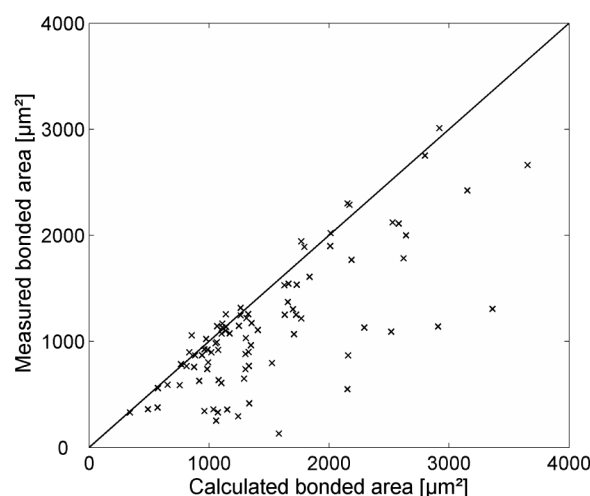
Fig 11. The calculated bonded area A_{calc} plotted versus the measured bonded area for each fiber-fiber bond. The geometric calculation overestimates the bonded area, which is mainly attributed to incomplete bonding ($B_{incomplete}$), compare *Table 1*.

Analyzing the influence of fiber morphology on incomplete bonding

The examined data set showed that the bonded area is to a large extent explained by basic geometry and regions that are unbonded, even though the fibers are overlapping (incomplete bonding, $B_{incomplete}$). The final step of the analysis is to determine which fiber morphological parameters might be responsible for these overlapping but unbonded regions.

Multiple linear regression was again performed, using incomplete bonding ($B_{incomplete}$) as the response variable and the morphological parameters as the predictor variables. *Table 2* shows which variables can be used to explain incomplete bonding ($B_{incomplete}$) (white) and which cannot (shaded gray).

Only 5.3% of the incomplete bonding ($B_{incomplete}$) can be explained by fiber collapse, which is related to fiber conformability. Fibers that easily collapse also usually have higher conformability. Still, a larger interrelation between conformability related fiber morphology and incomplete bonding of overlapping fiber parts was expected.

Table 2. Results of multiple linear regression and ANOVA with incomplete bonding ($B_{incomplete}$) as the response variable. The fiber morphological parameters were used as predictor variables. Significant parameters have a white background, while non-significant parameters are shaded gray.

Variable	R^2 stepwise	R^2 alone	p-Value	Sign of Coeff.
Fiber collapse	0.053	0.053	0.011	+
Fiber cross sectional area		0.010	0.092	
Fiber wall thickness		0.003	0.452	
Fiber width		0.004	0.722	
Crossing angle		0.005	0.230	
Fiber perimeter		0.004	0.968	

Discussion

Preparation of fiber-fiber bonds

When working with single fibers or single fiber-fiber bonds, the pre-selection of only a certain kind of fibers can be problematic. This is especially true when single fibers are manipulated, as straight and long fibers are more easily separated from the pulp. This effect is strongly reduced when the bonds are made from suspension. Still there occurs some pre-selection, only longer fibers were used in the present work, as the bonds must be glued across a hole with a diameter of 1 mm. This is only possible with fibers longer than approximately 3 mm.

The drops of suspension were dried in a conventional sheet dryer, and the pressing and drying conditions were similar to laboratory sheet forming.

Measurement of bonded area

To verify if the results for bonded area are in a realistic range, the bonded areas were compared to values given in the literature. The values given by Page et al. (1962) and Stratton (1992) cannot be directly compared, as a pulp with differing fiber diameter was used. Still, the distributions were similarly found to be positively skewed.

Mayhood et al. (1962) also used pulp from a mixture of spruce and pine. The pulp was produced from both, sulfite and kraft cooking, and the bonded area was determined for both pulps separately. The fiber-fiber bonds were also made from an unbleached and unbeaten pulp and dried in a sheet dryer without additional pressing. Polarized light microscopy had been used for the determination of bonded area, using the method developed by Page (1960). Mayhood et al. (1962) point out that polarized light microscopy gives more reliable results when flat and ribbon shaped springwood fibers are used. This is why only bonds of ribbon-shaped springwood fibers were analyzed. A comparison of the bonded areas from both methods is presented in *Table 3*. For both pulps (sulfite and kraft) the values for bonded area given by Mayhood et al. (1962) are clearly larger than ours (*Fig 9*). The standard deviation is also smaller. The pre-selection of only ribbon-shaped and collapsed springwood fibers might explain the differences between the measured values. There also might be a systematic increase in the size of the bonded area. If the fibers are fully collapsed, the fiber width will be larger. Calculation of the bonded area (A_{calc}) showed the significant influence of the fiber width. The restriction to only one type of fibers could also be the reason for the smaller standard deviation. However, this is only based on speculation as no objective evidence for this exists.

A benefit of the method used in the present study is that holes and unbonded regions can be correctly identified. Information is not available if holes in the bond cannot be detected with dyeing methods, for example, used by Torgnysdotter et al. (2007). According to Mayhood et al. (1962), it is also unclear whether holes in the bond can be identified with polarized light microscopy. The current results showed that holes in the bond only have a moderate size. Although percentage of the total bonded area due to holes was between 0 and 46.9%, the average value was only 5.1%. Thus it was found that

Table 3. Comparison of values for bonded area given in the literature with results from our measurements.

Author	Pulp	Fiber diameter	Method	Bonded area	Standard deviation	Skewness
(Mayhood et al. 1962)	Mixed spruce and pine sulfite pulp	25-45 µm	Polarized light microscopy	1591 µm^2	478 µm^2	NA
(Mayhood et al. 1962)	Mixed spruce and pine Kraft pulp	25-45 µm	Polarized light microscopy	2097 µm^2	321 µm^2	NA
(Kappel et al. 2009)	Mixed spruce and pine Kraft pulp	25-45 µm	Microtome serial sectioning	1130 µm^2	602 µm^2	0.9495

it is more important to measure incomplete bonding at the border of the bond than holes in the bond.

It has to be pointed out that only the optically bonded area was measured, since light microscopy was used. A 50x objective was used and the pixel size was 0.161 μm. Although the resolution was high enough to see details like fiber collapse, it is difficult to make any statement about actual bonding between the fibers on a nanometer scale, i.e. molecular contact.

It is believed that the bonded area in paper is mainly influenced by fiber morphology, namely the fiber conformability. However, a connection between fiber morphology and bonded area was not observed in this study. An explanation might be that the single fiber-fiber bonds that were examined are almost two-dimensional structures. In contrast, paper is a truly three-dimensional network. Conformability might not be so important to develop the bonded area in the two-dimensional case. The effect of beating or higher wet pressing during the sample preparation procedure still needs to be examined. In this case a stronger interrelation between fiber-fiber bonded area and morphology might be found. The results might also be different for hardwood pulp.

The main disadvantage of microtome methods is that the bonds are destroyed during the analysis, and further measurements cannot be performed. It would be possible with a non-destructive method to additionally measure, for example, the bonding force. This would allow the specific bond strength to be measured. Investigating the formerly bonded areas after rupturing the bond, as performed by Jayme, Hunger (1961), is not possible after microtome serial sectioning.

Conclusions

The proposed method seems to be a useful tool to investigate the bonded area as well as the morphology of the fiber cross sections and the bonding region. The method is able to measure the area of holes in the bond and overlapping but unbonded fiber regions. This combined measurement of fiber morphology and bonded area morphology might contribute to a comprehensive understanding of fiber-fiber bonding.

A comparison of the measured and geometrically calculated bonded area (only dependent on fiber width and crossing angle) showed great difference for an unbeaten, unbleached softwood kraft pulp. The actual bonded area was on average 60% lower than geometrically calculated bonded area. Incomplete bonding of overlapping fiber regions was mainly responsible for this difference. It occurred preliminarily at the edges of the bond. Holes in the bond had less impact.

Morphological fiber parameters that can be related to conformability (fiber wall thickness, fiber cross sectional area, fiber collapse) could not explain the bonded area and incomplete bonding. This stands in opposition to the papermaker's experience that fiber conformability controls bonded area. This leads to the conclusion that the currently used technique to prepare single fiber-fiber bonds does not reflect the development of bonded area in

paper sheets. Modified specimen preparation, potentially including beating and strong wet pressing, might deliver a closer similarity between development of the bonded area in paper, which is a three-dimensional structure, and development of the bonded area of single fiber-fiber bonds, which are almost two-dimensional structures.

Literature

Asunmaa, S. and Steenberg, B. (1958): Beaten Pulps and the Fibre-to-Fibre Bond in Paper, Svensk Papperstidning, 61, 686.

Forsström, J. and Torgnysdotter, A. (2005): Influence of fibre/fibre joint strength and fibre flexibility on the strength of papers from unbleached kraft fibers, Nord Pulp Paper Res. J. 20(2), 186.

Jayme, G. and Hunger, G. (1961): Electron microscope 2- and 3-dimensional classification of fibre bonding, in Formation and Structure of Paper, IInd Fundamental Research Symposium, Oxford, 135.

Kang, T., Paulapuro, H. and Hiltunen, E. (2004): Fracture mechanism in interfibre bond failure – microscopic observations, Appita J. 57(3), 199.

Kritzinger, J., Donoser, M., Wiltsche, M. and Bauer, W. (2008): Examination of Fiber Transverse Properties Based on a Serial Sectioning Technique, Progress in Paper Physics Seminar Proceedings, Helsinki, 157.

Mayhood, C.H., Kallmes, O.J. and Cauley, M.M. (1962): The Mechanical Properties of Paper Part II: Measured Shear Strength of Individual Fiber to Fiber Contacts, Tappi, 45(1), 69.

McIntosh, D.C. (1963): Tensile and Bonding Strengths of Loblolly Pine Kraft Fibers Cooked to Different Yields, Tappi, 46(5), 273.

Neter, J., Kutner, M.H., Nachtsheim, C.J. and Wassermann W. (1996): Applied Linear Statistical Models, Fourth Edition, Richard D. Irwin, Illinois (USA).

Page, D.H. (1960): Fibre-to-fibre bonds Part 1 – A method for their direct observation, Paper Technology, 1(4), 407.

Page, D.H., Tydeman, P.A. and Hunt, M. (1962): A Study of Fibre-to-Fibre Bonding by Direct Observation, in Formation and Structure of Paper, IInd Fundamental Research Symposium, Oxford, 171.

Stratton, R.A. (1992): Fundamentals of Internal Strength Enhancement Part 2 – Studies on the Bonding of Single Fibers, Progress Report, Institute of Paper Science and Technology, Atlanta, Georgia.

Thomson, C.I. (2007): Probing the Nature of Cellulosic Fibre Interfaces with Fluorescence Resonance Energy Transfer, PhD Thesis, Georgia Institute of Technology.

Thorpe, J.L., Mark, R.E., Eusufzai, A.R.K. and Perkins, R.W. (1976): Mechanical properties of fiber bonds, Tappi, 59(5), 96.

Torgnysdotter, A., Kulachenko, A., Gradin, P. and Wågberg, L. (2007): The Link Between the Fiber Contact Zone and the Physical Properties of Paper: A Way to Control Paper Properties, Journal of Composite Materials, 41(13), 1619.

Wiltsche, M., Donoser, M., Bauer, W., Bischof, H. (2005): A New Slice-Based Concept for 3D Paper Structure Analysis Applied to Spatial Coating Layer Formation, in Advances in Paper Science and Technology, Fundamental Research Symposium, Cambridge, 853.

Yang, C.F., Eusufzai, A.R.K., Sankar, R., Mark, R.E. and Perkins Jr, R.W. (1978): Measurement of geometrical parameters of fiber networks Part 1 – Bonded surfaces, aspect ratios, fiber moments of inertia, bonding state probabilities, Svensk Papperstidning, 13, 426.

Paper II

Revisiting polarized light microscopy for fiber-fiber bond area measurement - Part I: Theoretical fundamentals

Lisbeth Kappel, Ulrich Hirn, Eduard Gilli, Wolfgang Bauer and **Robert Schennach**, Graz University of Technology, Austria

SUMMARY: Polarized light microscopy is a powerful approach to measure the bonded area of fiber-fiber bonds, because it is a non-destructive measurement. Still the results are often misleading and hard to interpret. Part one of our study treats polarization microscopy for *undyed* fiber-fiber bonds. The results for bonds between one dyed and one undyed fiber are discussed in part two of the work.

In our study we offer a comprehensive fundamental understanding why polarization microscopy of undyed fiber-fiber bonds works better for fibers of equal fiber wall thickness and not good for wrinkled fibers or fibers with considerably different fiber wall thickness.

In order to understand the mechanism of polarized light microscopy we apply a physical model that simulates the path of light through the fibers and the microscope. We compare the results of this model to individual fiber-fiber bond specimens, which are analyzed with polarization microscopy. Additionally these specimens are embedded in resin and cut with a microtome and the cross section of the bond is investigated.

The combination of these three methods showed that polarized light microscopy only yields correct results if the fibers in the bond are parallel and have similar fiber wall thickness. However, the fibers do not necessarily have to be bonded to appear dark under the polarized light microscope. Also *unbonded*, parallel fibers with similar fiber wall thickness look dark under polarized light. All in all 59 fiber-fiber bonds were analyzed and in 63 % of all bonds polarized light microscopy yielded misleading results.

Still it is shown that, if the above conditions are fulfilled - i.e. the fibers are parallel and have similar thickness - polarized light microscopy gives the correct area of a fiber-fiber bond.

ADDRESSES OF THE AUTHORS: Lisbeth Kappel (lisbeth.kappel@tugraz.at), **Ulrich Hirn** (ulrich.hirn @tugraz.at) and **Wolfgang Bauer** (wolfgang.bauer @tugraz.at): Graz University of Technology, Institute for Paper, Pulp and Fiber Technology, CD-Laboratory for Surface Chemical and Physical Fundamentals of Paper Strength, Kopernikusgasse 24, 8010 Graz, Austria.
Eduard Gilli (gilli@tugraz.at) and **Robert Schennach** (robert.schennach@tugraz.at) Graz University of Technology, Institute for Solid State Physics, CD-Laboratory for Surface Chemical and Physical Fundamentals of Paper Strength, Petersgasse 16, 8010 Graz, Austria.
Corresponding author: Ulrich Hirn

Introduction

Paper strength depends on the strength of single fibers and on the strength of fiber-fiber bonds. This fiber-fiber bond strength again depends on the size of the bonded area and on the specific bonding strength. In order to measure specific bonding strength, bonded area has to be measured *non-destructively* before measuring bonding strength. Polarized light microscopy, as introduced by Page (1960), meets this criterion, which makes it a powerful approach for fiber-fiber bond area measurement.

Page (1960) states that under polarized vertical illumination bonded area appears dark while unbonded areas are bright. He investigated fiber-fiber bonds in thin sheets. In order to absorb unwanted reflections and light scattering from surrounding fibers 70 % of the fibers were dyed black using Chlorazol Black. Thus the bonds between the remaining undyed fibers became visible and bonds between one dyed and one undyed fiber showed exceptionally high contrast under the polarized light microscope (Page et al. 1962).

A drawback of polarization microscopy seems to be that it works better for some types of bonds and less good for others. Generally it was found that the appearance of bonded area tends to be more clearly dark if the fibers are ribbon-shaped and fully collapsed springwood fibers (Page et al. 1962). Mayhood et al. (1962) investigated undyed fiber-fiber bonds and found that the bonded area of bonds between two flat springwood fibers can be measured more accurately than when un-collapsed or wrinkled fibers are bonded. Schniewind et al. (1964) state that polarized light microscopy was not generally applicable for their undyed bonds, but they do not discuss the problem or give any explanation. Stratton, Colson (1990) investigated fiber-fiber bonds between one dyed and one undyed fiber, which they found to be unproblematic.

In summary polarized microscopy is a very powerful approach for fiber-fiber bond area measurement because it is non-destructive and thus permits successive measurement of bonding force between individual fiber-fiber bonds (Stratton, Colson 1990). Still it is unclear why it works well

for some types of fiber-fiber bonds and not so well for others.

In part one of this study we will clarify the physical mechanisms of bond area measurement with polarized light microscopy. We will provide an explanation why it works only for some types of fiber-fiber bonds. In this part we will investigate only bonds between undyed fibers. Although literature suggests that the method works better for bonds between dyed and undyed fibers, we first study undyed bonds to investigate the fundamental theoretical background without any changes in reflection and transmission due to the dye.

In part two of the study we will deal with bonds between one dyed and one undyed fiber. Based on the theoretical ideas developed in this paper we will explain why the method works better with bonds between dyed and undyed fibers.

In this paper we analyze individual fiber-fiber bonds between undyed fibers. The bonds are first imaged with polarized light microscopy, then embedded in resin and cut with a microtome. In this way the cross section of the fiber-fiber bond can be inspected and the result of polarized light microscopy can be verified. In order to understand the mechanism of polarized light microscopy we apply a physical model that simulates the path of light through the fibers and the microscope (Gilli et al. 2009). The results from this model are verified with empirical data. Based on the analysis of the fiber cross sections and the physical model we can provide a comprehensive interpretation of the polarization microscopy results.

Materials and Methods

All investigations were performed with an unbleached softwood kraft pulp. The pulp was a mixture from spruce and pine wood and was once-dried and unbeaten. The fiber-fiber bonds were made from suspension, as described in Kappel et al. (2009).

Polarized light microscopy for bond area measurement

Page (1960) introduced polarized light microscopy for bond area measurement of fiber-fiber bonds. The phenomenology of the method can be described as follows. Light is linearly polarized, so waves with only one plane of oscillation are directed through the objective and to the surface of the sample, where it is reflected. The second polarizing filter is rotated 90° towards the first one, so that only optically modified light is able to pass it. Light that is reflected at surfaces under vertical illumination does

not change its state of polarization. Therefore reflexes at surfaces are of negligible intensity. The geometry of the optical system at the fiber-fiber bond yields very small reflected over-all intensities, so that fiber-fiber bonds appear dark, while the inner reflection at the back surface of a single fiber yields reflected light with quite a high intensity and a changed polarization direction. Thus single fibers appear bright.

The visibility of the dark bonded area depends on the angle between the transmission axis of the polarizing filter and the fibers forming the bond. *Fig 1* shows eight different rotary positions of the fiber-fiber bond under the polarized light microscope. The drawing in the left upper corner of each image indicates the position of the strip of paper where the bond is fixed under the microscope. In this example dark bonded area is only observable if the fibers forming the bond enclose an angle of approximately 45° with the transmission axis of the polarizing filters. This has also been observed experimentally by Page (1960). This phenomenon can also be explained with the optical model, as will be discussed later.
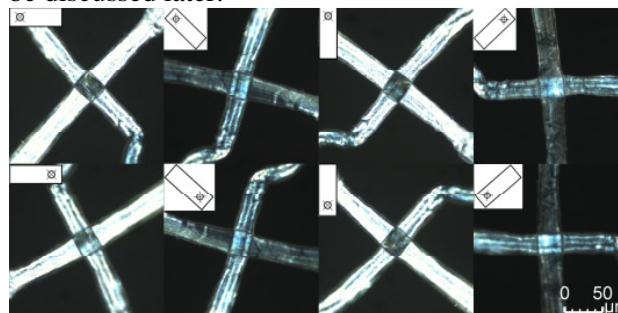
Fig 1. Dependence of the visibility of dark bonded area on the rotary position of the fiber-fiber bond under the polarized light microscope.

The polarized light microscopy investigations were performed with a Leica Leitz DMRX microscope[1], which was equipped with crossed polarizing filters. A 20-fold objective with an optical resolution of 0.255 µm/Pixel was used. The images were taken with a Leica DFC290 camera[1]. Each fiber-fiber bond was rotated and imaged in eight different positions, as shown in *Fig 1*. The image with highest contrast was used for further analysis.

Microtome method for three-dimensional bond area measurement

The method for the measurement of the three-dimensional bonded area is based on microtome serial sectioning and image analysis. A detailed description of the method can be found in Kappel et al. (2009). Here only the most important steps are described.

---

[1] http://www.leica-microsystems.com/

A single fiber-fiber bond is embedded in resin and clamped in a microtome. Slices with a thickness of 3 µm are cut off the embedded sample and the cutting area is imaged using an automated light microscope with an optical resolution of 0.161 µm/Pixel. *Fig 2* shows an image of a fiber-fiber bond cross section. The area where the fibers are in optical contact is determined image analytically, yielding a bonding line for every cut, as it is indicated by the white line in *Fig 2*. Bonded area is calculated from bond line length and cut thickness. A three dimensional visualization of the bonding region is obtained by plotting these consecutive bonding lines (*Fig 2*, right).
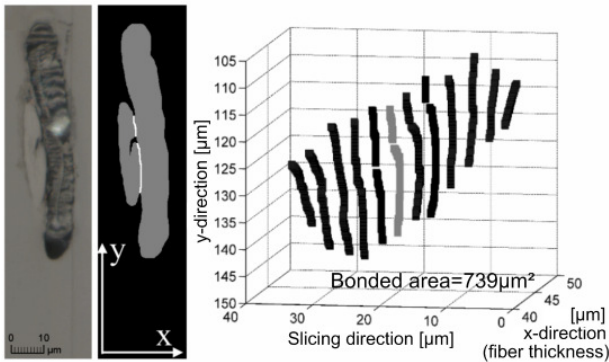
Fig 2. Fiber-fiber bond cross section after microtome serial sectioning and after image analysis and visualization of the 3D bonding area.

An optical model for fiber-fiber bonds under polarized light

An optical model describing reflection and transmission at pulp fiber surfaces under polarized vertical illumination has been developed (Gilli et al. 2009). The model applies the Jones formalism and calculates the run of the time averaged light waves through the fibers and the microscope. The formalism considers phase shift in the fiber bulk and at interfaces. Furthermore the model employs Fresnel's formulas for calculation of light intensities returned at different interfaces (fiber-air, different fiber walls). The model gives a *quantitative* prediction of the light collected in the camera, thus it is able to calculate if a fiber-fiber bond looks dark or bright. The calculations yield the mean intensities of the reflected light for plane parallel layer systems. The big advantage of this formalism is the possibility to combine different layers by multiplication of the corresponding Jones matrices, which allows the modelling of the layered structure of fiber-fiber bonds. A detailed mathematical description as well as verification of the model results can be found elsewhere (Gilli et al. 2009).

Fig 3 (left) shows a fiber-fiber bond and a dashed line indicating the cross section depicted in *Fig 3* (right). The hatching refers to the fiber walls (////

lower fiber wall, \\\\ upper fiber wall). Each wall is modelled separately considering that the refractive index in the fiber walls is anisotropic. The refractive indices in longitudinal and transversal direction of a pulp fiber are given in the literature with n_l=1.618 and n_t=1.554 (Brandrup, Immergut 1975). As the S2-layer of the fiber forms 80-90% of the fiber wall, it dominates the physical properties of the fiber (Wang et al. 2001). This is why the other layers (P-, S1- and S3-layer) are not taken into account in the calculation. It is assumed that a collapsed fiber can be approximated as consisting of two oriented layers. The fibril angle determines the direction of the optical axis of each layer (Bestsense, Ye 1995), so the polarization main axis is parallel to the fibril angle. For springwood fibers fibril angles between 20° and 30° are given by Gullichsen, Paulapuro (2000), so the fibril angle in our calculations was set to 25°.

In *Fig 3* the resulting Jones vectors (E_1-E_5) show where light is reflected: at the outer surfaces of the fibers, at the interface between upper and lower fiber wall (collapsed lumen) and at the fiber-fiber interface. The intensities of these reflections are calculated and give a good prediction of how fiber-fiber bonds with varied geometries and fiber morphologies will appear under the polarized light microscope.

Calculations were performed assuming that the fibers are completely collapsed and lying flat one upon the other.
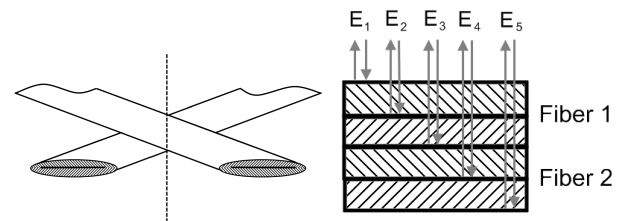
Fig 3. Fiber-fiber bond cross section and possible reflections at surfaces and interfaces that are considered in the calculation.

The model calculations help to predict the intensities of the reflections E_1 to E_5. E_1 is a normal surface reflex and thus its polarization is not altered. Therefore E_1 is completely filtered by the analyzer. The intensities of the vectors E_2, E_3 and E_4 tend to zero due to very small reflectivities at the respective interfaces between media of similar refractive indices. The phase of E_5 is shifted in respect to E_1 by the optical anisotropy of the fiber bulk. This shift depends to some extent on the fiber wall thickness of the bonded fibers, thus at certain fiber wall thickness configurations the phase shift of E_5 reaches 180° and bonded area appears dark. The influence of fiber wall thickness configuration on

the effect of dark bonded area will be addressed in more detail later.

Results

Model results

Page (1960) found that the contrast in the polarized light microscopy images can be influenced by rotating the fiber-fiber bond under the microscope. This is shown experimentally in *Fig 1*, the visibility of the effect of dark bonded area depends on the angle enclosed by the polarizing filter and the fibers forming the bond. At an angle of about 45° bonded area appears dark, while it is bright at an angle of 90°. The computation of this angle dependency is shown in *Fig 4*. Depending on the rotation of the optical axes the polarization direction of the reflection E_5 changes due to differences in phase shifts. Therefore also the intensity transmitted through the analyzer changes. These results indicate that the model yields correct predictions of the returned light intensity of fiber-fiber bonds under the polarized light microscope.
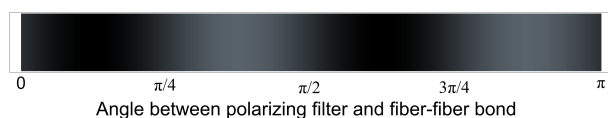
Fig 4. Computation of the returned intensity depending on the rotary position of the fibers forming the bond under the polarized light microscope. Bonded area shows the highest contrast at an angle of approximately 45°.

Comparison of theoretical and experimental results

The optical model allows predicting the behaviour of fibers and fiber-fiber bonds under the polarized light microscope. To verify these predictions fiber-fiber bonds were first analyzed with polarized light microscopy and then cut with the microtome to get images of the bond cross sections. The combination of these three methods explains why the effect of dark bonded area is not always observable under the polarized light microscope. The fundamentals of the method together with its restrictions and benefits are clarified.

For the discussion of the results the fiber-fiber bonds are divided into four distinct forms of appearance, as these four cases behave differently under the polarized light microscope. These distinct forms of appearance are:

1. bonds between two completely collapsed springwood fibers, lying flat one upon the other
2. bonds between fibers with unequal fiber wall thickness, lying flat one upon the other
3. bonds between fibers where one or both fibers are folded and
4. partly or completely unbonded but parallel fibers.

Bonds between two completely collapsed springwood fibers, lying flat one upon the other

Fig 5 (left) shows an example of a bond between two completely collapsed springwood fibers that lie flat one upon the other. This fiber-fiber bond resembles a system of plane parallel plates with equal layer thickness. This type of bonds appears dark under the polarized light microscope (*Fig 5*, right). The reflected light waves behave as it is described above using the example in *Fig 3*. So in this case polarized light microscopy yields correct results, as it has been suggested in the literature (Mayhood et al. 1962, Page et al. 1962). The optical model also predicts that this type of fiber-fiber bonds shows dark bonded area under the polarized light microscope.
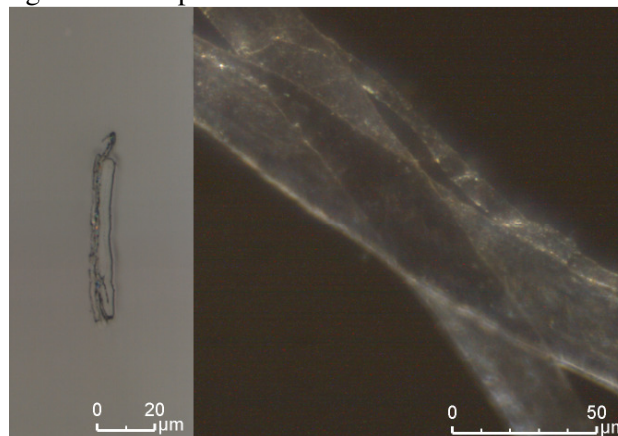
Fig 5. Fiber-fiber bond between two completely collapsed springwood fibers, lying flat one upon the other. The effect of dark bonded area is visible under the polarized light microscope.

Bonds between fibers with unequal fiber wall thickness, lying flat one upon the other

Fig 6 (left) shows the cross section of a bond between two flat and collapsed fibers that are completely bonded. However, bonded area does not appear dark under the polarized light microscope (*Fig 6*, right). Model calculations showed that the unequal fiber wall thickness is responsible for this misleading result.
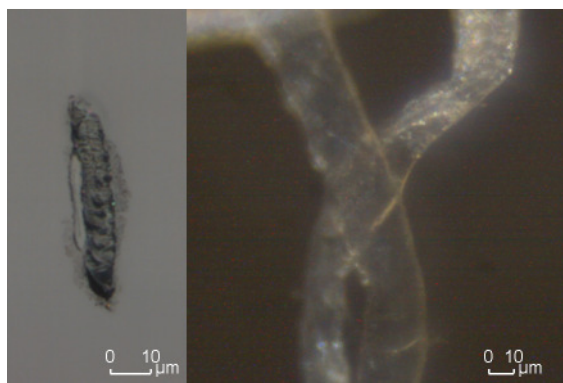
Fig 6. Fiber-fiber bond between two completely collapsed fibers, lying flat one upon the other, with unequal fiber wall thickness. The effect of dark bonded area is not visible under the polarized light microscope.

The physical explanation for this phenomenon is that the reflection E_5 (see *Fig 3*) changes its phase shift, depending on the ratio of the fiber wall thicknesses. This means that bonded area only looks dark under the polarized light microscope if the fiber wall thicknesses of the bonded fibers are either equal or at a certain ratio. For a wide range of unequal fiber wall thickness configurations polarized light microscopy suggests that the fibers are unbonded.

Model calculations were performed with varying fiber wall thickness of both fibers to verify this explanation. Modelling results are shown in *Fig 7* (right), the x and y axes give the fiber wall thickness and the color coding directly illustrates the intensity of the returned light. If the fibers have similar fiber wall thickness, the intensity of reflection is low and so bonded area appears dark in the polarized light microscope. This is confirmed experimentally as shown in example A in *Fig 7*. The fiber-fiber bond cross section shows that both fibers have almost the same fiber wall thickness, a dark bonded area is evident in polarized light microscopy. Example B refers to unequal fiber wall thickness. The bonded area does not appear dark in the polarized light microscope. This result is in good agreement with the calculated intensity of over all reflection, as marked in the plot in *Fig 7* (right).
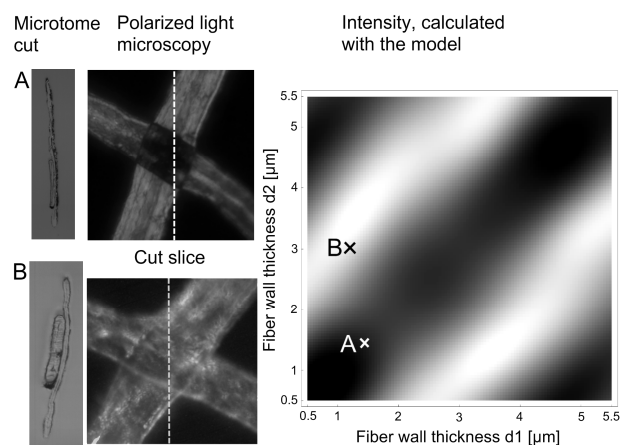
Fig 7. Comparison of microtome cuts (left), the according bonds under polarized light microscope (middle) and the modeled light remission (right).

Bonds between fibers where one or both fibers are folded

An example for a fiber-fiber bond where both fibers are folded is shown in *Fig 8*. The microtome image (left) shows that the fibers are completely bonded, but the polarized light microscope image on the right suggests that the fibers are at least partly unbonded, the lower part of the bonding region (marked with the black arrow) is even brighter than the unbonded fiber surfaces. However, the region above the bond appears as dark as part of the bonding region. This indicates that the fold resembles bonded fibers and cannot always be distinguished from the actual fiber-fiber bond.
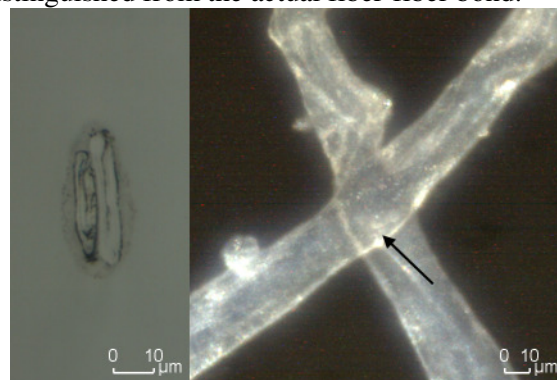
Fig 8. Fiber-fiber bond between two folded fibers. The effect of dark bonded area is only partly visible under the polarized light microscope due to additional phase shifts and reflections caused by the fold.

The folded fibers in the bonding region disturb the system of plane parallel plates with equal thickness, so the defined configuration, as described in *Fig 3* is no longer valid. The folds cause additional phase shifts and reflections so that dark bonded area is in many cases not observable.

5

Partly or completely unbonded but parallel fibers

Fig 5 showed that the bonded fibers have to resemble plane parallel plates with equal thickness to show dark bonded area under the polarized light microscope. However, even if this requirement is fulfilled, the fibers do not necessarily have to be bonded to look dark under polarized light, as it is shown in *Fig 9* and *Fig 10*. The microtome image in *Fig 9* (left) shows that the fibers are unbonded in the upper part of the bond. The white bonding line in the label image (middle) highlights where the fibers are bonded. Still, in the polarized light microscope image on the right it seems as if the fibers were completely bonded. Even though part of the bonding region is slightly brighter, the entire crossing region is framed dark, suggesting that at least the fiber edges were completely bonded.
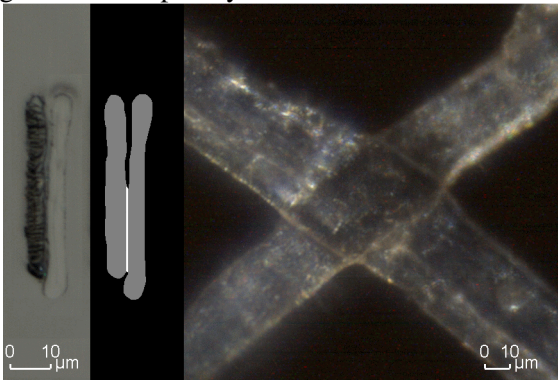
Fig 9. Partly unbonded fibers, parallel and lying flat one upon the other. The polarized light microscope image suggests that most parts of the fibers are bonded.

This effect is shown even clearer in *Fig 10*, where the fibers are not even close to each other, nevertheless the crossing region appears dark in the polarized light microscope image on the right.
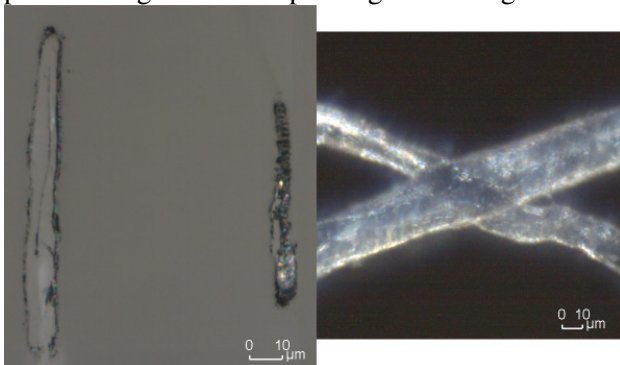
Fig 10. Completely unbonded and parallel fibers. The polarized light microscope image shows a dark crossing region and suggests that the fibers are bonded.

The optical model provides an explanation why crossed but unbonded fibers may appear dark under the polarized light microscope as long as they resemble plane parallel plates with equal fiber wall thickness. In the case of crossed but unbonded

fibers, an additional reflection (E_6) has to be considered in the calculation, as shown in *Fig 11*.
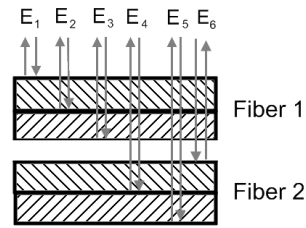
Fig 11. Fiber-fiber crossing (unbonded fibers) with possible reflections at surfaces and interfaces that are considered in the calculation.

The reflection E_3 occurs at an interface from a medium with a higher refractive index to a medium with a lower refractive index (internal reflection), for E_6 this is vice versa (external reflection). So E_6 is shifted by 180°, while E_3 is not. All the other parts of the optical path of E_3 and E_6 are identical because the air gap does not alter the polarization state. So the phase shift of E_6 leads to a negative interference between E_3 and E_6, they are cancelling each other, resulting in a dark appearance of this region. So unbonded, but parallel fibers (or fiber regions), may look dark under the polarized light microscope, just as bonded fiber regions.

Quantifying the amount of correctly analyzed bonds

The results above show that only certain types of bonds will be analyzed correctly by polarized light microscopy. In order to quantify the amount of bonds that may be analyzed correctly 59 fiber-fiber bonds were examined with polarized light microscopy and with microtomy. A classification into the four distinct forms of appearance as shown in *Fig 5* to *Fig 10* was performed, the results are given in *Fig 12*. Among all bonds only 12 (20 %) were bonds between two completely bonded, collapsed, flat spring wood fibers, showing dark bonded area. At 10 samples (17 %) there was no bonding and the crossing region did not appear dark, as the fibers were not parallel. In these two cases (shaded dark in *Fig 12*) polarized light microscopy was reliable. But in all other cases (63 % of the samples) polarized light microscopy yielded incorrect results (shaded bright in *Fig 12*). Either the bonded area did not appear dark because the fiber wall thicknesses were not in a proper ratio (25 %) or the fibers were folded in the bonding region (27 %) so that the effect of dark bonded area was disturbed or fibers were unbonded and parallel and therefore showed dark in the crossing region (10 %), suggesting bonding.
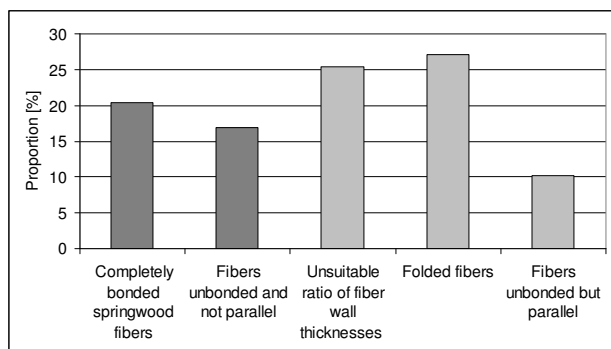
Fig 12. Proportion of bonds in the distinct forms of appearance. Bonds where polarized light microscopy yields correct results are shaded dark, bonds where it yields incorrect results are shaded bright.

Comparison of size of bonded area

Polarized light microscopy seems to work correctly if the fiber-fiber bond resembles a system of plane parallel plates with equal fiber wall thickness. As an example bonded area was first measured by polarized light microscopy and then re-measured with microtome serial sectioning as described in Kappel et al. (2009). A comparison of the results is shown in *Fig 13*. The values for bonded area are given below the respective image of the bonded area and show good agreement.
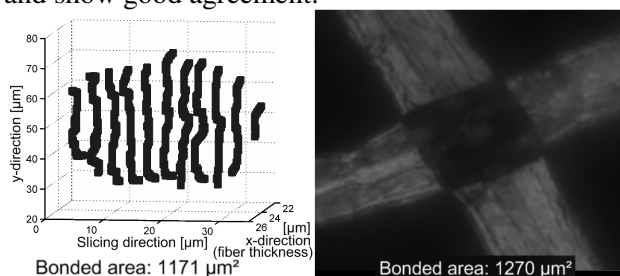
Fig 13. Comparison of shape and size of bonded area measured with microtomy (left) and polarized light microscopy (right).

However, this good agreement of the results only exists if the borders of the fibers are completely bonded, as unbonded but parallel fiber edges might be evaluated as bonded with polarized light microscopy as shown in *Fig 9*. Even a small unbonded border area of the bond will cause quite high deviations in size of bonded area.

Conclusions

Polarized light microscopy is a powerful approach for measuring bonded area of fiber-fiber bonds, especially because the measurement is non-destructive. However, if the method is applied to undyed fiber-fiber bonds it may yield misleading results. The work introduced in this paper has offered a comprehensive interpretation of the shortcomings of polarization microscopy for the analysis of *undyed* fiber-fiber bonds. Results of

polarization microscopy were compared to microtomy of the bond cross sections and results from an optical model that calculates the light remission of fiber-fiber bonds in polarized light microscopy. Both, theoretical and empirical results suggest that undyed fiber-fiber bonds do look dark under polarized light if the fibers have equal fiber wall thickness and if they are parallel. Nevertheless even in that case the results are not totally reliable, as also the crossing region of parallel but unbonded fibers will show dark under the polarized light microscope. Furthermore it could be demonstrated that bonded fibers, that are folded or have considerably differing fiber wall thickness will appear unbonded in polarized light microscopy.

All in all 59 undyed fiber-fiber bonds were analyzed with the polarized light microscope and then cut with the microtome to get additional information on fiber cross sectional morphology in the bonding region. In 63 % of all samples polarized light microscopy yielded incorrect results, as either bonded fibers showed bright or unbonded fibers appeared dark.

Literature

Bestsense, O. and Ye, C. (1995): Method and device for determining the orientation angle of the optical axis and the relative phase retardation of a birefingent specimen, International Patent Number: WO 96/10168.

Brandrup, J. and Immergut, E. (1975): Polymer Handbook, Wiley, New York.

Gilli, E., Kappel, L., Hirn, U. and Schennach, R. (2009): An optical model for polarization microscopy analysis of pulp fibre-to-fibre bonds, Composite Interfaces 16 (2009) 5, S. 901 - 922.

Gullichsen, J. and Paulapuro, H. (2000): Forest Products Chemistry, in Fapet Oy, Book 3, 24.

Kappel, L., Hirn, U., Bauer, W. and Schennach, R. (2009): A novel method fort he determination of bonded area of individual fiber-fiber bonds, Nordic Pulp and Paper Research Journal, 24 (2), 199.

Mayhood, C.H., Kallmes, O.J. and Cauley, M.M. (1962): The Mechanical Properties of Paper Part II: Measured Shear Strength of Individual Fiber to Fiber Contacts, Tappi, 45 (1), 69.

Page, D.H. (1960): Fibre-to-fibre bonds Part 1 – A method for their direct observation, Paper Technology, 1(4), 407.

Page, D.H., Tydeman, P.A. and Hunt, M. (1962): A Study of Fibre-to-Fibre Bonding by Direct Observation, in Formation and Structure of Paper, IInd Fundamental Research Symposium, Oxford, 171.

Schniewind, A.P., Nemeth, L.J. and Brink, D.L. (1964): Fiber and Pulp Properties Part I. Shear Strength of Single Fiber Crossings, Tappi, 47 (4), 244.

Stratton, R.A. and Colson, N.L. (1190): Dependence of Fiber/Fiber Bonding on Some Papermaking Variables, IPST Technical Paper Series, Institute of Paper Science and Technology Atlanta, Georgia.

Wang, H.H., Drummond, J.G., Reath, S.M., Hunt, K. and Watson, P.A. (2001): An improved fibril angle measurement method for wood fibres, Wood Science and Technology, 34, 493.

Paper III

Revisiting Polarized Light Microscopy for Fiber-Fiber Bond Area Measurement - Part II: Proving the Applicability

Lisbeth Kappel, Ulrich Hirn, Eduard Gilli, Wolfgang Bauer and **Robert Schennach**, Graz University of Technology, Austria

SUMMARY: In this paper the applicability of polarized light microscopy for fiber-fiber bond area measurement is investigated. Fiber-fiber bonds between one dyed and one undyed fiber were first analyzed with the polarized light microscope. Then the bonds were cut with the microtome to obtain a series of cross sectional images of the bond. Polarized light microscopy images and cross sectional images were compared and bonded area was measured with both methods. For the pulp used in this study the results showed good agreement although it is shown that bonded area is overestimated with polarized light microscopy by an average of 12.5%.

Some results were additionally computed with an optical model that describes the behavior of fibers and fiber-fiber bonds under polarized light. The combination of theoretical results and measurements provide a comprehensive understanding of the fundamental theory of polarized light microscopy for fiber-fiber bond area measurement. Specifically the results explain why polarization microscopy does *not* work for undyed fiber-fiber bonds but *does* work for bonds with one dyed fiber.

Provided that a factor for overestimation is considered, polarized light microscopy proved to be a suitable method for fiber-fiber bond area measurement.

ADDRESSES OF THE AUTHORS: Lisbeth Kappel (lisbeth.kappel@tugraz.at), **Ulrich Hirn** (ulrich.hirn @tugraz.at) and **Wolfgang Bauer** (wolfgang.bauer @tugraz.at): Graz University of Technology, Institute for Paper, Pulp and Fiber Technology, CD-Laboratory for Surface Chemical and Physical Fundamentals of Paper Strength, Kopernikusgasse 24, 8010 Graz, Austria.
Eduard Gilli (gilli@tugraz.at) and **Robert Schennach** (robert.schennach@tugraz.at) Graz University of Technology, Institute for Solid State Physics, CD-Laboratory for Surface Chemical and Physical Fundamentals of Paper Strength, Petersgasse 16, 8010 Graz, Austria.
Corresponding author: Ulrich Hirn

Introduction

Paper strength depends on the strength of single fibers and on the strength of fiber-fiber bonds. This fiber-fiber bond strength again depends on the size of the bonded area and on the specific bonding strength. In order to measure specific bonding strength, bonded area has to be measured *non-destructively* before measuring bond strength. Polarized light microscopy, as introduced by Page

(1960), meets this criterion, which makes it a powerful approach for fiber-fiber bond area measurement.

In part one of our study we investigated fiber-fiber bonds between *undyed* fibers. However, in this approach polarized light microscopy yielded incorrect results in more than 60 % of all cases. According to the theoretical and experimental results we identified four different types of fiber-fiber bonds.

1. Bonds between two completely collapsed springwood fibers, lying flat one upon the other: In this case the bond resembles a system of plane parallel plates with equal thickness and *polarized light microscopy yields correct results*, bonded area appears dark.
2. Bonds between fibers with unequal fiber wall thickness, lying flat one upon the other: Model calculations showed that the fiber wall thickness of the bonded fibers has to be equal or at a certain ratio, as the intensity of returned reflection depends on the fiber wall thickness configuration. Experiments confirmed that bonded area does not always look dark, even though the fibers are bonded.
3. Bonds between fibers where one or both fibers are folded: The folds in the bonding region cause additional reflections and phase shifts of the light, the fibers are not plane parallel. In most cases the bonded area does not appear dark.
4. Partly or completely unbonded fibers: Model calculations as well as experimental results showed that *unbonded* but parallel fibers show a dark crossing region under the polarized light microscope. This leads to incorrect interpretation of unbonded crossed fibers as bonded and to overestimation of bonded area if the fiber edges are not completely bonded.

To analyze bonds between one dyed and one undyed fiber seems to be a more promising method. Page (1960) investigated fiber-fiber bonds in thin sheets. 70 % of the fibers were dyed black using Chlorazol Black. This was aimed to absorb unwanted reflections and light scattering from surrounding fibers. He observed that bonds between one dyed and one undyed fiber showed exceptionally high contrast under the polarized light microscope. Based on these findings Stratton, Colson (1990) applied polarized light microscopy to bonds between one dyed and one undyed fiber, which they found to work well.

We will discuss each of the four cases of fiber-fiber bonds introduced above. Based on the theoretical ideas developed in part one of this study we will provide an explanation why polarization microscopy works well with bonds between one dyed and one undyed fiber. Finally a quantitative comparison between bonded area measured with polarized light microscopy and bonded area measured with microtomy will be given. It shows that bonded area is overestimated with polarized light microscopy.

Materials and Methods

Fiber-fiber bonds between one dyed and one undyed fiber were first analyzed with the polarized light microscope. Then they were embedded in resin and serially sectioned with a microtome to examine the cross section of the bond. Bonded area was measured with the microtome method (Kappel et al. 2009). The shape and the size of the bonded area measured with polarized light microscopy and with the microtome method were compared.

To explain the experimental observations some results of polarized light microscopy were additionally discussed using a physical model (Gilli et al. 2009). The model simulates the path of light through the fibers and the microscope and calculates the brightness of the bonded area under polarized light microscopy.

A description of the applied methods is given in part one of our study.

All experiments were performed with an unbleached softwood kraft pulp. The pulp was a mixture from spruce and pine wood and was once-dried and unbeaten. 50 % of the fibers were dyed with Chlorazol Black.

Dyeing of the fibers

Page (1960) dyed 70 % of the fibers with Chlorazol Black, the same dye was used in these trials. For lack of further indications in the literature, an appropriate procedure for dyeing of the fibers was developed. 1 g of the powdered dye was added to 100 ml ethanol (96%) and stirred for 30 minutes under environmental conditions. Because of the poor swellability of the pulp in ethanol, the pulp was allowed to swell in de-ionized water for 15 hours before dyeing. The pulp was dewatered to a dry solids content of 20 % and subsequently completely covered with the dye. The pulp remained in the dye for one hour under environmental conditions and was stirred several times. Then the excess dye was removed and the pulp was washed until the filtrate was absolutely clear.

For bond formation the dyed and the undyed pulp were mixed in equal shares and fiber-fiber bonds were made from suspension, as described in Kappel et al. (2009).

Bond area measurement with polarized light microscopy

Equipment and imaging procedure were the same as described in Part 1, with the only difference that now the upper and the lower side of the bond were imaged, as the method works much better if the dyed fiber lies beneath the undyed fiber. *Fig 1* shows the influence of the position of the dyed fiber. In the left image the dyed fiber lies beneath the undyed fiber, the contrast is high and bonded area is clearly darker than the rest of the fibers. In the right image the dyed fiber lies above the undyed fiber. The contrast is lower and bonded area does not show as clearly as in the left image.
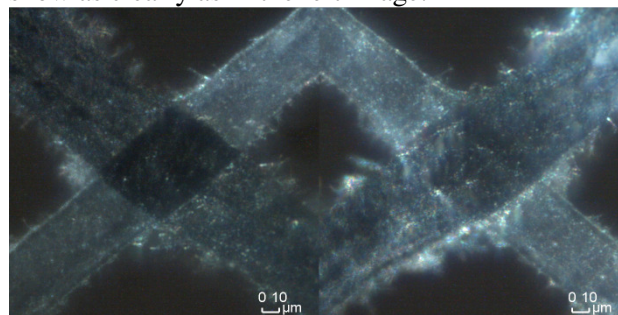
Fig 1. Polarized light microscopy image of a fiber-fiber bond. Left: dyed fiber lies beneath the undyed fiber, right: dyed fiber lies above the undyed fiber.

After the bond had been imaged in eight different rotary positions from both sides, the image with the highest contrast was chosen for further analysis and bond area measurement.

For bond area measurement the dark area in the microscope images was digitally drawn by hand. The amount of pixels in this area was counted image analytically and bond area was calculated.

An optical model for fiber-fiber bonds under the polarized light microscope

Fig 2 shows the cross section of a fiber-fiber bond where the lower fiber is dyed. As in Part 1 the hatching refers to the fiber walls (//// lower fiber wall, \\\\ upper fiber wall). The vectors E_1-E_5 show where light is reflected: at the outer surfaces of the fibers at the interface between upper and lower fiber wall (collapsed lumen) and at the fiber-fiber interface. According to the model of Gilli et al. (2009) E_1 is completely filtered by the analyzer, as it is a normal surface reflex and its polarization is not altered. The reflections E_2, E_3 and E_4 are almost zero, as they are reflected at interfaces between media of similar refractive indices. The reflection E_5 is almost completely absorbed by the black dye, so

its intensity tends to zero. All five reflections are either very small or filtered by the analyzer in the microscope so independently of the fiber morphology and of the bonding geometry, bonded area looks dark.
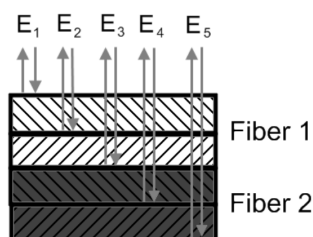
Fig 2. Cross section of a fiber-fiber bond between one dyed and one undyed fiber and possible reflections at surfaces and interfaces that are considered in the calculation.

Results

Experimental results

For the comparison of polarized light microscopy images and images of microtome cuts the results are discussed separately for the following four types of fiber-fiber bonds:

1. bonds between two completely collapsed springwood fibers, lying flat one upon the other
2. bonds between fibers with unequal fiber wall thickness, lying flat one upon the other
3. bonds between fibers where one or both fibers are folded and
4. partly or complete unbonded but parallel fibers.

Bonds between two completely collapsed springwood fibers, lying flat one upon the other

Fig 3 shows a fiber-fiber bond between two completely collapsed and flat springwood fibers. They behave as described in *Fig 2* and bonded area looks dark under the polarized light microscope.
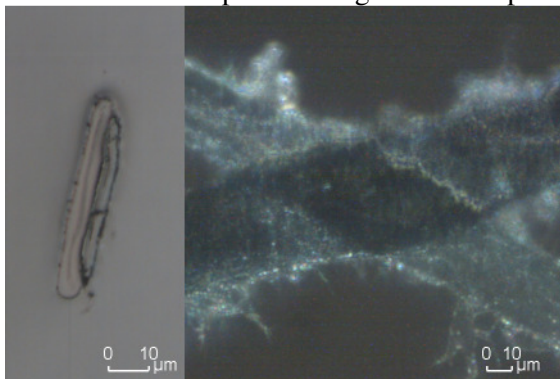
Fig 3. Fiber-fiber bond between two completely collapsed springwood fibers, lying flat one upon the other. The effect of dark bonded area is visible under the polarized light microscope.

Bonds between fibers with unequal fiber wall thickness, lying flat one upon the other

If the lower fiber of the fiber-fiber bond is dyed black, the reflection E_5 has zero intensity, as it is almost completely absorbed by the dye. Thus the phase shifts induced by the lower fiber are irrelevant. There is much less influence of the fiber wall thickness configuration on the appearance of the bond than it is for undyed fibers.

The reduced influence of fiber wall thickness is shown experimentally in *Fig 4*. The microtome image on the left shows that the fibers have unequal fiber wall thicknesses, still, bonded area shows dark under polarized light (*Fig 4*, right).
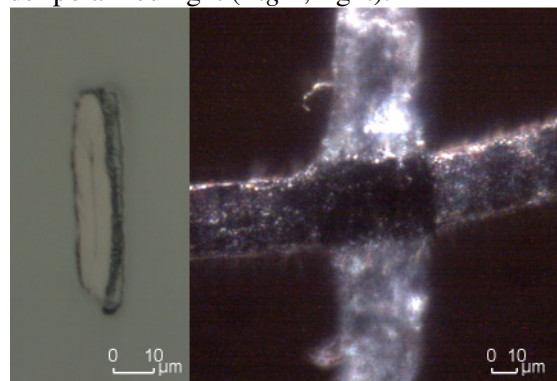
Fig 4. Fiber-fiber bond between two completely collapsed fibers, lying flat one upon the other, with unequal fiber wall thickness. The effect of dark bonded area is visible under the polarized light microscope.

Bonds between fibers where one or both fibers are folded

A fold in the bonding region causes additional reflections and phase shifts to the ones shown in *Fig 2*. Dyeing of one fiber reduces this problem, as a dyed and folded fiber will not disturb the effect of dark bonded area. Even though the fold causes additional interfaces, they will have hardly any influence on the appearance of bonded area under the polarized light microscope because the black dye reduces the intensity of the incident light, so that additional phase shifts and reflections will have little effect.

Fig 5 shows a bond, where one fiber is folded, bonded area appears dark under the polarized light microscope and even the interruption in the bond caused by the fold shows by the bright spot under polarized light.
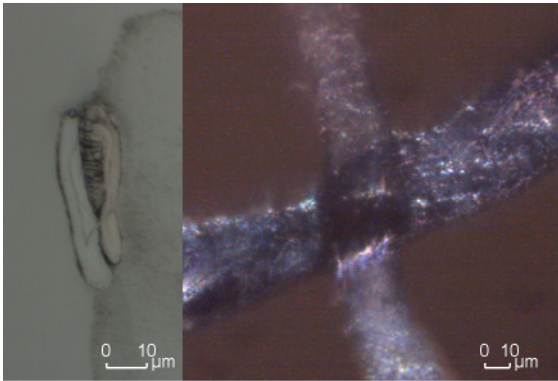
Fig 5. Fiber-fiber bond between one folded and one unfolded fiber. The effect of dark bonded area is visible under the polarized light microscope, as the folded fiber is dyed black.

However, if the undyed fiber is folded, the additional interfaces caused by this fold can be problematic, as the additional reflections will not necessarily have zero intensity or interfere destructively.

Partly or completely unbonded but parallel fibers

In the case of *crossed but unbonded* fibers, there is an additional reflection E_6 at the upper surface of the second fiber (see cross sections of the fiber-fiber crossing in *Fig 6*). If the unbonded fibers are *undyed* and parallel, the reflections E_3 and E_6 interfere destructively, so no difference between bonded and crossed but unbonded fibers can be seen under the polarized light microscope. This has already been shown experimentally in Part 1 of this study and theoretically in Gilli et al. (2009). If the lower fiber is dyed, the reflection E_6 is strongly reduced. E_3 and E_6 still interfere destructively, but they do not cancel each other out as E_6 has much lower intensity. So crossed but unbonded fibers are identified correctly.
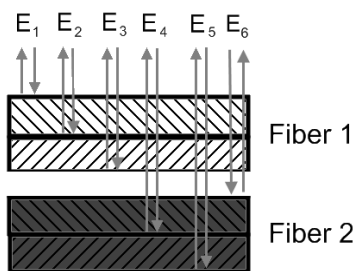
Fig 6. Optical model dyed fibers - unbonded fibers.

Fig 7 (left) shows a fiber-fiber bond between two flat and collapsed springwood fibers. The scale-up shows that the fibers are unbonded over a certain length. Even though the fibers are parallel in that area, a bright area shows under the polarized light microscope (*Fig 7*, right).
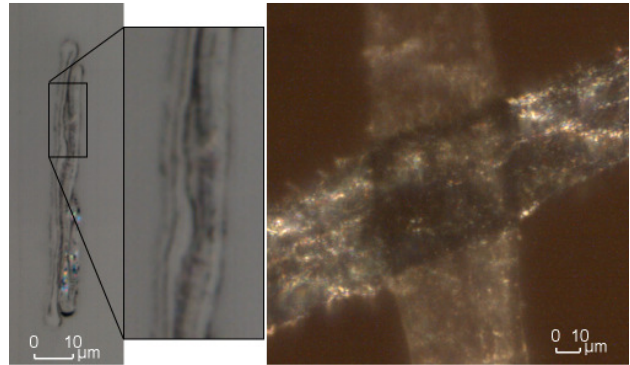
Fig 7. Partly unbonded fibers, parallel and lying flat one upon the other. The unbonded area shows bright under the polarized light microscope.

Measurement of bonded area

To verify the results of polarized light microscopy for fiber-fiber bond area measurement, the bonded area of 73 bonds between one dyed and one undyed fiber was first measured with polarized light microscopy and then the bonds were embedded in resin and cut with the microtome to measure the three-dimensional bonded area (Kappel et al. 2009). Results for size and shape of bonded areas were compared.

Fig 8 shows a comparison of all values for bonded area obtained with both methods. In general the results show quite good agreement, although bonded area is overstimated more often by polarized light microscopy. Deviations between the methods can be illustrated using the examples in *Fig 9* and *Fig 10*.
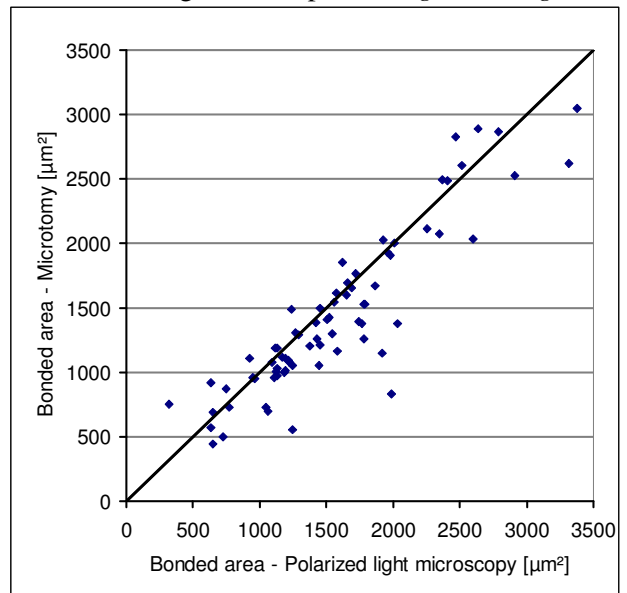
Fig 8. Comparison of the results of bond area measurement with the microtome method and with polarized light microscopy.

An example for *underestimation* of bonded area with polarized light microscopy is given in *Fig 9*. The microtome image (left) shows variations in fiber wall thickness of the left fiber. These variations seem to have an influence on phase shifts and intensity of reflections under the polarized light

microscope. The polarized light microscopy image (right) shows brighter areas in the crossing region, which will be evaluated as unbonded areas, while the microtome image shows that the fibers are bonded over the entire length.
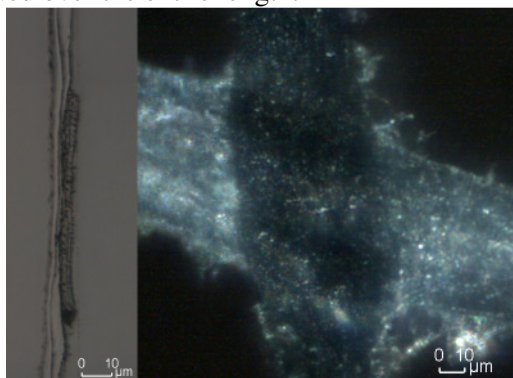
Fig 9. Completely bonded fibers, variations in fiber wall thickness of the left fiber are evaluated as unbonded fiber surfaces with polarized light microscopy.

Fig 10 shows an example where fiber-fiber bonded area is *overestimated* with polarized light microscopy. The microtome image (left) shows that the left fiber is folded in the lower part of the bond. Here the fibers are not bonded, a small gap between the fibers is evident (see scale up in *Fig 10*, left). This unbonded fiber edges do not show under the polarized light microscope. It is rather suggested that the bonded area reaches over the border of the fiber-fiber crossing region, as the fold also appears as bonded fiber (marked with the white arrow, right).

Generally unbonded fiber edges cannot always be identified under the polarized light microscope, independent of folds in the bonding region. The reason why these unbonded regions can only be identified in some cases is still under study.
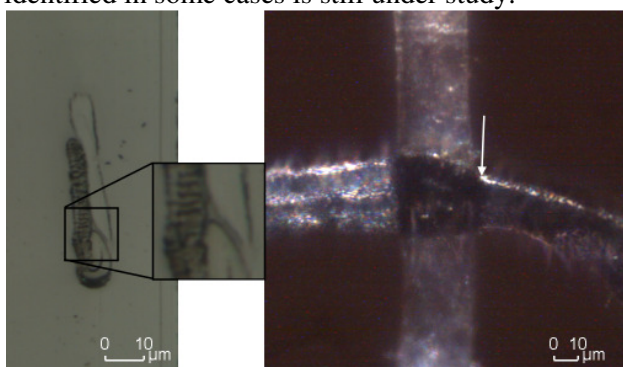
Fig 10. Overestimation of bonded area with polarized light microscopy: the left fiber is folded at the border of the bond. This region appears dark under polarized light although the fibers are unbonded (marked with white arrow).

So these two examples show that also bonds between one dyed and one undyed fiber cannot always be unambiguously identified under the polarized light microscope. If the undyed fiber is folded, folds still can cause problems under the polarized light microscope. Unbonded fiber regions or fiber edges cannot always be identified.

All in all bonded area measured with polarized light microscopy on average was 12.5 % higher than bonded area measured with microtomy for the 73 investigated bonds. To explain this overestimation of bonded area, a multiple linear regression model was built. The deviation between the methods was the response variable, morphological parameters that were assumed to be explanatory were taken as the predictor variables. The morphological parameters are: Fiber wall thickness, angle between the fibers, fraction of unbonded fiber edges and fraction of holes in the bond. The exact definition of these parameters and a description of how they are measured can be found in Kappel et al. (2009). *Table 1* shows the significance (p-value of the F*-statistics) and the impact (ANOVA) of the variables (Neter et al. 1996). The results of the model are interpreted on basis of the stepwise R^2 values, i.e. the ANOVA. Because of redundancies and interaction the R^2 values alone are not really meaningful and are not used for interpretation of the results. The p-value shows the significance of the parameters on a 95% confidence level. Only the significant parameters are given in *Table 1*. It can be shown that unbonded fiber edges account for 56.7 % of the deviations (the R^2 value is 0.567). By adding the fraction of holes in the bond to the model, the stepwise R^2 value is increased from 0.567 to 0.590, indicating that the holes in the bond explain further 2.3 % of the deviations. This confirms what has already been shown experimentally - partly unbonded fibers might be overestimated, when the bonds are analyzed with the polarized light microscope, even though one of the fibers is dyed.

The fiber wall thickness and the angle between the fibers are not significant on a 95 % confidence level (i.e. $p>0.05$). As both of these two parameters may change the run of light waves through the fiber-fiber bond we would have expected an influence on the polarization microscopy image, but they did not show significant influence.

Table 1. Results of multiple linear regression and ANOVA with the deviation of bonded area between microtomy and polarized light microscopy as the response variable.

Variable	R^2 stepwise	R^2 alone	p-Value	Sign of Coeff.
Unbonded fiber edges	0.567	0.567	$<10^{-5}$	-
Holes in the bond	0.590	0.092	0.03	-

Discussion

The influence of dyeing on paper strength was also analyzed. Standard hand sheets were formed with dyed and with undyed pulp and tensile strength and burst strength were measured. The results showed that the paper strength of dyed sheets was slightly higher, however overlapping confidence intervals indicate that this difference is statistically not significant. Since the dye is weakly cationic it is assumed that the increase in paper strength is only caused chemically and that the size of bonded area is not influenced by dyeing the fibers.

The factor for the overestimation of bonded area with polarized light microscopy (12.5 %), as determined in this study, is not generally applicable, because only unbeaten softwood pulp was used for the experiments. Almost 60 % of the deviation between the results for bonded area can be explained with incomplete bonding (overlapping but unbonded fiber edges and holes in the bond). Refining might reduce the fraction of unbonded fiber edges and lead to less overestimation of bonded area with polarized light microscopy. Further trials with beaten pulp will have to be performed. The results may also be different for hardwood pulp. So the correction factor given in this paper is only valid for the pulp that was used in this study. It also has to be considered, that the statistics are based on only 73 investigated bonds. Given that the results for bonded area scatter strongly, a higher number of samples might slightly change the correction factor.

Conclusions

The comparison of polarized light microscopy images with fiber-fiber bond cross sectional images indicates that polarized light microscopy is an appropriate method for fiber-fiber bond area measurement as long as one of the bonded fibers is dyed black. An optical model, which describes the behaviour of fibers and fiber-fiber bonds under the polarized light microscope, confirms and explains these experimental results. In contrast to undyed fiber-fiber bonds now in most cases bonded area can be identified correctly.

Bonded area was first measured with the polarized light microscope and then with a three-dimensional measurement method based on microtome serial sectioning and image analysis. The results of these two methods were compared and showed good agreement. However, bonded area is overestimated with polarized light microscopy in most cases. On average bonded area was 12.5 % too high for the investigated pulp. If this factor for overestimation is considered, polarized light microscopy is an appropriate basis for specific bond area measurement. The theoretical and experimental results verify its applicability as a non-destructive method for fiber-fiber bond area measurement.

Literature

Gilli, E., Kappel, L., Hirn, U. and Schennach, R. (2009): An optical model for polarization microscopy analysis of pulp fibre-to-fibre bonds, Composite Interfaces, in press

Kappel, L., Hirn, U., Bauer, W. and Schennach, R. (2009): A novel method fort he determination of bonded area of individual fiber-fiber bonds, Nordic Pulp and Paper Research Journal, 24 (2), 199

Neter, J., Kutner, M.H., Nachtsheim, C.J. and Wassermann, W. (1996): Applied Linear Statistical Models, Fourth Edition, Richard D. Irwin, Illinois (USA)

Page, D.H. (1960): Fibre-to-fibre bonds Part 1 – A method for their direct observation, Paper Technology, 1(4), 407

Stratton, R.A. and Colson, N.L. (1190): Dependence of Fiber/Fiber Bonding on Some Papermaking Variables, IPST Technical Paper Series, Institute of Paper Science and Technology Atlanta, Georgia

Paper IV

An Optical Model for Polarization Microscopy Analysis of Pulp Fibre-to-Fibre Bonds

E. Gilli [a,c], **L. Kappel** [b,c], **U. Hirn** [b,c] **and R. Schennach** [a,c,*]

[a] Institute for Solid State Physics, Graz University of Technology, 8010 Graz, Austria

[b] Institute for Paper, Pulp and Fibre Technology, Graz University of Technology, Austria

[c] Christian Doppler Laboratory for Surface Chemical and Physical Fundamentals of Paper Strength, Austria

Abstract

Pulp fibre-to-fibre bonds were studied using polarization microscopy and microtome cuts. The experiments showed considerable discrepancies between these two experimental methods. While microtome cuts clearly show if a bond between two fibres has formed, polarization microscopy cannot unambiguously discern between crossed unbonded fibres and bonded fibres; also certain bonds cannot be detected with this method. To examine these shortcomings, a physical model of polarization microscopy of bonded and unbonded pulp fibers was built. Experimental validation of the model gave good agreement between calculations and reflectance measurements. Calculations based on this model clearly demonstrate that only bonded fibres resembling a plane parallel plate show as bonds. However, crossings of unbonded fibers also appear as bonds if the two fibres are flat and plane parallel to each other. The model provides a consistent interpretation for polarization microscopy imaging of pulp fibre bonds, an important topic in research of mechanical and optical properties of fibrous composites like paper.

© Koninklijke Brill NV, Leiden, 2009

1. Introduction

The tensile strength of paper mainly depends on the strength of the individual pulp fibres and on the ability to form fibre-to-fibre bonds [1]. The strength of the bonds is controlled by the size of the bonded area and the specific bonding force, i.e., the bonding force per area [2]. Consequently an increase of paper strength is usually achieved by pulp fibre flexibilization, which increases bonding area, or im-

---

provement of bond strength by means of fibre treatment, e.g., refining, or chemical additives [2].

Several methods for determining the bonded area of fibre-to-fibre bonds have been published. Yang *et al.* [3] determined the bonded area using images of samples that were cut with a microtome. Jayme and Hunger [4] used an electron microscope to analyze the previously bonded areas of fibre-to-fibre bonds that were torn apart. Torgnysdotter [5] investigated the contact zone between fibres using light microscopy and a staining technique. Thomson [6] used fluorescence resonance energy transfer to analyze fibre-to-fibre bonds. Already in the 1960s Page and Tydeman [7, 8] introduced a method where the bonded area of a fibre-to-fibre bond was determined with polarized light microscopy. Figure 1 shows a fibre-to-fibre bond in reflection polarization microscopy between crossed polarizers. Whenever the fibres and the transmission directions of the polarizing filters enclose an angle of about 45°, the fibres appear bright, while the bonded area appears almost completely dark (Fig. 1(a), left frame). If the fibres and the transmission directions are parallel or perpendicular, the fibres appear in a minimal intensity, while the bonded area appears brighter than the single fibres (Fig. 1(a), right frame). However, the physical explanation for the dark appearance of the fibre bond given in the original paper [7] does not hold. Furthermore the bond area cannot be observed with all fibre-to-fibre bonds, e.g., Fig. 1(b), left frame.

In this paper we will present an optical model that describes the imaging of fibre-to-fibre bonds in polarization microscopy as described by Page and Tydeman [7, 8].

Experimental results will be presented that further underline the validity of the proposed model. The presented model explains why some fibre-to-fibre bonds are visible under polarization microscopy while others are not.

2. Experimental and Computational Details

The optical experiments were carried out on a Leitz DM RX polarization microscope in reflection and transmission mode. An Olympus BX 51 microscope with rotatable polarizer and analyzer was used in transmission.

The samples were prepared from unbleached and unrefined spruce kraft pulp fibres. To get an insight into the structure of the analyzed fibre-to-fibre bonds, single bonds were embedded in epoxy resin and cut with a Leica RM 2155 microtome. The exact description of the method can be found in Ref. [9].

The analysis of the experimental data was carried out using Matlab 7.1 R14, and the theoretical computation was assisted with the algebra system Mathemetica 5.2.

3. Experimental Results

A cellulose fibre between two crossed polarizers appears in distinct colors in reflection microscopy. Its intensity depends on the angles that are enclosed by the principal axis of the fibre and the transmission directions of the polarizing filters.
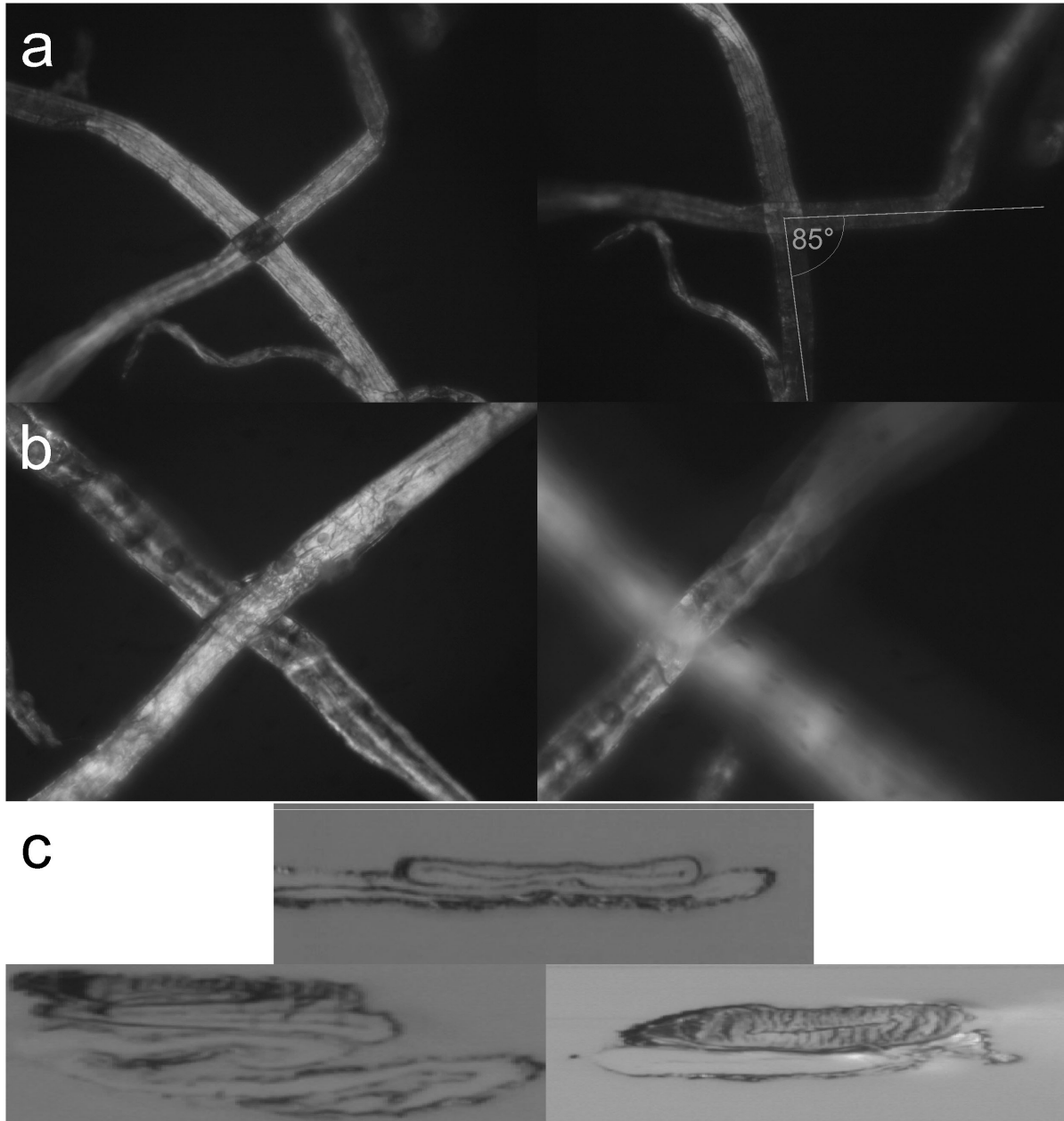
Figure 1. Fibre-to-fibre bond in reflection polarization microscopy with the polarizer vertical and the analyzer horizontal. (a) left: Fibres under a 45°-angle to the transmission direction of the polarizer, right: one fibre parallel to the transmission direction of the polarizer, the other orthogonal. The discussed effect is visible: The bond appears dark under a 45° angle between the transmission axis of the polarizing filters and the fibres. (b) Fibres under a 45°-angle to the transmission direction of the polarizer, left: before tearing apart, right: after tearing apart. The discussed effect is not visible: Bonded area and single fibre are of similar intensity. (c) Photos of microtome cuts of fibre-to-fibre bonds. Top: cut of the bond shown in (a), the effect of a dark bonding area is visible, the fibre is fully collapsed and approximately of the shape of a plane parallel plate, bottom: two bonds which did not show the effect of dark bond areas: left: not well collapsed fibres with multiple reflecting surfaces, right: fully collapsed fibres with an elliptic shape, not similar to a plane parallel plate.

Let ψ_p be the angle enclosed by the principal axis of a fibre and the transmission axis of the polarizer and let ψ_a be the angle enclosed by the principal axis of a fibre and the transmission axis of the analyzer. If the angles are close to 45°, the fibre

appears in its maximum intensity (see Fig. 1(a), left frame). If one of the angles is ≈0° and the other ≈90°, the fibre appears under a minimal intensity (see Fig. 1(a), right frame). The situation is quite different with fibre-to-fibre bonds. The bonded region appears dark when the principal axis of one fibre encloses an angle close to 45° with the transmission axes of the polarizing filters (Fig. 1(a), left frame), and it appears brighter than the single fibres when the fibres are parallel or orthogonal to the transmission axes (Fig. 1(a), right frame).

Crossings between two unbonded fibres almost always appear brighter than the single fibre, and there are fibre-to-fibre bonds that behave like unbonded crossings (see Fig. 1(b)). The fibre-to-fibre bond shown in Fig. 1(b), left frame, appears like a crossing of two unbonded fibres under crossed polarizers in reflection. This is a bond that cannot be observed in the polarization microscope, but its existence could be shown by tearing it apart after observation in the microscope (Fig. 1(b), right frame). Therefore polarization microscopy cannot observe all fibre-to-fibre bonds.

All bonds that were observed in the polarization microscope were cut with a microtome to understand their morphology. A microtome was used to cut the fibre-to-fibre bond shown in Fig. 1(a), and microscope images of a section are presented in Fig. 1(c). In this case the effect of the dark bonded area was visible. Both fibres of the bond are fully collapsed and flat springwood fibres. Two examples of bonds that could not be observed by polarization microscopy are shown in Fig. 1(c), bottom left and bottom right frame.

The left image shows a bond of not fully collapsed and folded fibres, resulting in an irregular geometry. The right image shows a bond consisting of fully collapsed fibres, with an elliptical shape.

As will be shown later, a fibre-to-fibre bond can only be seen in reflection polarization microscopy if both fibres are fully collapsed and lie flat, one upon the other (see Section 4). In the following, we will discuss these conditions and build an optical model for a cellulose fibre that can provide the required accuracy to describe the optical behaviour of fibre-to-fibre bonds.

4. Optical Model

In this section a model for the optical behavior of pulp fibres will be developed [10]. The behaviour of a fibre in polarization microscopy can be accurately modeled as an anisotropic plane parallel plate. To show that the assumption of plane parallel plates is feasible, a numerical simulation of the optical path length of collapsed fibres, as they can be seen in cutting areas of microtome cuts, was carried out for the collapsed fibre shown in Fig. 1(a) (the corresponding image of the cutting area is shown in Fig. 1(c), top frame).

A simulation of the optical path length difference between the beam that is refracted at the front surface to the back surface and the beam that is reflected at the back surface to the front surface, over the width of the fibre, is shown in Fig. 2. The difference between the two lengths stays well below 70 nm for a wide interval
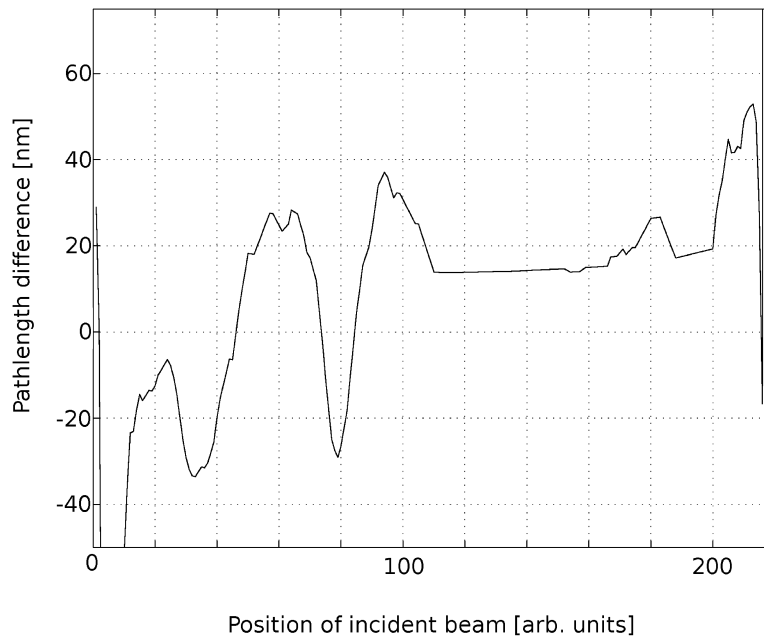
Figure 2. Numerically calculated optical path length difference between the incident and the reflected beam within the fibre shown in Fig. 1(a). The small difference is indicating the possibility of approximating the fibre as a plane parallel plate (see text).

(for a plane parallel plate it would be exactly zero). The points where the values go below -30 nm or over $+40$ nm are numerical artifacts due to the position close to the edge of the fibre, which causes errors in the automated edge detection. The difference moves towards $\pm\infty$ at the edges of the fibre where the beam is refracted at great angles. That means that the differences in the optical path length are smaller than the wavelength of visible light by an order of magnitude, justifying the approximation of the fibre as a plane parallel plate.

Taking this into account and considering the fact that cellulose fibres are optically anisotropic [11] leads to a suitable theory. An optical model will therefore be outlined to describe all of the observable phenomena very accurately.

The following premises have been used:

(1) Fibres showing an effect of dark bonded area can be approximated as birefringent plane parallel plates (fully collapsed fibres that lie upon each other). As shown above, the effect of a dark bonded region only shows if this assumption is fulfilled.

(2) The optical axes of the fibres correspond to the median angle of the microfibrils in the thickest layer of the fibre, the s_2 layer (see [12]). This leads to opposite directions of the fibrils in the two layers separated by the collapsed lumen.

Both of these premises have been used successfully with cellulose fibres before [13].

(3) Neglect of the interference effects within the fibres. The fibres are thick enough for sizeable internal reflections. However, multiple reflections and, therefore,

any interference effects within the fibre do not play an important role for the intensity in comparison to the intensity caused by birefringence within the first reflex. This is due to the low reflectivity of the fibre–air interface, of about 0.22 (see equation (18) with the parameters given in Section 5, equation (48)). For multiple reflexes the beam would have to reflect at least three times, i.e., there would be two additional reflections with a reflectivity of 0.22 each. This makes the second reflection by more than an order of magnitude ($\approx$0.05) smaller than the first one. The intensity being the norm square of the Jones vectors (see later) thus would be altered by about $\pm$0.25% from interference effects by multiple reflections within the fibre.

The model does not show an effect without birefringence, which is also shown in the experiment. If interference would play a role in the transmission or reflection intensity of fibers, these fibers would have to appear in different colors, depending on their thickness, without the usage of polarization filters, and this clearly is not the case in the experiments.

With these three premises, the system can be calculated using the Jones formalism [14], which yields mean intensities over time for plane parallel layer systems. The great advantage of the Jones formalism is the possibility to combine different layers by multiplying their corresponding Jones matrices. Figure 3(a) shows the most important parameters for the model. The Jones matrix for a birefringent plane parallel plate (see Fig. 3(b)) with its fast axis parallel to the normal polarization direction (*s*) is given by:

$$\mathcal{P}_{\mathrm{pc}} = \begin{pmatrix} e^{\mathrm{i}\varepsilon_p} & 0 \\ 0 & e^{\mathrm{i}\varepsilon_s} \end{pmatrix}, \tag{1}$$

with ε_p and ε_s the phase retardation in parallel and normal directions (see, for example, Ref. [14]). The phase difference between *s*- (normal) and *p*-direction (parallel polarization) is given by $\Delta\phi = |\varepsilon_p - \varepsilon_s|$. For $\varepsilon_s = \Delta\phi/2$ and $\varepsilon_p = -\Delta\phi/2$ this gives:

$$\mathcal{P}_{\mathrm{pc}}(\Delta\phi) = \begin{pmatrix} e^{-\mathrm{i}(\Delta\phi/2)} & 0 \\ 0 & e^{\mathrm{i}(\Delta\phi/2)} \end{pmatrix}. \tag{2}$$

For an arbitrary angle, α, between the fast axis and the *s*-direction, the Jones matrix can be written as (see Fig. 3(b)):

$$\begin{aligned} \mathcal{P}_{\mathrm{pc}}(\Delta\phi, \alpha) &= \mathbb{R}(\alpha)\mathcal{P}_{\mathrm{pc}}(\Delta\phi)\mathbb{R}(-\alpha) \\ &= e^{\mathrm{i}(\Delta\phi/2)} \begin{pmatrix} e^{-\mathrm{i}\Delta\phi}\cos^2\alpha + \sin^2\alpha & (e^{-\mathrm{i}\Delta\phi} - 1)\cos\alpha\sin\alpha \\ (e^{-\mathrm{i}\Delta\phi} - 1)\cos\alpha\sin\alpha & \cos^2\alpha + e^{-\mathrm{i}\Delta\phi}\sin^2\alpha \end{pmatrix}, \end{aligned} \tag{3}$$

with the rotation matrix, $\mathbb{R}(\alpha)$, defined by:

$$\mathbb{R}(\alpha) = \begin{pmatrix} \cos(\alpha) & -\sin(\alpha) \\ \sin(\alpha) & \cos(\alpha) \end{pmatrix}. \tag{4}$$
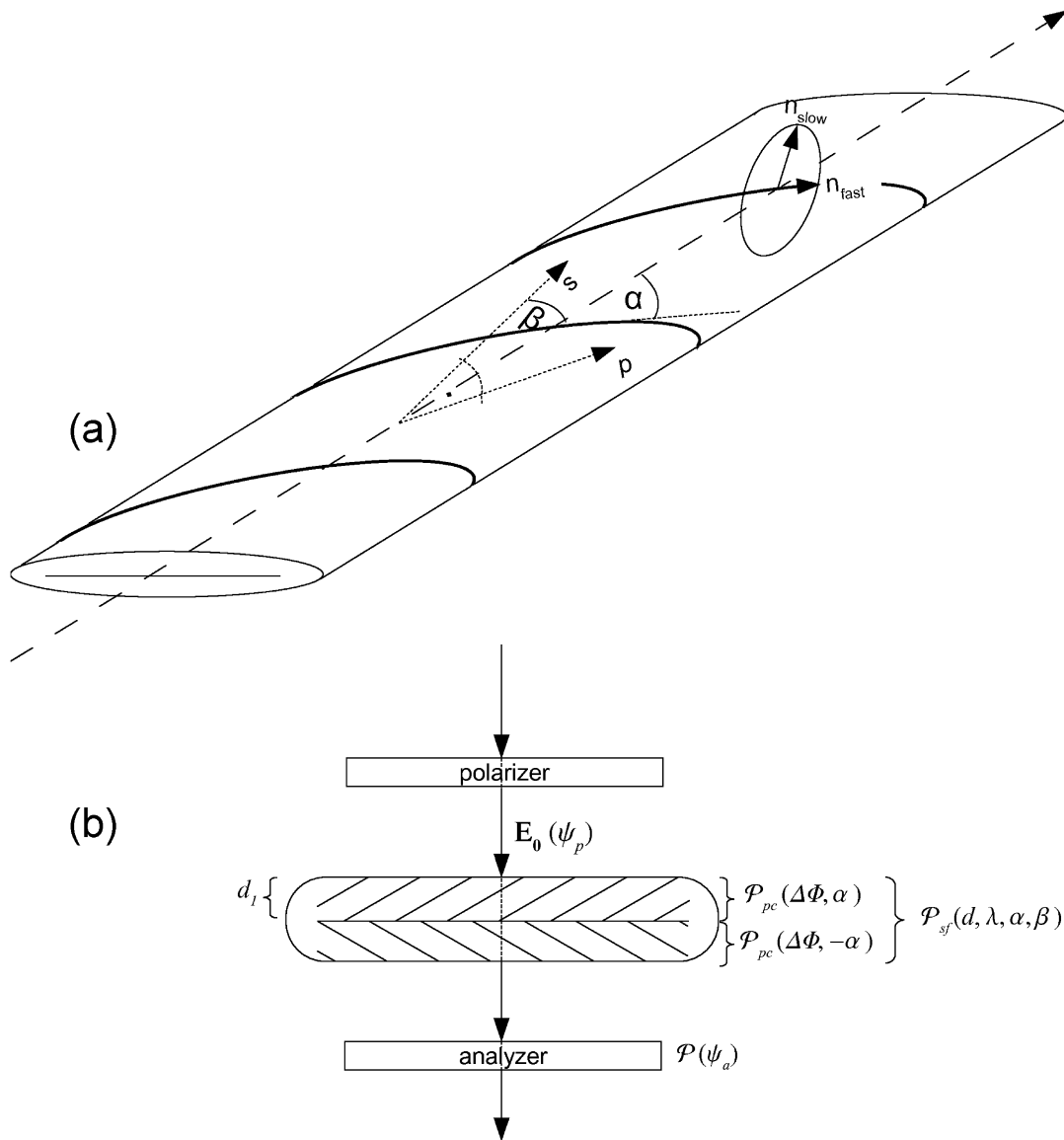
Figure 3. Important parameters and operators (Jones matrices) used by the model: (a) a fully collapsed fibre with its microfibrillar angle α, the ellipse of refraction with the two refractive indices n_{slow} and n_{fast}, the total rotation angle of the fibre, and the normal (s)- and parallel (p)-direction of polarization. (b) Single fibre with the wall thickness d_1 in transmission polarization microscopy, and the used Jones matrices for this case: The linearly polarized incident Jones vector $E_0(\psi_p)$, with ψ_p the angle enclosed by the transmission direction of the polarizer and the s-direction, the Jones matrices of the two birefringent plates $\mathcal{P}_{pc}(\Delta\phi, \pm\alpha)$ and the combined Jones matrix of the entire fibre $\mathcal{P}_{sf}(d, \lambda, \alpha, \beta)$, and the Jones matrix of the analyzer $\mathcal{P}(\psi_a)$.

The phase difference, $\Delta\phi$, of a wave traveling through an anisotropic plate can be described by the following [14]:

$$\Delta\phi(\lambda, d) = \frac{2\pi}{\lambda} \cdot d(n_{slow} - n_{fast}), \qquad (5)$$

with λ being the wavelength, d the thickness of the plate, and n_{slow} and n_{fast} the ordinary and extraordinary refractive indices of the anisotropic plate, respectively (see Figs 3(a) and 4).
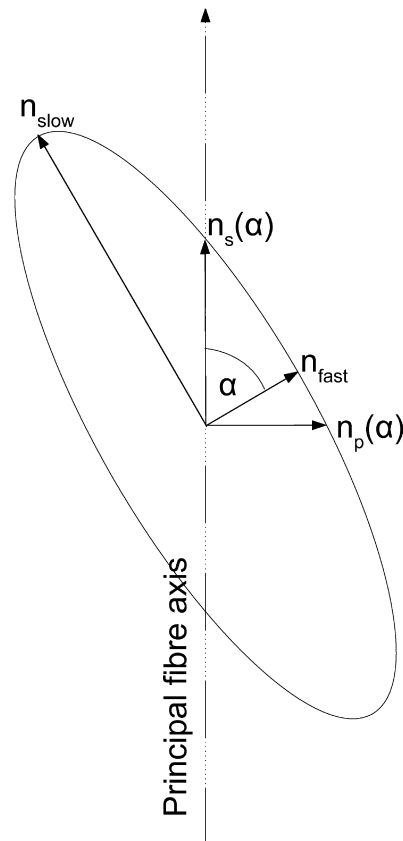
Figure 4. The ellipse of refractive indices of an anisotropic medium. α: angle between the fast optical axis and the normal (s)-direction of polarization, n_{slow} and n_{fast}: refractive indices in the directions of the optical axes of the medium, n_s and n_p: refractive indices in parallel (p)- and normal (s)-direction of polarization.

The Jones matrix for a linear polarizer with its transmission axis in the s-direction is given by

$$\mathcal{P}_v = \begin{pmatrix} 0 & 0 \\ 0 & 1 \end{pmatrix}, \tag{6}$$

which yields for an arbitrary angle between the transmission axis and the s-direction:

$$\mathcal{P}(\alpha) = \mathbb{R}(\alpha)\mathcal{P}_v\mathbb{R}(-\alpha) = \begin{pmatrix} \sin^2(\alpha) & -\cos(\alpha)\sin(\alpha) \\ -\cos(\alpha)\sin(\alpha) & \cos^2(\alpha) \end{pmatrix}. \tag{7}$$

Finally, the Jones vector of a linear polarized wave is represented by:

$$\mathbf{E} = \begin{pmatrix} p \\ s \end{pmatrix}, \quad \text{with } p, s \in \mathbb{R}, \tag{8}$$

with p and s being the amplitudes of the electric field in the p- and in the s-direction, respectively. For an arbitrary polarization angle, ψ_p, the Jones vector for the incident beam becomes:

$$\mathbf{E}_0(\psi_p) = \mathbb{R}(\psi_p)\begin{pmatrix} 0 \\ 1 \end{pmatrix} = \begin{pmatrix} -\sin(\psi_p) \\ \cos(\psi_p) \end{pmatrix}. \tag{9}$$

These are the operators needed for the calculation of the phase differences. For quantitative calculations of returned intensities, the well-known Fresnel formulas are required [14]:

$$\tau_s = \frac{2\sin\delta\cos\gamma}{\sin(\gamma+\delta)},\tag{10}$$

$$\tau_p = \frac{2\sin\delta\cos\gamma}{\sin(\gamma+\delta)\cos(\gamma-\delta)},\tag{11}$$

$$\rho_s = -\frac{\sin(\gamma-\delta)}{\sin(\gamma+\delta)},\tag{12}$$

$$\rho_p = \frac{\tan(\gamma-\delta)}{\tan(\gamma+\delta)},\tag{13}$$

where τ is the coefficient of transmittivity, ρ is the coefficient of reflectivity (indices s and p for normal and parallel polarization), γ is the angle between the incident beam and the optical plummet and δ is the angle between the optical plummet and the refracted beam.

Taking into account the projection of the beams onto the interface between the two media and the mean value of the amplitude over time yields an additional factor $\sqrt{n_2/n_1 \cdot \cos\delta/\cos\gamma}$ for transmission, which cancels to 1 for reflection (see, for example, Ref. [15]):

$$t_{s,p} = \sqrt{\frac{n_2\cos\delta}{n_1\cos\gamma}} \cdot \tau_{s,p},\tag{14}$$

$$r_{s,p} = \rho_{s,p},\tag{15}$$

where t is the coefficient of transmission, r is the coefficient of reflection (indices s and p for normal and parallel polarization), n_1 and n_2 are the refractive indices of the two media.

For the case of plane parallel plates only the limits for $\gamma \to 0$ and $\delta = \sin^{-1}(n_1/n_2 \cdot \sin(\gamma))$ (Snell's law) are required. This yields:

$$t_s(n_1,n_2) = 2\frac{\sqrt{n_1n_2}}{n_1+n_2},\tag{16}$$

$$t_p(n_1,n_2) = 2\frac{\sqrt{n_1n_2}}{n_1+n_2},\tag{17}$$

$$r_s(n_1,n_2) = \frac{n_1-n_2}{n_1+n_2},\tag{18}$$

$$r_p(n_1,n_2) = -\frac{n_1-n_2}{n_1+n_2},\tag{19}$$

where n_1 is the refractive index of the first medium and n_2 is the refractive index of the second medium.

These refractive indices depend on the angle α of the optical axis (anisotropic media), such that the actual refractive index is an elliptic 2-vector function of the angle between the principal axis of the fibre and the fast axis (see Figs 3(a) and 4). This cannot be described by the Jones formalism because an elliptically polarized wave rotates its incident polarization angle around 2π within one period with changing intensities. The Jones matrices already give the mean value over an entire period, therefore losing basis invariance at the reflections and the transmissions. An exact solution must be made by calculating the time dependent electromagnetic wave with all the interactions in the different layers and building the mean value over time at the end, which would go far beyond the scope of this paper. For the sake of simplicity, the surfaces of the fibres are approximated as being isotropic (with the mean value of the two refractive indices as a refractive index). This is feasible because the difference in the refractive indices of the fibres is very small (an estimate of the error, caused by this approximation is given in equation (50) in Section 5). The refractive index at the surface thus is defined by:

$$n_{\text{surf}} = \frac{n_{\text{fast}} + n_{\text{slow}}}{2}. \tag{20}$$

This gives the operators of transmission ($\mathcal{T}$) and reflection ($\mathcal{R}$):

$$\mathcal{R}(n_1, n_2) = \begin{pmatrix} r_p(n_1, n_2) & 0 \\ 0 & r_s(n_1, n_2) \end{pmatrix}, \tag{21}$$

$$\mathcal{T}(n_1, n_2) = \begin{pmatrix} t_p(n_1, n_2) & 0 \\ 0 & t_s(n_1, n_2) \end{pmatrix}. \tag{22}$$

The angle α can be interpreted physically. A cellulose fibre consists of multiple layers which consist of microfibrils [12]. The thickest layer, s_2, has a high degree of crystallinity and its microfibrils are arranged non-parallel to the principal axis of the fibre (see Fig. 3(a)).

The other layers are an order of magnitude thinner and show a less ordered structure. Uncollapsed fibres are hollow, and the microbrils form a helix around the principal axis at an angle of $\alpha \approx 20°$ to $30°$ for springwood. A fibre with a collapsed lumen can be approximated as consisting of two oriented layers. Seen from above, one fibre is rotated by α and the other fibre by $-\alpha$ (see Fig. 3(b)). It is inevitable that this orientation influences the optical properties of the fibre, and it is very plausible to assume that the angle α gives the orientation of the optical axes of the fibre (see also Ref. [13]).

The fibre can therefore be modeled as a set of two anisotropic plane parallel plates on top of each other, one with its fast optical axis oriented in $+\alpha$ and the other in $-\alpha$-direction, with a general rotation β of the principal fibre axis (see Fig. 3(a)). The Jones matrix for a single fibre therefore becomes:

$$\begin{aligned}
&\mathcal{P}_{\text{sf}}(d, \lambda, \alpha, \beta) \\
&= \mathcal{P}_{\text{pc}}(\Delta\phi(\lambda, d), -\alpha + \beta) \overbrace{\mathcal{T}(n_{\text{surf}}, n_{\text{surf}})}^{=\mathbb{1}} \mathcal{P}_{\text{pc}}(\Delta\phi(\lambda, d), \alpha + \beta) \\
&= \mathcal{P}_{\text{pc}}(\Delta\phi(\lambda, d), -\alpha + \beta) \mathcal{P}_{\text{pc}}(\Delta\phi(\lambda, d), \alpha + \beta), \tag{23}
\end{aligned}$$

with $\mathbb{1}$ being the unity matrix. In the case of $\alpha = \pi/4$, the two layers would be exactly inverse to each other and have no effect on the wave:

$$\mathcal{P}_{pc}(\Delta\phi, \pi/4)\mathcal{P}_{pc}(\Delta\phi, -\pi/4) = \begin{pmatrix} 1 & 0 \\ 0 & 1 \end{pmatrix} = \mathbb{1}. \tag{24}$$

With $\alpha = 0$ (or both layers in the same α) the layers form one layer with doubled phase shift:

$$\mathcal{P}_{pc}(\Delta\phi, \alpha)\mathcal{P}_{pc}(\Delta\phi, \alpha) = \mathcal{P}_{pc}(2\Delta\phi, \alpha). \tag{25}$$

The two layers with an arbitrary angle behave similar to a linear combination of transmission and a phase retarder.

4.1. Transmission

The intensities for transmission polarization microscopy are modeled using all the previously defined operators (see Fig. 3(b)).

4.1.1. Single Fibre
The single fibre between two polarizers is modeled by:

$$\begin{aligned} \mathbf{E}_{\text{sf,trans}}&(\psi_p, \psi_a, \lambda, \alpha) \\ &= \mathcal{P}(\psi_a)\mathcal{T}(n_{\text{surf}}, n_{\text{air}})\mathcal{P}_{\text{sf}}(d_1, \lambda, \alpha, 0)\mathcal{T}(n_{\text{air}}, n_{\text{surf}})\mathbf{E}_0(\psi_p). \end{aligned} \tag{26}$$

4.1.2. Fibre-to-Fibre Bond
Here the wave travels through two fibres which enclose the angle β_f:

$$\begin{aligned} \mathbf{E}_{\text{bond,trans}}&(\psi_p, \psi_a, \lambda, \alpha, \beta_f) \\ &= \mathcal{P}(\psi_a)\mathcal{T}(n_{\text{surf}}, n_{\text{air}})\mathcal{P}_{\text{sf}}(d_2, \lambda, \alpha, \beta_f) \\ &\quad \times \underbrace{\mathcal{T}(n_{\text{surf}}, n_{\text{surf}})}_{=\mathbb{1}}\mathcal{P}_{\text{sf}}(d_1, \lambda, \alpha, 0) \cdot \mathcal{T}(n_{\text{air}}, n_{\text{surf}})\mathbf{E}_0(\psi_p) \\ &= \mathcal{P}(\psi_a)\mathcal{T}(n_{\text{surf}}, n_{\text{air}})\mathcal{P}_{\text{sf}}(d_2, \lambda, \alpha, \beta_f) \\ &\quad \times \mathcal{P}_{\text{sf}}(d_1, \lambda, \alpha, 0)\mathcal{T}(n_{\text{air}}, n_{\text{surf}})\mathbf{E}_0(\psi_p). \end{aligned} \tag{27}$$

4.1.3. Crossing of Two Unbonded Fibres

$$\begin{aligned} \mathbf{E}_{\text{cross,trans}}&(\psi_p, \psi_a, \lambda, \alpha, \beta_f) \\ &= \mathcal{P}(\psi_a)\mathcal{T}(n_{\text{surf}}, n_{\text{air}})\mathcal{P}_{\text{sf}}(d_2, \lambda, \alpha, \beta_f) \\ &\quad \times \mathcal{T}(n_{\text{air}}, n_{\text{surf}})\mathcal{T}(n_{\text{surf}}, n_{\text{air}})\mathcal{P}_{\text{sf}}(d_1, \lambda, \alpha, 0)\mathcal{T}(n_{\text{air}}, n_{\text{surf}})\mathbf{E}_0(\psi_p). \end{aligned} \tag{28}$$

The resulting intensities are obtained by the absolute square of the resulting E-vector:

$$I = |\mathbf{E}|^2. \tag{29}$$

For information on the reflected or transmitted color of a single fibre the intensity for a single fibre ($I_{\text{ref,sf}}$) can be integrated over the visible spectrum, with a spectral sensitivity function as weight. For the spectral sensitivity, the CIE functions for the human eye (red, green and blue) were used [16], because these functions are the

basis of all RGB-coordinate systems.

$$I_{\text{total}} = \left| \int_{\lambda_{\min}}^{\lambda_{\max}} d\lambda \, \mathbf{E}(\lambda) S(\lambda) \right|^2, \tag{30}$$

$$I_{\text{r,g,b}} = \left| \int_{\lambda_{\min}}^{\lambda_{\max}} d\lambda \, \mathbf{E}(\lambda)[\text{r, g, b}](\lambda) \right|^2, \tag{31}$$

with $S(\lambda) = (\text{r}(\lambda) + \text{g}(\lambda) + \text{b}(\lambda))/3$, and $[\text{r, g, b}](\lambda)$ the spectral sensitivity functions as functions of the wavelength λ, for red green and blue [16].

4.2. Reflection

Reflection models are more complicated than transmission models due to multiple beams and reflections on different interfaces. This results in longer algebraic expressions, but is not qualitatively different from the transmission model. For the different situations (single fibre, fibre-to-fibre bond, crossed fibres), nine different reflected Jones vectors have to be defined. Their respective intensity vectors are shown in Fig. 5(a).

(1) All cases: reflection at the surface:

$$\mathbf{E}_1(\psi_\text{p}, \psi_\text{a}, \alpha) = \mathcal{P}(\psi_\text{a}) \mathcal{R}(n_{\text{air}}, n_{\text{surf}}) \mathbf{E}_0(\psi_\text{p}). \tag{32}$$

(2) All cases: reflection at the interface within the first fibre:

$$\begin{aligned}
\mathbf{E}_2&(\psi_\text{p}, \psi_\text{a}, \lambda, \alpha) \\
&= \mathcal{P}(\psi_\text{a}) \mathcal{T}(n_{\text{surf}}, n_{\text{air}}) \mathcal{P}_{\text{pc}}(\Delta\phi(\lambda, d_1), \alpha) \underbrace{\mathcal{R}(n_{\text{surf}}, n_{\text{surf}})}_{=0} \\
&\quad \times \mathcal{P}_{\text{pc}}(\Delta\phi(\lambda, d_1), \alpha) \mathcal{T}(n_{\text{air}}, n_{\text{surf}}) \mathbf{E}_0(\psi_\text{p}) \\
&= 0.
\end{aligned} \tag{33}$$

(3) Fibre-to-fibre bond: reflection at the fibre-to-fibre interface:

$$\begin{aligned}
\mathbf{E}_3&(\psi_\text{p}, \psi_\text{a}, \lambda, \alpha, 0) \\
&= \mathcal{P}(\psi_\text{a}) \mathcal{T}(n_{\text{surf}}, n_{\text{air}}) \mathcal{P}_{\text{sf}}(d_1, \lambda, -\alpha, 0) \\
&\quad \times \underbrace{\mathcal{R}(n_{\text{surf}}, n_{\text{surf}})}_{=0} \mathcal{P}_{\text{sf}}(d_1, \lambda, \alpha, 0) \mathcal{T}(n_{\text{air}}, n_{\text{surf}}) \mathbf{E}_0(\psi_\text{p}) \\
&= 0.
\end{aligned} \tag{34}$$

(4) Fibre-to-fibre-bond: reflection at the interface within the second fibre:

$$\begin{aligned}
\mathbf{E}_4&(\psi_\text{p}, \psi_\text{a}, \lambda, \alpha, \beta_\text{f}) \\
&= \mathcal{P}(\psi_\text{a}) \mathcal{T}(n_{\text{surf}}, n_{\text{air}}) \mathcal{P}_{\text{sf}}(d_1, \lambda, -\alpha, 0) \\
&\quad \times \underbrace{\mathcal{T}(n_{\text{surf}}, n_{\text{surf}})}_{=\mathbb{1}} \mathcal{P}_{\text{pc}}(\Delta\phi(\lambda, d_2), \alpha + \beta_\text{f}) \\
&\quad \times \underbrace{\mathcal{R}(n_{\text{surf}}, n_{\text{surf}})}_{=0} \mathcal{P}_{\text{pc}}(\Delta\phi(\lambda, d_2), \alpha + \beta_\text{f}) \underbrace{\mathcal{T}(n_{\text{surf}}, n_{\text{surf}})}_{=\mathbb{1}} \\
&\quad \times \mathcal{P}_{\text{sf}}(d_1, \lambda, \alpha, 0) \mathcal{T}(n_{\text{air}}, n_{\text{surf}}) \mathbf{E}_0(\psi_\text{p}) \\
&= 0.
\end{aligned} \tag{35}$$
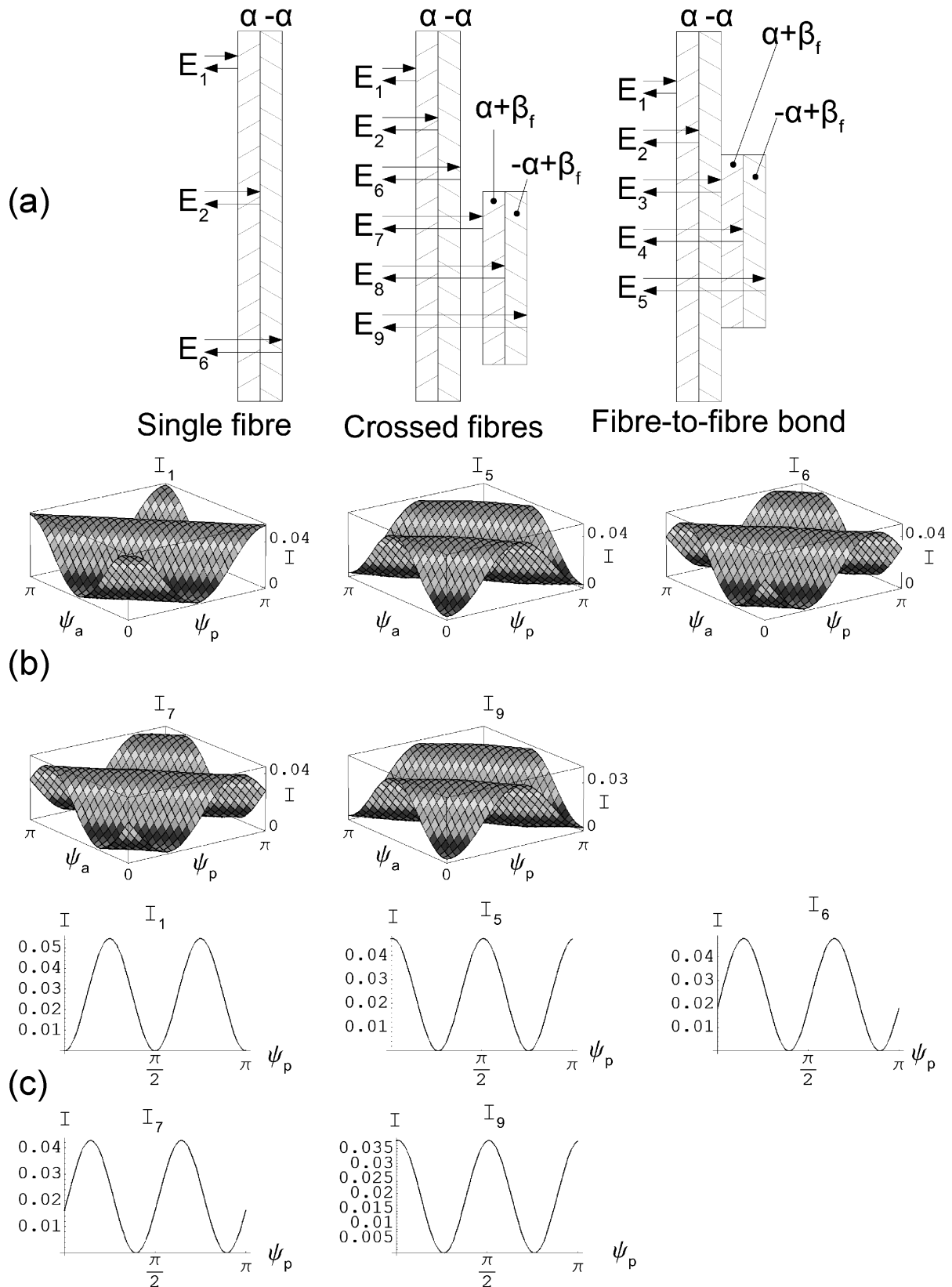
Figure 5. (a) Optical setup of the model, and reflections taken into account for single fibres, unbonded crossed fibres and fibre-to-fibre bonds. (b) The simulated non-zero intensities of the reflections shown in (a), as functions of polarizer (ψ_p) and analyzer (ψ_a) angle (see text). (c) Same as (b), but for crossed polarizers ($\psi_a = \psi_p + \pi/2$).

(5) Fibre-to-fibre bond: reflection at the back surface:

$$
\begin{aligned}
\mathbf{E}_5(&\psi_p, \psi_a, \lambda, \alpha, \beta_f) \\
&= \mathcal{P}(\psi_a)\mathcal{T}(n_{surf}, n_{air})\mathcal{P}_{sf}(d_1, \lambda, -\alpha, 0) \\
&\quad \times \underbrace{\mathcal{T}(n_{surf}, n_{surf})}_{=\mathbb{1}}\mathcal{P}_{sf}(d_2, \lambda, -\alpha, \beta_f)\mathcal{R}(n_{surf}, n_{air}) \\
&\quad \times \mathcal{P}_{sf}(d_2, \lambda, \alpha, \beta_f)\underbrace{\mathcal{T}(n_{surf}, n_{surf})}_{=\mathbb{1}}\mathcal{P}_{sf}(d_1, \lambda, \alpha, 0) \\
&\quad \times \mathcal{T}(n_{air}, n_{surf})\mathbf{E}_0(\psi_p) \\
&= \mathcal{P}(\psi_a)\mathcal{T}(n_{surf}, n_{air})\mathcal{P}_{sf}(d_1, \lambda, -\alpha, 0) \\
&\quad \times \mathcal{P}_{sf}(d_2, \lambda, -\alpha, \beta_f)\mathcal{R}(n_{surf}, n_{air})\mathcal{P}_{sf}(d_2, \lambda, \alpha, \beta_f) \\
&\quad \times \mathcal{P}_{sf}(d_1, \lambda, \alpha, 0)\mathcal{T}(n_{air}, n_{surf})\mathbf{E}_0(\psi_p).
\end{aligned}
\tag{36}
$$

(6) Single fibre and unbonded crossed fibres: reflection at the back surface of the first fibre:

$$
\begin{aligned}
\mathbf{E}_6(&\psi_p, \psi_a, \lambda, \alpha, \beta_f) \\
&= \mathcal{P}(\psi_a)\mathcal{T}(n_{surf}, n_{air})\mathcal{P}_{sf}(d_1, \lambda, -\alpha, 0) \\
&\quad \times \mathcal{R}(n_{surf}, n_{air})\mathcal{P}_{sf}(d_1, \lambda, \alpha, 0)\mathcal{T}(n_{air}, n_{surf})\mathbf{E}_0(\psi_p).
\end{aligned}
\tag{37}
$$

(7) Unbonded crossed fibres: reflection at the front surface of the second fibre:

$$
\begin{aligned}
\mathbf{E}_7(&\psi_p, \psi_a, \lambda, \alpha, \beta_f) \\
&= \mathcal{P}(\psi_a)\mathcal{T}(n_{surf}, n_{air})\mathcal{P}_{sf}(d_1, \lambda, -\alpha, 0) \\
&\quad \times \mathcal{T}(n_{air}, n_{surf})\mathcal{R}(n_{air}, n_{surf})\mathcal{T}(n_{surf}, n_{air}) \\
&\quad \times \mathcal{P}_{sf}(d_1, \lambda, \alpha, 0)\mathcal{T}(n_{air}, n_{surf})\mathbf{E}_0(\psi_p).
\end{aligned}
\tag{38}
$$

(8) Unbonded crossed fibres: reflection at the interface within the second fibre:

$$
\begin{aligned}
\mathbf{E}_8(&\psi_p, \psi_a, \lambda, \alpha, \beta_f) \\
&= \mathcal{P}(\psi_a)\mathcal{T}(n_{surf}, n_{air})\mathcal{P}_{sf}(d_1, \lambda, -\alpha, 0) \\
&\quad \times \mathcal{T}(n_{air}, n_{surf})\mathcal{T}(n_{surf}, n_{air})\mathcal{P}_{pc}(\Delta\phi(\lambda, d_2), \alpha + \beta_f) \\
&\quad \times \underbrace{\mathcal{R}(n_{surf}, n_{surf})}_{=0}\mathcal{P}_{pc}(\Delta\phi(\lambda, d_2), \alpha + \beta_f)\mathcal{T}(n_{air}, n_{surf}) \\
&\quad \times \mathcal{T}(n_{surf}, n_{air})\mathcal{P}_{sf}(d_1, \lambda, \alpha, 0)\mathcal{T}(n_{air}, n_{surf})\mathbf{E}_0(\psi_p) \\
&= 0.
\end{aligned}
\tag{39}
$$

(9) Unbonded crossed fibres: reflection at the back surface of the second fibre:

$$
\begin{aligned}
\mathbf{E}_9(&\psi_p, \psi_a, \lambda, \alpha, \beta_f) \\
&= \mathcal{P}(\psi_a)\mathcal{T}(n_{surf}, n_{air})\mathcal{P}_{sf}(d_1, \lambda, -\alpha, 0) \\
&\quad \times \mathcal{T}(n_{air}, n_{surf})\mathcal{T}(n_{surf}, n_{air})\mathcal{P}_{sf}(d_2, \lambda, -\alpha, \beta_f)\mathcal{R}(n_{surf}, n_{air}) \\
&\quad \times \mathcal{P}_{sf}(d_2, \lambda, \alpha, \beta_f)\mathcal{T}(n_{air}, n_{surf})\mathcal{T}(n_{surf}, n_{air})\mathcal{P}_{sf}(d_1, \lambda, \alpha, 0) \\
&\quad \times \mathcal{T}(n_{air}, n_{surf})\mathbf{E}_0(\psi_p).
\end{aligned}
\tag{40}
$$

The non-zero single intensities are shown in Fig. 5(b and c). (The chosen parameters will be discussed in Section 5.) The reflected Jones vectors $\mathbf{E}_1$ to $\mathbf{E}_9$ (see Fig. 5(a)) can be combined to total intensities by the absolute squares of their sums:

- Single fibre:

$$I_{\text{ref,sf}} = |\mathbf{E}_1(\psi_p, \psi_a, \alpha) + \mathbf{E}_2(\psi_p, \psi_a, \lambda, \alpha) + \mathbf{E}_6(\psi_p, \psi_a, \lambda, \alpha, \beta_f)|^2. \quad (41)$$

- Fibre-to-fibre bond:

$$\begin{aligned} I_{\text{ref,bond}} = |\mathbf{E}_1(\psi_p, \psi_a, \alpha) &+ \mathbf{E}_2(\psi_p, \psi_a, \lambda, \alpha) + \mathbf{E}_3(\psi_p, \psi_a, \lambda, \alpha, \beta_f) \\ &+ \mathbf{E}_4(\psi_p, \psi_a, \lambda, \alpha, \beta_f) + \mathbf{E}_5(\psi_p, \psi_a, \lambda, \alpha, \beta_f)|^2. \end{aligned} \quad (42)$$

- Crossing of two unbonded fibres:

$$\begin{aligned} I_{\text{ref,cf}} = |\mathbf{E}_1(\psi_p, \psi_a, \alpha) &+ \mathbf{E}_2(\psi_p, \psi_a, \lambda, \alpha) \\ &+ \mathbf{E}_6(\psi_p, \psi_a, \lambda, \alpha, \beta_f) + \mathbf{E}_7(\psi_p, \psi_a, \lambda, \alpha, \beta_f) \\ &+ \mathbf{E}_8(\psi_p, \psi_a, \lambda, \alpha, \beta_f) + \mathbf{E}_9(\psi_p, \psi_a, \lambda, \alpha, \beta_f)|^2. \end{aligned} \quad (43)$$

5. Computational Results

With the intensities of the different geometries, given in Fig. 5(a), the system of plane-parallel plates, describing the fibres can be simulated, given the geometric parameters of the fibre. The refractive indices and the wavelength of the light used are known.

The angle of the bond, $\beta_f = 85°$, can be obtained from Fig. 1(a). The microfibrilar angle, α, was chosen to be $\alpha = -27° = -0.471$ rad. Absolute values for the fibril angle of spruce pulp, the fibers used in our experiments, vary for individual fibers between $0°$ and $50°$ [17], an average angle of $27°$ is a reasonable choice. Cellulose fibrils in wood always form a right handed spiral along the fiber principal axes [18]. According to Fig. 4(a) the parameter of the microfibrillar angle, α, therefore has a negative sign. The refractive indices of a cellulose fibre in the longitudinal and transversal direction are $n_l = 1.618$ and $n_t = 1.554$, as given in [11].

The refractive indices in the fast and slow optical axes are given by the ellipse of refraction (see Fig. 4). For a given n_{slow} and n_{fast}, the transversal and longitudinal refractive indices are:

$$n_l = \sqrt{n_{\text{fast}}^2 \cos^2 \alpha + n_{\text{slow}}^2 \sin^2 \alpha}, \quad (44)$$

$$n_t = \sqrt{n_{\text{fast}}^2 \sin^2 \alpha + n_{\text{slow}}^2 \cos^2 \alpha}. \quad (45)$$

Solving the system for n_{slow} and n_{fast} yields:

$$n_{\text{slow}} = \sqrt{\frac{n_t^2 \cos^2 \alpha - n_l^2 \sin^2 \alpha}{\cos^4 \alpha - \sin^4 \alpha}} \quad (46)$$

and

$$n_{\text{fast}} = \sqrt{\frac{n_{\text{t}}^2 \sin^2 \alpha - n_{\text{l}}^2 \cos^2 \alpha}{\sin^4 \alpha - \cos^4 \alpha}}. \tag{47}$$

It is to be expected that the refractive indices in the longitudinal and transversal direction are a function of the microfibrillar angle and that the refractive indices in the direction of the fast and slow optical axis stay rather constant. If the indices n_{slow} and n_{fast} were to be considered as a function of α, one would arrive at false answers for the intensity as a function of α (see Fig. 7). Equation (46) still gives a useful approximation of the refractive indices. With α chosen as above, this yields:

$$n_{\text{slow}}(\alpha = -0.471) = 1.63985, \tag{48}$$

$$n_{\text{fast}}(\alpha = -0.471) = 1.53092. \tag{49}$$

The thickness of the fibre can be measured from images taken from the micro-tome cuts. For the fibre-to-fibre bond shown in Fig. 1(a), the thickness of the first fibre is 3.054 µm and the thickness of the second fibre is 2.090 µm. The parameter d represents the thickness of only one s_2 layer (see Fig. 3(b)), while the thickness measured from the microtome images is the thickness of two s_2 layers. Thus the thickness has to be taken as half the measured thickness: 1.527 µm for the first fibre and 1.045 µm for the second fibre. The assumption that the fibre wall thickness equals the thickness of the s_2 layer is feasible, because this layer contains 80–95% of the fibre material [13]. The wavelength of the incident light was chosen in the visible range, $\lambda = 400$ nm for monochromatic calculations.

Figure 5(b) shows the calculated reflected, non-zero single intensities ($I_n = |E_n|^2$) as a function of the polarizer angle (ψ_{p}) and the analyzer angle (ψ_{a}). The different intensities show different periodic behavior. The reflected intensity on the top surface I_1, shows a phase shift of π resulting from the reflection on a medium with higher refractive index (equation (16)). The other intensities show a behavior similar to a $\lambda/2$ phase retarder plate (which also gives a phase shift of π) but with an additional shift in the maxima resulting from rotation of the polarization. Additionally, I_5 and I_9 (Fig. 5(b)) show a slight curve along the $\psi_{\text{a}} = -\psi_{\text{p}} + \pi/2$-direction, resulting from transmission-like behavior. The polarization rotation of the intensity maxima is higher at I_5 and I_9 than at I_6 and I_7 (Fig. 5(b)).

The case for crossed polarizers as a function of ψ_{p} is shown in Fig. 5(c). This represents a section through the intensities in Fig. 5(b) (along the line $\psi_{\text{a}} = \psi_{\text{p}} + \pi/2$). Here the shift of the maxima of intensity can be observed better. The intensities I_5 and I_9 (Fig. 5(c)) are shifted in respect to I_1 by $\pi/4$, while the intensities I_6 and I_7 (Fig. 5(c)) are shifted by about $\pi/6$. These shifts are the main reason for the effect of dark bonded areas, because the amplitude of the different intensity maxima is quite similar.

The intensities I_2, I_3, I_4 and I_8 are exactly zero (equations (33)–(35) and (39)). This is due to the fact that these are the intensities of reflection on the inner interface of a fibre, or on the bonded interface, where the index of refraction was set to

n_{surf} (equation (20)). This yields a reflectivity $\mathcal{R}(n_1 = n_2) = 0$ (equation (16)). The error arising from this approximation is not large. For a circular polarized wave, the difference in reflectivity cancels totally over a period: the biggest error is to be expected for a linear polarized wave, parallel to one of the optical axes of the two media (for example two s_2-layers of a pulp fibre), when these optical axes enclose an angle of 90°. The refractive index in the first medium would then be n_{slow} and in the second medium n_{fast} (or *vice versa*). This yields a reflectivity of:

$$\mathcal{R}(n_{\text{slow}}, n_{\text{fast}}) = \begin{pmatrix} -0.03 & 0 \\ 0 & 0.03 \end{pmatrix}, \tag{50}$$

with n_{slow} and n_{fast} chosen according to equation (46). This means a maximum error of 3% in every reflection or transmission, while most of these reflections and transmissions will take place with elliptically polarized light, making the error smaller.

The total intensities for reflection polarization microscopy are shown in the Figs 6 and 7. Figure 6(a) shows the resulting total intensity for a fibre-to-fibre bond, a single fibre, and crossed unbonded fibres as a function of the polarizer angle (ψ_{p}) enclosed by the principal axis of the fibre and the transmission axis of the polarizer, and the analyzer angle (ψ_{a}), enclosed by the transmission axis of the analyzer and the principal axis of the fibre. Fibre-to-fibre bond and an unbonded fibre crossing show the same shift of intensity maxima, resulting from the shift in the single intensities, while the behavior of the intensity of the single fibre is similar to a $\lambda/2$-phase retarder plate without a big shift (Fig. 6(a)). For a constant angle between the polarizer and the analyzer, it is always observed that the fibre-to-fibre bond has its maximum of intensity shifted in respect to the maximum of intensity of the single fibre by $\approx \pi/4$, such that it looks identical to the unbonded fibre crossing. This is due to the fact that the two reflections between the unbonded fibres (I_6 and I_7, Fig. 5(b)) interfere negatively while the reflection at the bonded surface (I_3) is zero because of the identical refractive indices on the two surfaces (equation (16)). The negative interference occurs because the reflection I_7 takes place at an interface from a medium with a lower refractive index to a medium with a higher index (specular reflection). This causes a phase shift of π at the reflection I_7, while the reflection I_6 (internal reflection) is not shifted (equation (16), Fig. 5(a)).

Experimentally the similarity between the bond and the crossing is a rather rare effect. This is not surprising because the probability of two fibres crossing each other exactly plane parallel is quite small. The difference in intensity between the fibre-to-fibre bond and the unbonded fibre crossing is only due to the relative alignment of the two fibres and, therefore, the correlation of dark bonded areas with the existence of fibre-to-fibre bonds is a purely statistical phenomenon.

The situation of Fig. 6(a) is plotted in Fig. 6(b) for crossed polarizers ($\psi_{\text{a}} = \psi_{\text{p}} + \pi/2$) for the case of a fibre-to-fibre bond, the two different single fibres (different thickness) and a crossing of the two unbonded fibres. The bond and the unbonded crossing yield an intensity that is smaller than the intensity of the single fibres by a factor 2. This is due to the fact that the single intensity I_6
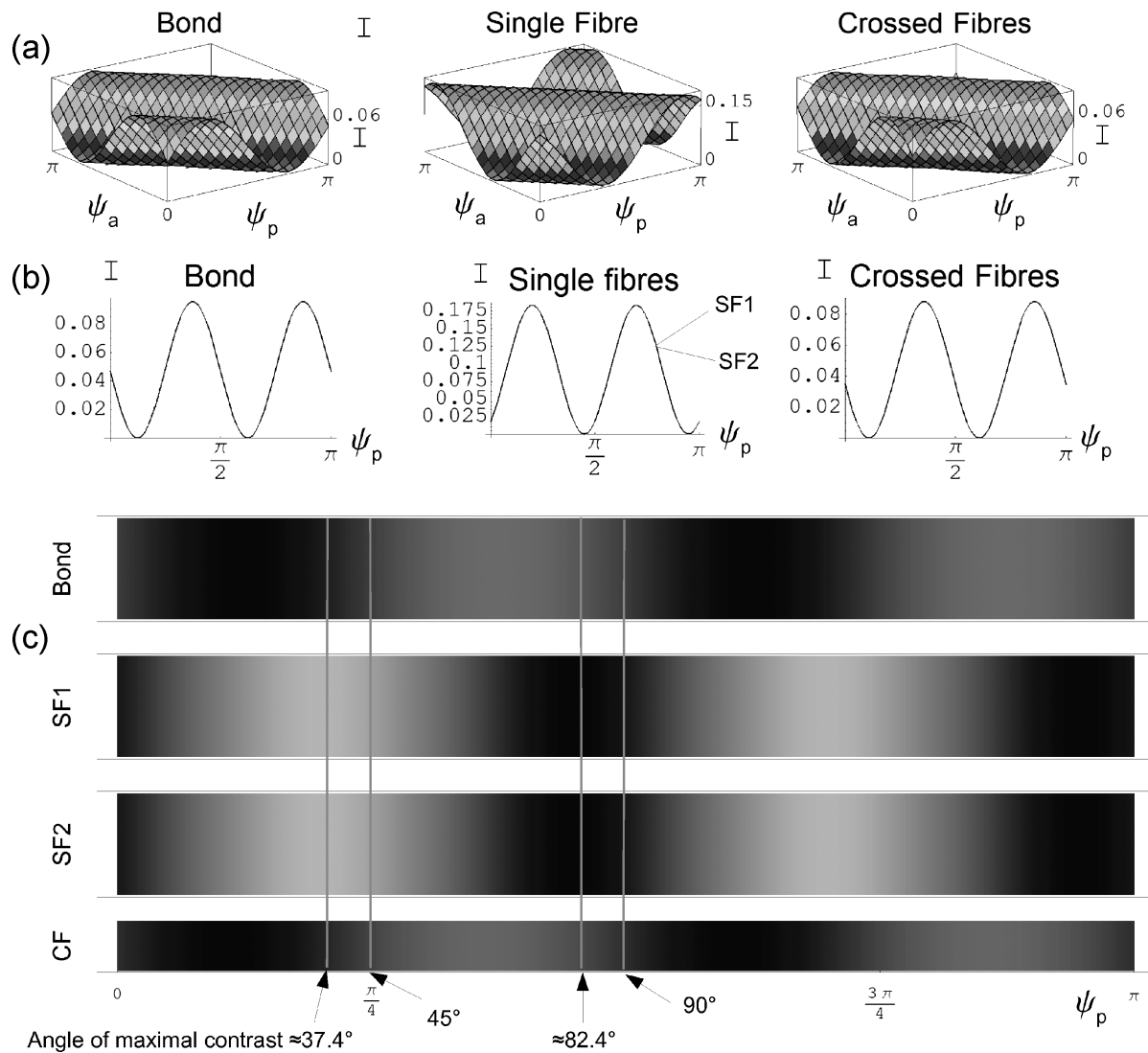
Figure 6. Reflected total intensities for two single fibres (SF1, SF2), their unbonded crossing (CF) and a fibre-to-fibre bond between them (bond). (a) As a function of polarizer (ψ_p) and analyzer angle (ψ_a), only one single fibre shown (SF1). (b) As a function of polarization angle (ψ_p) with crossed analyzer ($\psi_a = \psi_p + \pi/2$). (c) As a function of polarization angle (ψ_p) with crossed ($\psi_a = \psi_p + \pi/2$) analyzer and calculated reflection color. Compare the angles of high contrast to Fig. 1(a).

is preserved in the case of the single fibres, because it does not interfere negatively with I_7 (see Fig. 5(a)). A comparable illustration of the intensities and colors for $\alpha = -27°$ and crossed polarizers is given by Fig. 6(c). This result is in very good agreement to the microscope picture in Fig. 1(a), the bond area is clearly darker than the fibre (which can even be seen in the greyscale). Please note that two unbonded crossing fibres (Fig. 6(c), CF) would also form a crossing area that is darker than the fibers. The color functions were calculated from the spectra of the returned intensities weighed with the CIE-sensitivity functions for the human eye [16]. The colors should only be considered as a rough estimate.

Some conclusions can be drawn about the behavior of the system with different microfibrilar angles α: in reflection for $\alpha \to \pm\pi/4$, the effect of the dark bonds
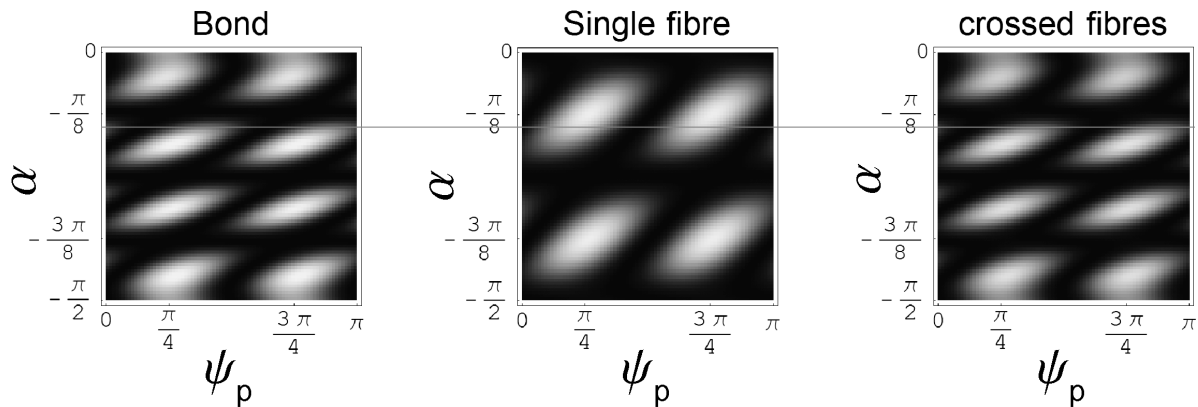
Figure 7. Reflection intensities for one single fibre (SF1), fibre-to-fibre bond and unbonded crossed fibres between crossed polarization filters, as a function of the angle of the polarizer (ψ_p) and the angle of the microfibrils (α). For $\alpha \to k \cdot \pi/4$ and $\alpha \to (2k+1) \cdot \pi/16$, with $k \in \mathbb{Z}$ the effect vanishes (see text). The line indicates the chosen parameter $\alpha = -27°$.

has to vanish due to the fact that the Jones matrices of a fibre for this case yield unity (see equation (24)). This fact is shown in Fig. 7 for crossed polarizers. The influence of the fibres vanishes at $\alpha = -\pi/4$, i.e., that the Jones matrices of the fibres at $\alpha = \pm\pi/4$ yield unity. With a microfibrillar angle $\alpha = \pm\pi/8, \pm3\pi/8$, the bond would appear completely dark for all polarizer angles ψ_p. For a microfibrillar angle α of $\pm\pi/16, \pm3\pi/16, \ldots$, the fibre-to-fibre bond and single fibres would have their intensity maxima at the same polarizer angle ψ_p (Fig. 7). Therefore it can be said that all the mentioned effects can only occur for microfibrillar angles $\alpha \neq k \cdot \pi/4$ and $\alpha \neq (2k+1) \cdot \pi/16$ with $k \in \mathbb{Z}$. The red line in Fig. 7 indicates the chosen angle $\alpha = -27°$.

To underline the validity of the model, further experiments regarding light dispersion of fibers under stress were carried out and simulated by the model. A comparison of experimental and computational results is shown in Fig. 8. Figure 8(a) presents a single fibre under longitudinally applied mechanical stress, in transmission microscopy. In this case the transmission axis of the analyzer was parallel to the principal axis of the fibre, while the polarizer was rotated (polarization angle, ψ_p indicated above the images). The fibre shows a dispersion that is depending on the polarization angle. The dispersion of this fibre under mechanical stress in longitudinal direction, was numerically analyzed. For the analysis, squares of 100×100 pixels from the middle of the fibre were extracted from the pictures and split into red, green and blue. Their mean values are shown in Fig. 8(b). A $\cos^2(\psi_p + \phi)$-dependency (with ψ_p being the angle enclosed by the principal axis of the fibre and the polarizer) with different phase-shifts ϕ for different colors can be observed. For fibres that were not under mechanical stress, the effect of phase-shifts between the different colors was not observable (see Fig. 8(d)).

Figure 8(c) shows the simulation of the same situation for the parameters $n_{\text{slow}} = 1.798$, $n_{\text{fast}} = 1.50$, $d = 2.46$ and $\alpha = -0.4$. The agreement between the calculated and the measured values is quite good, except for a total shift of the polarization angle by about 0.5 rad. It is impossible to make a distinct statement, as the geometric
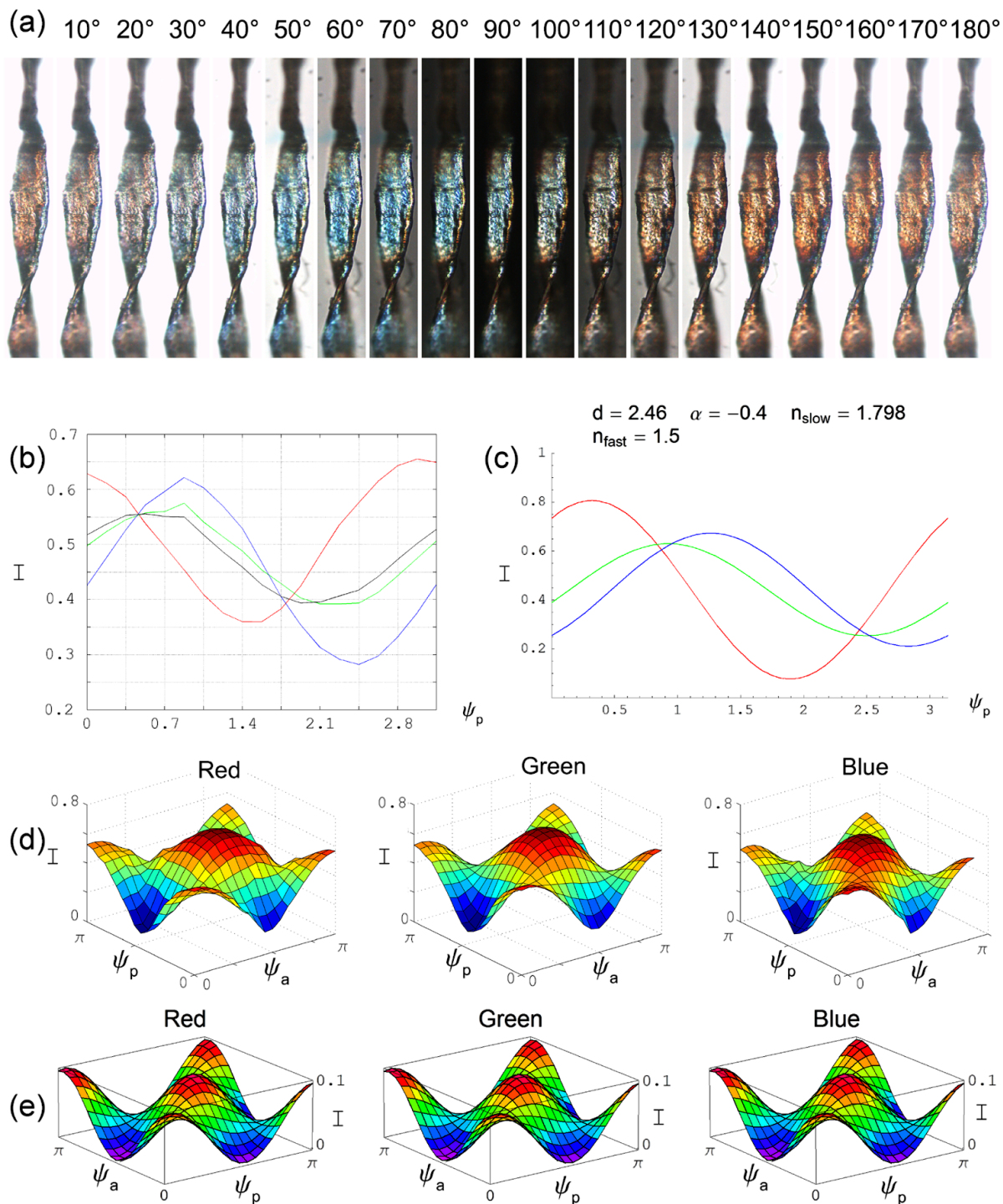
Figure 8. Comparison of measured data and calculation. (a) Single fibre under longitudinal mechanical stress in polarization transmission microscopy. The polarizer is rotated from $\psi_p = 0°$ to $\psi_p = 180°$, the analyzer stays parallel to the fibre. A dispersion, depending on the polarization angle can be observed. (b) Measured dispersion of a fibre in transmission under longitudinal mechanical stress, as a function of the polarization angle (shown in (a)), with the analyzer parallel to the fibre. (c) The effect of mechanical stress can be simulated with the model by reducing the absolute value of the angle of the microfibrils and increasing the anisotropy of refractive indices. (d) Measurement of transmission intensities for a single fibre as a function of polarizer and analyzer angle. Red, green and blue are separated numerically. (e) Simulation of (d) for polychromatic light (CIE color space R, G, B [16]).

parameters of the fibre investigated were not obtainable. A clear statement can be made: that the dispersion can indeed be described appropriately by the model, by increasing the optical anisotropy and by decreasing the microfibrillar angle.

The transmission intensity of a single fibre as a function of the angle between the transmission axis of the polarizer and the principal axis of the fibre (ψ_p) and the angle between the transmission axis of the analyzer and the principal axis of the fibre (ψ_a) was measured by a series of photographs. They were also analyzed for red, green and blue intensity. The results are shown in Fig. 8(d). The pictures show a behavior similar to a $\lambda/4$-phase retarder plate without noticeable dispersion, due to the absence of mechanical stress. Figure 8(e) shows the simulation of the same situation for a fibre with a thickness of $d = 1.85$ and with its microfibrillar angle $\alpha = -20°$. The calculation was carried out for polychromatic light, with the CIE red, green and blue functions [16] as weights (equation (30)). The experiment and the computation show a very high correlation. The broader peaks in the experimental data could be due to non-perfect polarization filters or ambient light.

6. Conclusions

A physical model is presented that describes reflection and transmission of pulp fibre surfaces under polarized vertical illumination. It employs the Jones formalism to model the optical appearance of pulp fibres and fibre-to-fibre bonds.

The model clearly shows that only for fibres that are fully collapsed and lie flat upon each other, thus resembling a system of plane parallel plates, the bonding areas appear as dark regions in polarization microscopy. If there are wrinkles or other irregularities in the fibre morphology no dark bonding region is visible under the microscope although the fibres are effectively bonded. Comparison of microscope images and microtome cuts of bonded fibres confirmed the model calculations. Not plane parallel fibre bonds, i.e., fibres with wrinkles in the bond or fibres with elliptic shape, did not show as bonds under polarization microscopy.

Furthermore it was found that fully collapsed, flat and parallel but unbonded fibres show a dark area in the crossing region, similar to the bonding region of bonded fibres. We know that paper has a highly layered structure where fibres are to a large extent aligned in the plane of the sheet, which makes it likely that a considerable amount of unbonded fibres in paper actually lie parallel to each other. Polarization microscopy on the one hand cannot identify all bonds between fibres and on the other hand some unbonded fibre crossings appear as bonds. Polarization microscopy cannot unambiguously discern between crossed unbonded fibres and bonded fibres, thus we find that this method is only to a limited extent suitable to determine bonded area of fibre-to-fibre bonds.

Calculations from the introduced model agreed very well with reflectance values measured from various bonded and unbonded chemical pulp fibres. It can be concluded that the presented model gives an accurate description of pulp fibre microscopy under polarized vertical illumination. Considering that the bonded area between fibres is a key factor for the mechanical and optical properties of paper,

a correct interpretation for polarized light microscopy images of pulp fibre-to-fibre bonds will contribute to a better understanding of paper network strength.

Acknowledgements

References

1. D. H. Page, A theory for the tensile strength of paper, *Tappi* **52**, 674–681 (1969).
2. T. Lindström, L. Wagberg and T. Larsson, On the nature of joint strength in paper — a review of dry and wet strength resins used in paper manufacturing, in: *13th Fundamental Research Symposium*, Cambridge, UK, pp. 457–562 (2005).
3. C. Yang, A. R. K. Eusufzai, R. Sankar, R. E. Mark and R. W. Perkins Jr., Measurements of geometrical parameters of fiber networks, Part 1. Bonded surfaces, aspect ratios, fiber moments of inertia, bonding state probabilities, *Svensk Papperstidning* **13**, 426–433 (1978).
4. G. Jayme and G. Hunger, Electron microscope 2- and 3-dimensional classification of fibre bonding, formation and structure of paper, in: *Transactions of the 2nd Fundamental Research Symposium*, Oxford, UK, pp. 135–170 (1961).
5. A. Torgnysdotter, The link between the fiber contact zone and the physical properties of paper: a way to control paper properties, *J. Compos. Mater.* **41**, 1619–1633 (2007).
6. C. I. Thomson, Probing the nature of cellulosic fibre interfaces with fluorescence resonance energy transfer, *PhD Thesis*, School of Chemistry and Biochemistry, Georgia Institute of Technology, USA (2007).
7. D. H. Page, Fibre-to-fibre bonds, Part 1. A method for their direct observation, *Paper Technol.* **1**, 407–411 (1960).
8. D. H. Page and P. A. Tydeman, Fibre-to-fibre bonds, Part 2. A preliminary study of their properties in paper sheets, *Paper Technol.* **1**, 519–530 (1960).
9. M. Donoser, M. Wiltsche and H. Bischof, A new automated microtomy concept of 3D paper structure analysis, in: *Proc. 9th IAPR Conference on Machine Vision Applications*, pp. 76–79 (2005).
10. E. Gilli, IR spectroscopic investigations on the chemical surface properties of cellulose fibres, *Master's Thesis*, Institute for Solid State Physics, Graz University of Technology, Austria (2008).
11. J. Brandrup and E. H. Immergut, *Polymer Handbook*. Wiley, New York, USA (1975).
12. J. Gullichsen and H. Paulapuro, Forest products chemistry, in: *Fapet Oy, Book 3*, pp. 24–26 (2000).
13. O. Bestsense and C. Ye, Method and device for determining the orientation angle of the optical axis and the relative phase retardation of a birefringent specimen, International Patent Number: WO 96/10168 (1995).
14. E. Hecht, *Optics*. Addison-Wesley Reading, MA, USA (1987).
15. W. Demtröoder, *Experimentalphysik 2*. Springer, Berlin, Germany (2006).
16. CIE Commission internationale de l'ecclairage, CIE 1964 Supplementary Standard Colorimetric Observer (1964), URL http://www.cie.co.at/publ/abst/datatables15_2004/x10.txt,/y10.txt,/z10.txt.
17. H. Jang, G. Weigel, R. Seth and C. Wu, The effect of fibril angle on the transverse collapse of papermaking fibers, *Paperi ja Puu* **84**, 112–115 (2002).
18. P. Viitaharju and K. Niskanen, Chiral curl in thin papers, *J. Pulp and Paper Soc.* **20**, J148–J152 (1994).